New Generation of PNT User Terminals Exploiting Hybridization with LEO Constellations

Francis Soualle(*), Markel Arizabaleta(*), Christian Lichtenberger(*), Thomas Pany(*)
Jose A. del Peral-Rosado(**), Xavier De Vaucorbeil(**), Gabriele Ligorio(**)
Luca Canzian(***), Federica Rozzi(***), Marco Rotoloni(***), Stefano Garlaschi(***)
Francesco Menzione(****), Ottavio Picchi(****), Juan Pablo Boyero(****)
Author Affiliation(s): (*) University of the Bundeswehr Munich
(**) Airbus Defence and Space GmbH
(***) Qascom
(****) European Commission

BIOGRAPHIES

Francis Soualle graduated from the French engineering schools, ICAM in 1998 and CentraleSupelec in 2000, and is currently working on his PhD at the University of the Bundeswehr Munich. He is a Senior R&D Navigation Engineer within Airbus Defence and Space GmbH where he started in 2000. He has been strongly involved in signal design and performance activities for the first and second generation of the European Galileo system, and for EGNOS V3 systems. His recent interests concentrate on architecture and performance of LEO- and alternative-PNT systems.

Markel Arizabaleta studied his Master's degree in Telecommunication Engineering at Universidad del Paʹıs Vasco (UPV-EHU) in Bilbao, Spain. He is currently a research associate at the University of the Bundeswehr Munich at the Institute of Space Technology and Space Applications (ISTA). His focuses his research topics on 4G/5G signal processing, LEO-PNT signals and authentication methods employed for the first and second generation of Galileo.

Christian Lichtenberger has been a research associate at the Institute of Space Technology and Space Applications (ISTA) at the University of the Federal Armed Forces Munich (UniBw M) since 2019. He holds a Master's degree in Geodesy and Geoinformation from the Technical University of Munich (TUM). Besides stochastic modeling of low-cost GNSS receivers and integrity analysis of safety-critical systems, his research field includes the extension of the Multi Sensor Navigation Analysis Tool (MuSNAT) for LEO-PNT signals.

Thomas Pany is with the University of the Bundeswehr Munich (UniBw M) at the Space Systems Research Center (FZ SPACE) where he leads the satellite navigation unit LRT 9.2 of the Institute of Space Technology and Space Applications (ISTA). He teaches navigation focusing on GNSS, sensors fusion and aerospace applications. He has a PhD from the Graz University of Technology (sub auspiciis) and worked in the GNSS industry for seven years. He authored around 200 publications including one monography.

Jose A. del Peral-Rosado is a Senior R&D Navigation Engineer within the Future Navigation Programs Department at Airbus Defence and Space GmbH since 2019. He received the PhD degree on Telecommunications Engineering from Universitat Autònoma de Barcelona (UAB) in 2014, and was a postdoctoral researcher of the SPCOMNAV research group at UAB until 2019. He authored seminal works on performance evaluation of 4G/5G signals for positioning, and conducted theoretical and experimental research activities on hybrid GNSS, LTE, and 5G localization.

Xavier De Vaucorbeil graduated from the French engineering school CentraleSupelec in 2021. Since 2022, he has been working as a satellite navigation system engineer at Airbus Defence and Space GmbH, with a particular interest in the architecture and performance of the second-generation Galileo system. His recent activities focus on the performance simulation of LEO-PNT systems.

Gabriele Ligorio has been working in the sensor fusion field since 2012, with particular focus on Kalman filters and inertial sensors. He has authored more than 10 publications (international journals and conferences) where innovative sensor fusion methods and sensor calibration procedures were proposed. Since 2019 he joined Airbus Defence and Space as a navigation system engineer where he has led as project manager and technical lead in several ESA/EUSPA activities on sensor fusion and on-board integrity monitoring for aviation and railway applications

Luca Canzian joined Qascom in 2015 and he is currently leading the R&D domain area. He has worked in several projects with ESA, ASI, NASA, the European Commission and Industry. His main expertise involves ground-based and space-based location systems, detection and location of interference signals, navigation using signals of opportunity, inertial navigation systems, orbit determination techniques, GNSS authentication and anti-spoofing techniques. He holds a MSc degree and a PhD in Electrical Engineering from University of Padova (Italy).

Federica Rozzi is an R&D Radio Navigation Engineer at Qascom, with a focus on of satellite-based position authentication and interference detection techniques. She is also involved in activities dealing with Precise Orbit Determination algorithms for Lunar navigation. She holds a MSc degree in Automation Engineering from the Università degli Studi di Padova.

Marco Rotoloni is a senior Software and Firmware Engineer at Qascom, he is responsible for the design and development of Qascom GNSS SDR simulator (QA707). He is also involved in several engineering activities concerning software design/development/testing for ESA and other organizations. He obtained his PhD in Information Engineering from Università degli Studi di Padova in 2011.

Stefano Garlaschi is an R&D Radio Navigation Engineer at Qascom. He works on on diffential GNSS techniques and GNSS-5G hybridization. He obtained his PhD in Physics from Università degli Studi di Padova in 2021. In the same year he joined Qascom where he is currently working as R&D Radio Navigation Engineer. He focuses on diffential GNSS techniques and GNSS-5G hybridization.

Francesco Menzione received Master degree (2012) and Ph.D. (2017) from the University of Naples Federico II in Aerospace Engineering and Satellite Navigation. From 2012 till 2021, he worked in the aerospace sector as navigation and control engineer. In 2021, he joined European Commission's Joint Research Centre as Technical and Scientific Officer. He currently provides technical and project management support to different funded DEFIS studies and research areas focusing on Precise Orbit Determination, Space Service Volume, LEO-PNT, Hybrid PNT, Galileo High Accuracy Service and GNSS based remote sensing.

Ottavio M. Picchi received the MSc degree in Telecommunications engineering and the PhD in information engineering from University of Pisa, in 2008 and 2012, respectively. From 2012 to 2021 he was with WISER S.r.l., working on signal processing for communications and navigation. In 2021 he joined Keysight Technologies, working on beamforming techniques for 5G-NR. In 2022 he joined MBI S.r.l., where he was Satellite communications engineer. From July 2023 he is external consultant for JRC, focusing on 5G-NTN and IRIS2.

Juan Pablo Boyero is since 2012 working at the EC on the definition of the evolution of the Galileo and EGNOS missions. He coordinated all EU Horizon 2020 Research and Development projects on EGNSS and is now working on Mission And Services projects under Horizon Europe. Currently he is responsible for the Galileo Mission baseline. Before joining EC, he worked within the Galileo System Performance team, both as System Prime as well as Technical Support to System Prime. He holds a M.Sc. by the Escuela Técnica Superior de Ingenieros de Telecomunicación of the Universidad Politécnica de Madrid.

ABSTRACT

This paper will provide the main outcomes of the first phase of the HybPNT project aiming at assessing the PNT capabilities of different LEO-PNT initiatives (dedicated, fused and opportunistic LEO-PNT) either considered standalone or properly combined (i.e. hybridized), using possible commonalities. To support those assessments, a detailed literature survey covering the Iridium, Globalstar, Starlink, Xona, Trustpoint constellations, and finally up-coming 5G NTN systems defined in the 3GPP standardization, will provide the required configurations for system volume simulations (SVSs). The study also benefits of the adaptation of and End-to-End simulator which has been enhanced to model specificities of LEO-COM. Extensive SVS campaigns allow to assess key performance indicator (KPI) focusing on the accuracy, robustness and resilience of the single point positioning (SPP) solution. The paper points out several limits intrinsic to the communication systems starting with the reduced observability, but also the non-continuous transmission of positioning signal patterns (PSP) exploited for time-of-arrival (ToA) and frequency-of-arrival (FoA) estimation. Mitigations are proposed either at UT or at system levels, such as the optimization of the signal layer but also of the orchestration for the positioning reference signal (PRS) transmission, applicable for 5G non-terrestrial networks (5G NTN) systems. The paper shows that the hybridization allows to go beyond the limits of each individual system, but requires a suitable design of the hybrid PNT terminal, especially for PNT services taking place in the higher frequency regions (Ku-/Ka-Band).

1 MOTIVATION OF THE HYBPNT STUDY

The potential to exploit low earth orbit (LEO) constellations for positioning is passing from a challenging research issue to a new strategic technology allowing to complement or back-up GNSSs with innovative positioning, navigation and timing (PNT) infrastructures and services by following three main approaches. The first one which recently gained renewed interest, proposes novel signal of opportunity (SoOP) techniques to exploit the signals spilling from pre-existent narrowband or broadband telecom systems. The new scenario of mega-constellations, comprising thousands of satellites for worldwide fast connectivity, anticipates unprecedented PNT performance even without service provider cooperation. Far to be at conceptual level, the numerous works (see for example Kassas et al., (2023), Benzerrouk et al., (2019) or Tan et al., (2019)) having demonstrated promising PNT performance with real signals captured from the legacy Iridium and Globalstar communication systems, or the more recent broadband Starlink and OneWeb ones have placed opportunistic PNT as a credible alternative. The second approach contemplates an increasing number of initiatives aiming at deploying dedicated PNT services through hosted navigation payloads or dedicated LEO-PNT constellations. Here the commercial systems Xona, Trustpoint, or Centispace, are currently pioneering this new PNT path. In the third approach, cost effective optimizations between navigation and communication functions are conducted to offer fused LEO-PNT, also building-up on 5G NTN infrastructures. On-going standardizations effectively propose to dedicate positioning signals and system orchestration to enable navigation services with minimum impact on LEO-COM system design and communication capacity. Hence, in the near future, a User Terminal (UT) will have access to hundreds of different signals from LEO systems reflecting one or either approach, with the promise of improved performance, robustness and resilience. This motivates the novel concept of a new generation of Hybrid Navigation Terminals (HNT) supporting different kinds of LEO systems, signal waveforms and navigation data integrated within the baseline GNSS navigation. In this context, the European Commission has launched the "Hybrid PNT" project aiming at identifying the different LEO navigation opportunities and design drivers of the next HNT generation. This project, whose study logic is depicted on **FIGURE 1**, is split into the two following main phases.

• In the first project phase (highlighted with a dashed frame), a detailed literature survey is firstly conducted with the main intention to categorize and bring better readability to the many existing or on-going LEO-PNT initiatives. The collected information permits evaluating the standalone performance of each system considered individually by means of system volume simulations (SVSs). Here single point positioning (SPP) is considered as core algorithm implemented in the position engine, and thermal noise will represent the main contribution to the measurement errors. The outcome of this first SVS campaign enables evaluating strengths and weakness of those LEO-PNT initiatives, with a main focus on the accuracy, on the robustness defined in the frame of the project as the capability to sustain harsh environments (e.g. urban/deep urban), and on the resilience defined as the capability to sustain non-intentional or intentional interferences. From the corresponding gap analyses the most promising hybridizations of systems operating in the same frequency region (FR), to ease HNT implementation, are firstly proposed to satisfy the needs of three target applications: handheld devices, automotive and UAVs. A second SVS campaign is then performed for those hybridized systems, with the objective to demonstrate that most of the formerly identified weaknesses could be mitigated. Finally, a second hybridization combining the first hybridized systems takes place, yielding to HNT operating in different frequency regions to foster PNT performance, robustness and resilience. It is worthwhile noticing that the results from the two campaigns conducted with the same SVS platform permits a balanced and systematic comparison between the different LEO-PNT initiatives, either considered individually or hybridized, and which participates to the reliability of the corresponding outcomes.

• The second and up-coming project phase aims at demonstrating former assessments with synthetic or real signals processed with a breadboard applying Software Defined Radio (SDR) technology.

The proposed analyses are essentially UT-centric and consider existing or future LEO systems as input for assessments, when available. Nevertheless, the SVS outcomes can support design work for up-coming constellations, and notably 5G NTN systems considering that the inclusion of the PNT service, intricated to the communication one, is still in a maturation phase.

The current article is articulated as follows. In section 2, the outcomes of the literature survey regarding different LEO-PNT initiatives are presented. In section 3 the generic HNT architecture is described, together with its main constitutive building-blocks. In the same section, the proposed algorithms applied to extract measurements from the LEO signals, and to process them for UT position and time estimation are also explained. In section 4 the SVS framework which will permit evaluating the performance for both standalone and hybridized scenarios will be described, and with a special focus on new modules, such as the orchestration, which are specific to the current activity. Sections 5 and 6 present the performance obtained from two successive SVS campaigns, the first for standalone and the second for hybridized LEO-PNT systems. Finally, section 6.3 concludes this work. The **APPENDIX** includes models and

closed-form expressions which support different analyses, together with different figures showing key performance indicators (KPI) for the studied scenarios.
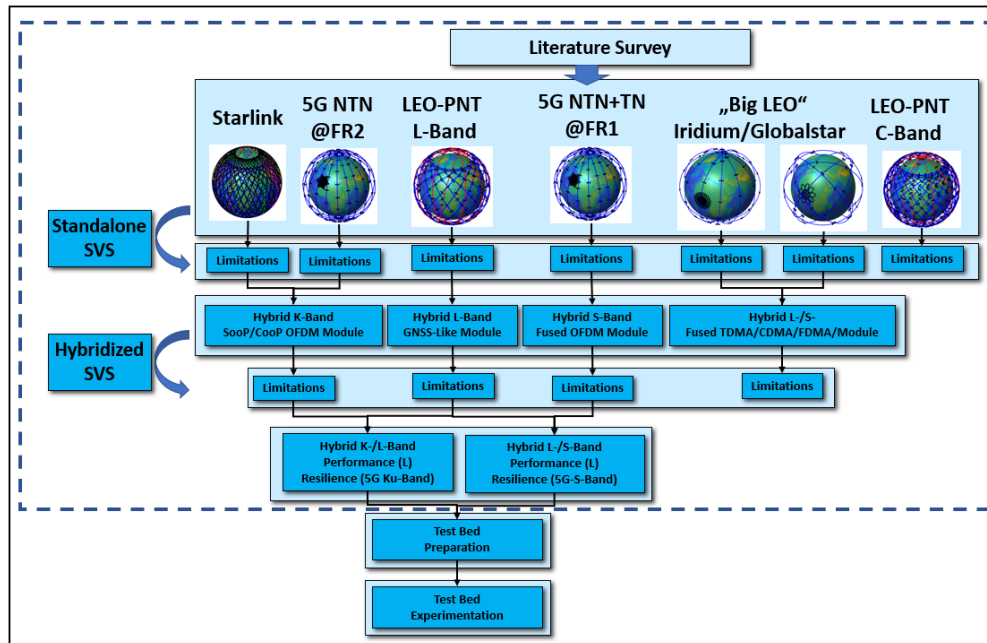

FIGURE 1*: Flow diagram for Hybrid PNT study logic*

2 REVIEW OF EXISTING AND FUTURE LEO-COM PROGRAMS OR DEDICATED LEO-PNT INITIATIVES

2.1 Introduction

This section presents the outcomes of a literature survey covering the different operational and future LEO-COM programs or dedicated LEO-PNT initiatives, with the intention to collect information supporting the configuration of the simulation framework. This concerns especially:

• The constellation topology which will permit to evaluate the satellite-to-UT visibility but also to derive the geometrical parameters (elevation, range, off-nadir angle (ONA) and azimuth) supporting link budget calculations and beam allocations. The cut-off angle for which system have been designed is also part of this set of geometrical information.

• The characteristics of the physical layer and comprising the down-link carrier frequency, the polarity, the signal structure and the applied modulation. More particularly, positioning signal patterns (PSP) such as tones or repetitive sequences usually applied by UTs for signal acquisition, locking, and data stream synchronization will be identified as they will enable the generation of observables (pseudo-range and pseudo-range rate) for UT positioning.

• The link access scheme, and especially the beam-to-cell allocation protocols for communication satellites equipped with multi-beam antennas. Contrarily to usual GNSS satellites broadcasting positioning signals to all "users in view", the communication satellites visibility does not obligatory imply accessibility to the corresponding communication signals, as it is strongly traffic dependent. Here, the allocation of the satellite resources, constituted of antenna beams and frequency channels to the UTs is of prime importance, as it will dictate the link availability and quality (i.e. carrier-to-noise density ratio, (C/N_0)), to support ranging and later positioning.

• The advertised PNT service, if any, provided by the system operator, but also the existing system or payload capabilities to support such a service.

In absence of information collected from the public domain, assumptions on a best guess basis are proposed.

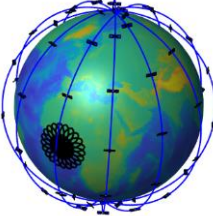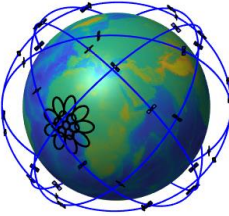### 2.2 Iridium and Globalstar as representatives of the "Big LEOs"

The first transmissions of radio signals from artificial satellites flying at low earth altitude date from the early 60s with the Russian Sputnik-1 and US SCORE missions, the latest one offering the first communication relay between two terrestrial nodes. Those pioneering missions settled the ground for the commercial exploitation of LEO satellites, which flourished in the 90s under the strong

demand for global mobile telephony with handheld terminals. Among the different planned initiatives only few became reality with the Iridium and Globalstar systems, so called the "big LEOs". Such systems offer voice and data communications, and short messaging, with moderate data rate, ranging from 10 KBps to several 100 KBps per satellite. They operate in the frequency region 1 (FR1), comprising the L-Band (~1.6GHz) and S-Band (~2.5GHz). Beyond their architectural commonalities, both systems also experienced similar ventures starting with a brief growing phase, rapidly followed by a bankruptcy caused by the fierce competition with terrestrial cellular technology and finally with a come-back enabled by a strong support of commercial and institutional investors, and which places now both systems into their second generation.

- **Constellation Topology of Iridium and Globalstar Systems:**

The characteristics of both Iridium and Globalstar constellations, together with their topology (see also Gaffney et al., (1994)) are presented in **TABLE 1**.

TABLE 1: Left: Iridium constellation topology, right: Globalstar constellation topology

Parameter	Iridium	Globalstar
Walker-Type	Star-Walker	Delta-Walker
Sat#	66	48
Planes Number	6	8
Sat. per Plane	11	6
Altitude [km]	780	1406
Inclination [deg]	86.4	52

- **Physical Layer of Iridium and Globalstar Systems:**

Iridium supports one and two-way communication to the UT by a combination of spatial, frequency and time division multiple access schemes (resp. SDMA, FDMA and TDMA). The frequency plan declared to the federal communications commission (FCC) identifies two main bands: the 1616-1626 MHz band allotted to duplex channels for broadcast, synchronization and traffic, and the 1626-1626.5 MHz band allotted to simplex channels for ring alert (RA) and messaging. The duplex band is fragmented into 30 sub-bands divided each in 8 duplex channels yielding to 240 duplex channels. The second band is decomposed in 12 simplex channels. Out of them 5 are actually exploited: 1 for the ring alert and 4 for the messaging. All channels, spaced with 41.667kHz occupy a bandwidth of 31.5kHz. Each frame of 90ms comprises a header burst transmitted in the simplex channels, followed by 4 pairs of up and down link bursts transmitted in the duplex channels. A common burst structure starts with an unmodulated carrier, followed by a unique word ('789' hex, binary phase shift keying (BPSK) modulated, as disclosed in Huang et al., (2022)) and the data stream (quadrature phase shift keying (QPSK) modulated at a 25 Ksymb/s rate), see **FIGURE 2**. The burst duration is channel dependent and equals 6.5ms for the ring alert, 8.28ms for the up/down link signals and 20.32ms for the messaging.

The Globalstar communication system exploits a combination of code division multiple access (CDMA) and SDMA schemes (see Globalstar. (2000)). The forward-link takes place in the 2483.5-2500MHz band, decomposed into 13 sub-bands of 1.2288MHz width. Each sub-band can accommodate 128 CDMA channels each modulated with a combination of pseudo-random noise (PRN) and Walsh sequences ensuring inter-channel orthogonality, themselves modulated with the communication symbols. Among those 128 channels, the pilot channel, as candidate position signal pattern, will thus play an important role for opportunistic positioning. The pilot channel applies a tiered code structure made of an inner PRN sequence comprising 1024 chips transmitted at 1.2288MCps and an outer sequence comprising 288 chips transmitted at 1.2KCps, yielding to an overall code periodicity of 240ms. It is transmitted continuously to support link acquisition, phase estimation for data demodulation and link power determination for traffic satellite handover. The other 127 channels comprising the synchronization, the paging, or the traffic channels could also be exploited for opportunistic positioning but their usage appears less straight-forward.
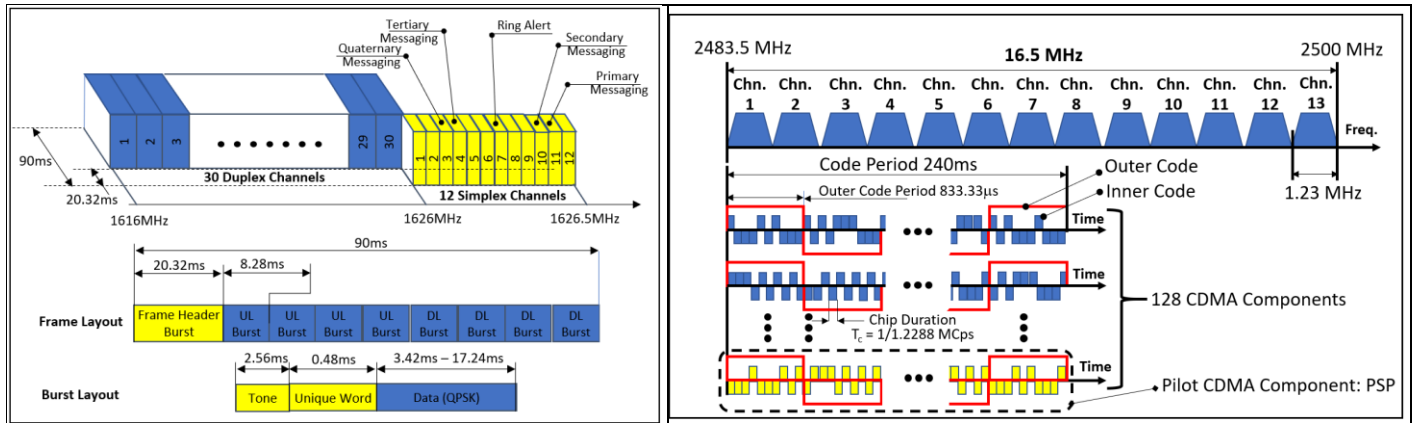
FIGURE 2: Left: Iridium signal structure and PSP component supporting ranging (yellow), Right: Globalstar signal structure and PSP component supporting ranging (yellow)

- **Payload:**

The Iridium Next antenna can form 48 beams distributed in a layout constituted of 4 rings, comprising respectively 3, 9, 15 and 21 cells and depicted on **FIGURE 3** (see also Claybrook, (2023)). To compensate for the larger space losses in the slant direction the equivalent isotropic radiated power (EIRP) is increased according to **FIGURE 3**, also showing the modelled antenna beam for each of the 4 rings and with a half-power beamwidth (HPBW) of 28.7°. The corresponding beam layout has been designed to guarantee the communication service for a minimal user masking angle of 8.2°. The 48 beams of Iridium Next antenna are arranged into 4 clusters of 12 beams. Each beam transmits 20 duplex channels, and the frequency re-use scheme ensures that the same channel is not transmitted on neighboured beams to reduce interferences. Regarding the simplex channels, the transmitted ring alert burst will revisit the same beam every 4.32s (see DecodeSystem., (2017)) and on an average the UE will receive one burst (paging or ring alert) every 1.4s (see DecodeSystem., (2017)) from the same satellite, ignoring the illumination from adjacent beams (as explained in Tan et al., (2019)), which could appear as parasites for a communication service but as enablers for a PNT one.

The Globalstar antenna layout is constituted of 3 rings, comprising respectively 1, 6 and 9 cells, to form 16 beams, as per Globalstar., (2000). As for Iridium, the EIRP increases for the 2nd and 3rd rings to balance the received power on ground (**FIGURE 3**). Each of the three beams has an HPBW of roughly 23°. The user down-link signals are transmitted in left-hand circular polarisation (LHCP). The EIRP level for the nadir beam and for the up-to 128-CDMA channels is derived from the EIRP per user (see ETSI, (1993)). All CDMA channels of the 13 sub-bands can be theoretically transmitted in each of the 16 beams (yielding to a maximum capacity of roughly 26.10^3 channels), but the overall number of channels per satellite is limited to 2500 due to power constraint (see Chang et al., (2005)).
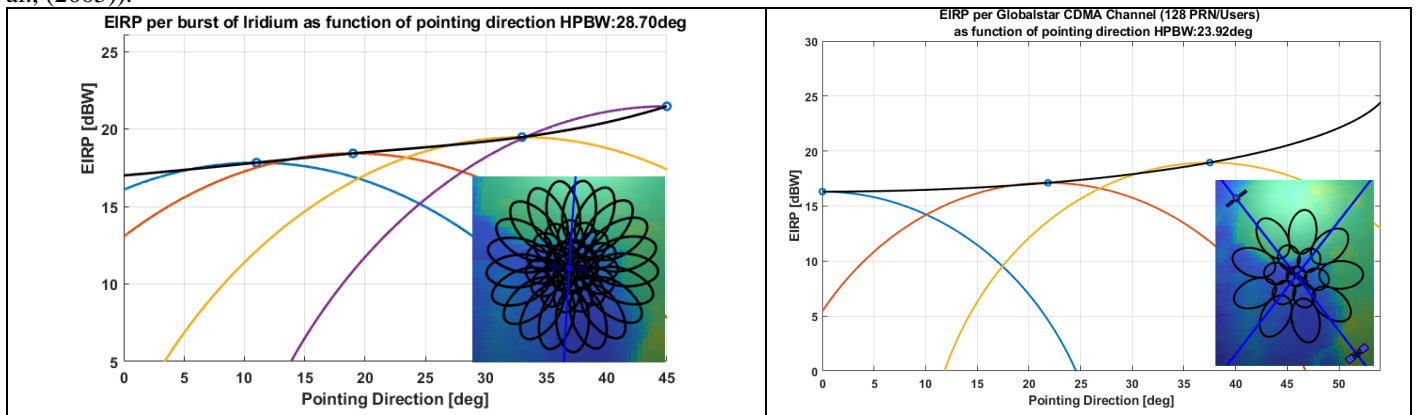

FIGURE 3: EIRP and antenna beam layout projected on earth surface - Left: Iridium – Right: Globalstar

Beyond the different combinations of multiple access schemes, two major features differentiate the Iridium and Globalstar payloads. Firstly, Iridium applies a re-generative payload while Globalstar payload is transparent. In that later case, a bent-pipe forward link combines the feeder link in C-Band between gateway and satellite and the user-link in S-Band. Secondly, to ease initial acquisition of the Globalstar link, and to reduce the apparent Doppler span to be scrutinized, a compensation takes place at Gateway, by wiping-off the actual Doppler experienced at beam centre from the transmitted signals, as explained in Neinavaie et al., (2021).

- **Payload and System Capabilities to support PNT service:**

To enter network, a 10km positioning accuracy is typically required for the handheld communication device (Levanon, (1998)). In the early 90's several works demonstrated how such a level could be achieved for both Iridium and Globalstar systems, and with two or only one satellite (see Narenthiran et al., (2000) and Levanon, (1999)). Besides this positioning service, intrinsic to the communication system, further investigations were conducted to identify payload or system capabilities offering enhanced and decoupled PNT service from the communication one.

Regarding Iridium, very few information is publicly available about the presence of a GNSS receiver interfaced to the regenerative communication payload, to provide satellite ephemeris or possibly steer local clock as for dedicated LEO-PNT systems (see section 3.2.6). The radio occultation payload, GEOscience, equipped with a precise GNSS receiver, or the attitude control unit of the platform (using star trackers as baseline and eventually accommodating a simpler GNSS receiver) appear decoupled from the main mission payload. Four inter-satellite link (ISL) units equipping each satellite, could represent a strong enabler for an orbit determination and time synchronization (ODTS) function implemented on-ground and independent from GNSS, assuming that ISL units can measure inter-satellite ranges (ISRs). To complete the list of payload items relevant for a PNT service, the local clock stability is better than 10ppb and a drift rate of 3Hz/s, according to the work of Tan et al., (2019). Despite obvious implementation of a LEO-PNT payload, Iridium has introduced a new PNT service to its portfolio, by incorporating the system time and location (STL) technology developed by Satelles (see Satellesportal.). This PNT technology exploits the short burst modulated on the simplex messaging, and notably both tones and unique word that have been tailored for improved frequency and time-of-arrival performance (see DecodeSystem., (2017)).

As for Iridium, the Globalstar system provides a low accuracy positioning service to support communication management with the user to gateway assignation and the registration. This service is completed with a high accuracy positioning service (at 300meters), as mentioned in Globalstar., (2000). The UT position can be determined either with an active two-way range (TWR), also called round-trip time, RTT, requesting at least two Globalstar satellites, or with a passive determinisation exploiting time difference of arrival (TDoA) technique and necessitating three satellites. In 2019, Globalstar and Echo Ridge announced the development of a PNT service, called augmented positioning system (APS), used as back-up to the GPS ones, as an answer to the department of transportation (DoT), (see Pressrelease., (2019)). Very few information on the actual ranging and positioning techniques implemented in the APS is however available in the public domain, although Hansen at al., (2021) mentions about a multilateration technique exploiting time-of-arrival.

2.3 Starlink

The last decade witnessed a renaissance of commercial initiatives for new LEO-constellations providing global and broadband (i.e. internet) communications. Among them OneWeb and Starlink represent the most emblematic operational systems, which should be soon followed by the Kuiper (Amazon), and the Chinese Thousand Sails, Guowang, Honghu-3 systems (see Pressrelease., (2024)). The high/very high data throughput per satellite (10 GBps to 40 GBps) is enabled firstly thanks to a migration to higher frequencies for the user and the feeder links, now taking place in the Ku-Band (10-12.7GHz) and Ka-Band (17-20GHz, 27-30GHz), and secondly with much more populated constellations, comprising several hundreds or even thousands of spacecrafts which attribute the name of "mega-constellations" to such systems. This technological renewal has been achieved with a significant reduction of launch cost (~5K€ per kg), and a profound rework of industrialization process built on the new space paradigm (see Soualle et al., (2019)).

- **Constellation:**

The final topology of the Starlink first-phase constellation is the result of mission analysis optimizations and adjustments following FCC recommendations (see FCC, (2020) and FCC, (2021a)). It is constituted of five shells comprising a mixed geometry of Walker-Star and -Delta (see Leyva-Mayorg et al., (2022)), yielding to an overall number of 4408 satellites, as shown on **FIGURE 4**.
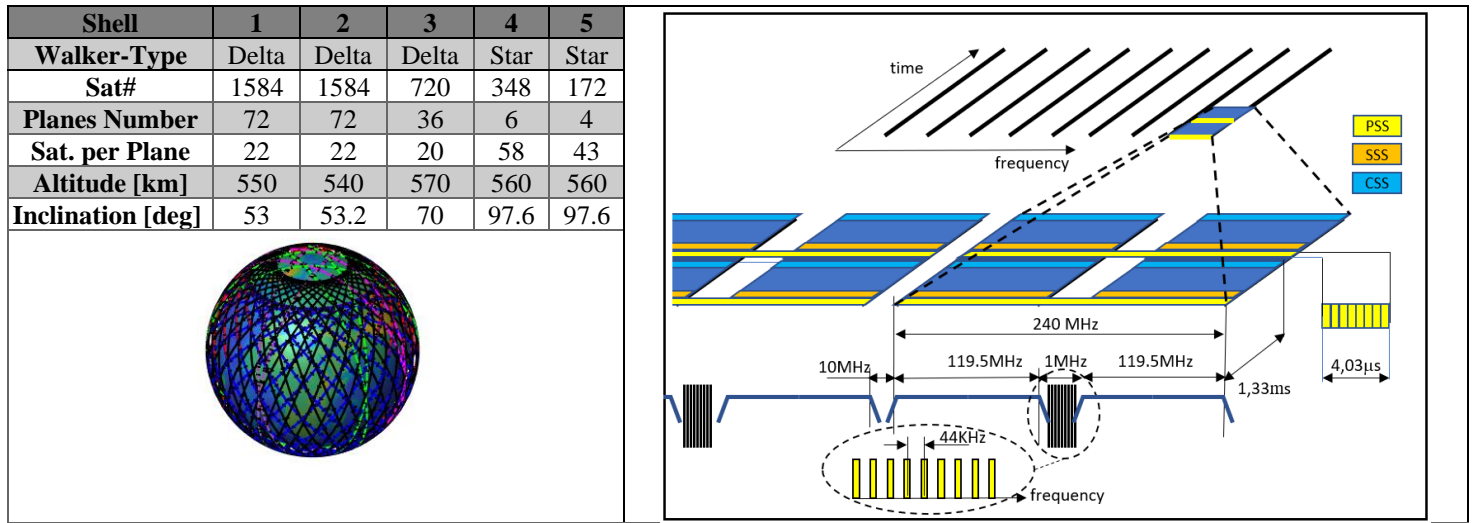
Shell	1	2	3	4	5
Walker-Type	Delta	Delta	Delta	Star	Star
Sat#	1584	1584	720	348	172
Planes Number	72	72	36	6	4
Sat. per Plane	22	22	20	58	43
Altitude [km]	550	540	570	560	560
Inclination [deg]	53	53.2	70	97.6	97.6

FIGURE 4: Left: Starlink constellation topology – Right: Starlink signal structure and PSP components supporting ranging

- **Physical Layer:**

The additional burden imposed by the high frequency in Ku-Band could not curb the enthusiasm and curiosity of several research groups to set-up dedicated signal monitoring equipment to pierce the Starlink signal structure. This quest has been facilitated by the significant cost decrease for the procurement of required components (antenna, analogue and digital front-end), also coupled with the availability of the new SDR technology. Furthermore, the plethora of operational Starlink satellites definitely intensified monitoring availability. Hence, in the recent years, a large number of publications aiming at unveiling Starlink signals have been issued out of three main communities: communication aiming at better characterizing system capacity, navigation aiming at recognizing specific features enabling ranging and positioning, and finally earth observation to exploit Starlink signals for bi-/multi-static passive radars.

The following summarizes the main characteristics of the user down-link signal structure essentially derived from Humphreys et al., (2021), and highlighted on **FIGURE 4**. The down-link signals are transmitted with a right-hand circular polarization (RHCP) in the 10.7 to 12.7 GHz band. This band is split into 8 channels of B_{ch}=240MHz bandwidth. The same physical layer, essentially based a OFDM signal modulation, is applied across channels. Each OFDM frame lasts T_{OFDM}=1/750s≈1.33ms and comprises N_{sc}=1024 sub-carriers with a sub-carrier interval F_{sc}= B_{ch}/N=234.375 kHz, and 302 symbols. The symbol duration T_{symb} (=1/F_{symb}) equals 4.4μs to support typical demodulation techniques based on FFT. The central part of the channel, called "gutter" with roughly 1MHz bandwidth is preserved from any OFDM transmission. Finally, guard intervals and guard bands improve isolation between channels, symbols and frames.

Two main types of position signal patterns have been identified in the Starlink signal structure, and their characteristics but also their accessibility will drive ranging and positioning availability and performance.
- The first PSP type englobes wide-band synchronization sequences prone for time-of-arrival (ToA) estimation. The designated primary synchronization sequence (PSS), defined in Humphreys et al., (2021), appears as the most promising sequence for opportunistic or cooperative navigation. The PSS, with T_{symb} duration, plays the role of a frame header occupying the complete bandwidth (including gutter), and starts with a cycle prefix followed by 8 repetitions of the same sub-sequence, the first one having inverted polarity. The PSS is identical over all OFDM frames and satellites, which will yield to an ambiguity for both pseudo-range and satellite identification for opportunistic PNT (see section 3.2.7). Two other sequences, namely the secondary synchronization sequence (SSS) and coda synchronization sequence (CSS) are OFDM symbols delimiting each frame. All three sequences show a periodicity equal to the OFDM frame. In addition to those permanent sequences, a second category of occasional sequences, having the same periodicity, seems to be transmitted "on demand" and also appears especially suitable for ranging (see Neinavaie et al., (2023)).
- The second PSP type comprises a comb of 9 tones, also called beacons, equally spaced with 44kHz apart and transmitted in the gutter. Such tones, not contaminated by any Doppler compensation, appear suited for frequency of arrival (FoA) estimation.

Regarding the comb availability, spectrograms (Blázquez-García et al., (2022)) show simultaneous reception of (at least) two combs from different satellites. However, not all satellites in view seem transmitting comb to the UT (i.e. hexa-cell it belongs to) but rather only the ascending ones. Amplitude variations of the single tones permit supposing transmission of data at a low rate. Hence, still according to Blázquez-García et al., (2022) and Iannucci et al., (2022) the tones could support network entry, possibly by offering a simpler signal and VSAT beam acquisition scheme, and by providing ancillary data to initiate the traffic. This could explain why descending satellites "leaving" the Hexa-Cell do not transmit tones, as the UT has passed network entry. As a conclusion, it is proposed to consider availability of tones for all ascending satellites seen with more than 25°, corresponding to the cut-off angle of the Starlink (see FCC, (2020)).

It is important to notice that the Starlink structure is not frozen but seems to evolve over years of operation. For example, Kozhaya et al., (2024) identified from real measurements a power reduction of the transmitted tone, and which occurred since December 2023. Despite those signal-in-space (SIS) modifications, the main signal structure and attributes are preserved which still permit applying the same signal processing techniques for both ToA or FoA estimation, despite those SIS variations. For example, Lichtenberger et al., (2024) showed after tone structure alteration that it was still possible to detect and track with a low noise block converter (LNB) a single tone out of nine.

- **Payload:**

The satellite earth panel accommodates three electronically steerable antenna (ESA) capable of simultaneously generating up to 8 beams each. According to FCC(2020), the maximal EIRP levels of every beam increases from 27.6dBW to 33dBW per 250MHz channel for an ONA varying between nadir to the end of coverage (EoC) to compensate for the larger free space losses (FSL) in slant directions. For nadir pointing, the beam with a HPBW of 2.25° projects into a circular footprint of 25km in diameter (see Blázquez-García et al., (2022)). Following the approach of terrestrial mobile networks, a geographical partitioning, also called tessellation, of the earth surface is applied, yielding to an overall number of roughly 1.3 million of hexagonal cells (hexa-cell). For slant links, the beam projection spreads in the along pointing direction and could cause inter-cell interference (ICI). To reduce ICI level, a further compensation mechanism reduces the HPBW for larger ONA (FCC (2016) and Sayin et al., (2019)). Regarding the capability, or not, to dynamically steer each beam, the time variations of the signal-to-noise ratio SNR measured from ground over a satellite pass show a train of main "lobe cuts" which permit inferring a fixed steering direction per beam (see Neinavaie et al., (2022) and Palacios et al., (2021)). Finally, illumination to the communication terminals has to be ensured from a cut-off-angle of 25°.

Aforementioned EIRP levels apply to the OFDM frame and will help estimating the received power on ground (PoG) to derive ranging performance based on synchronization sequences. Similar radiometric information is needed to support Doppler estimation from the tone processing. From Jardak et al., (2023), a range of (C/N_0) lying between 24 and 36 dB-Hz is proposed for single tones measured with an LNB. Considering a typical gain of 13dBi and a polarization mismatch loss of 3dB, yields to (C/N_0) lying between 14 and 29 dB-Hz at an isotropic and circular polarized antenna.

- **Link-Access Scheme and Channel Allocation**:

The dynamic allocation, also called orchestration, of the satellite resources, constituted of antenna beams and frequency channels to the hexa-cells is of prime importance, as it will impact link availability and quality. Two models, one for the OFDM frames (for ToA) and another for the tones (for FoA) have been developed as it seems that their orchestration differs according to satellite roles along the phase of the communication exchange (acquisition for network entry, or traffic provision).

Considering the three ESAs capable of forming up the 8 Beams, dedicated to a specific channel, yields up to 24 co-frequency beams per satellite, and a pool of roughly 105000 co-frequency beams over the complete network. Furthermore, to comply with equivalent power flux density (EPFD) limits, each cell can be illuminated by a single co-frequency beam at a time, out of the aforementioned pool (as per FCC (2016) and Sayin et al., (2019)). However, the hexa-cell can be illuminated simultaneously by different satellites in different channels Iannucci et al., (2022). Few information is however available on the frequency re-use factor (FRF), indicating the distribution of hexa-cells illuminated by co-frequency beams from the same satellite, and the FRF has been set to 3, as a working assumption (see Blázquez-García et al., (2023)). On the basis of those information an empirical and tentative orchestration model is proposed with the following rules:

- Each satellite cannot transmit to two neighboured hexa-cells with the same frequency channel (FRF=3).

• Two neighboured hexa-cells can be illuminated at the same frequency channel by two different satellites.

• A satellite cannot transmit more than 3 times the same frequency channel

• Handover to the next traffic satellite applies when the current traffic satellite reaches a 25° elevation threshold (Cakaj et al., (2021))

Based on those rules, **FIGURE 5** represents the allocation of co-frequency beams to hexa-cells lying in the vicinity of a UT (symbolized with a grey point) for a given epoch. Each number indicates the SV-ID. Eight different colours are associated to the 8 different channels. **FIGURE 5** also represents the time variations of the geometrical characteristics (elevation, range and range-rate) for the single traffic satellite illuminating the hexa-cell the UT belongs to. It indicates the change of SV-ID over time (here 5 traffic satellites over a time period of 10 minutes).
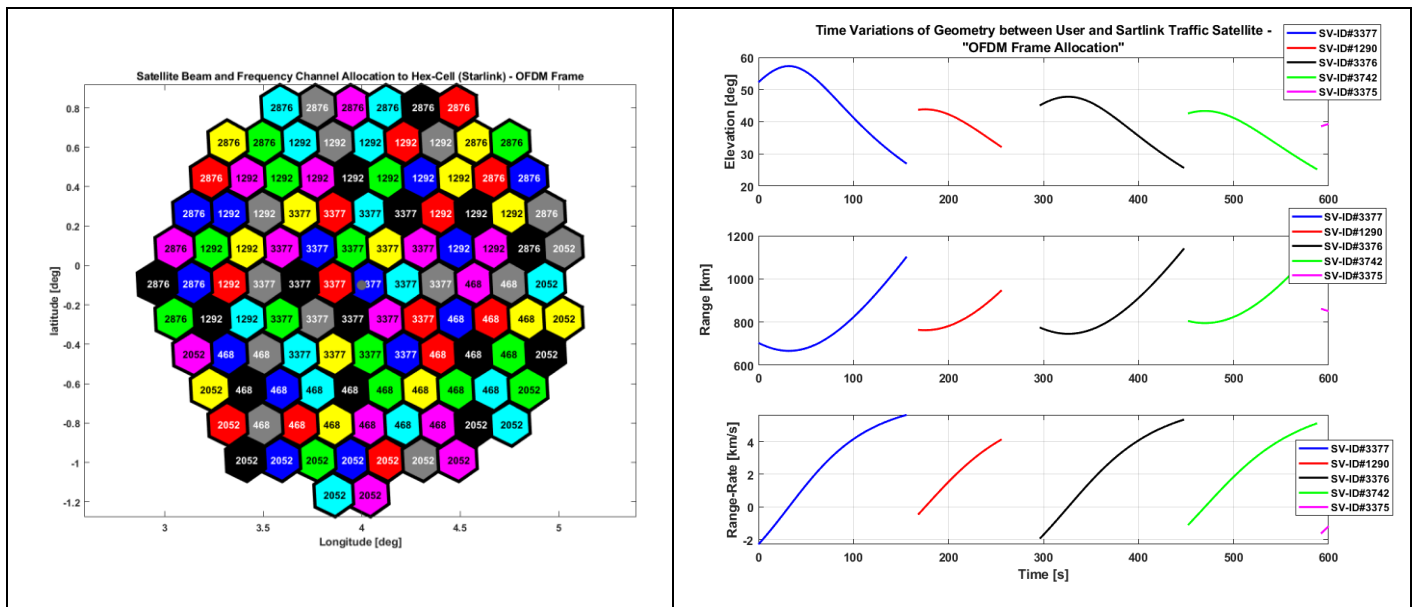

FIGURE 5: Illustrative allocation of beams to hexa-cells for OFDM signals transmitted by Starlink satellites

A similar approach has been followed for the elaboration of the orchestration model for the reception of comb of tones. The main difference resides in the satellite number, now set to two, transmitting tone combs towards the same hexa-cell (minimal value based on Blázquez-García et al., (2022)). Furthermore, prioritization to the ascending satellites from a hexa-cell perspective is given for the satellite selection. The tone transmission cessation is still maintained for a masking angle of 25°. **FIGURE 6** provides similar views on the Sat-ID illuminating each hexa-cell together with the time variations of the main geometrical parameters.

The proposed heuristic model for the resource allocation has not the pretention to exactly align to the actual allocation algorithm operated by the Starlink system. Important aspects, such that density of the subscribers, are for example not accounted. Furthermore, if a solution for the SV-beam selection algorithm can be derived to the adjacent first "rings" of hexa-cells to the UT, it is expected that no convergence is found at a more global scale. However, it is considered that the results of the selection algorithm are sufficiently representative to support SVSs, notably by generating occasional situations of neighboured cells illuminated at the same frequency channel (exploiting beam spread effect), and which could represent an enabler, as identified in Iannucci et al., (2022).
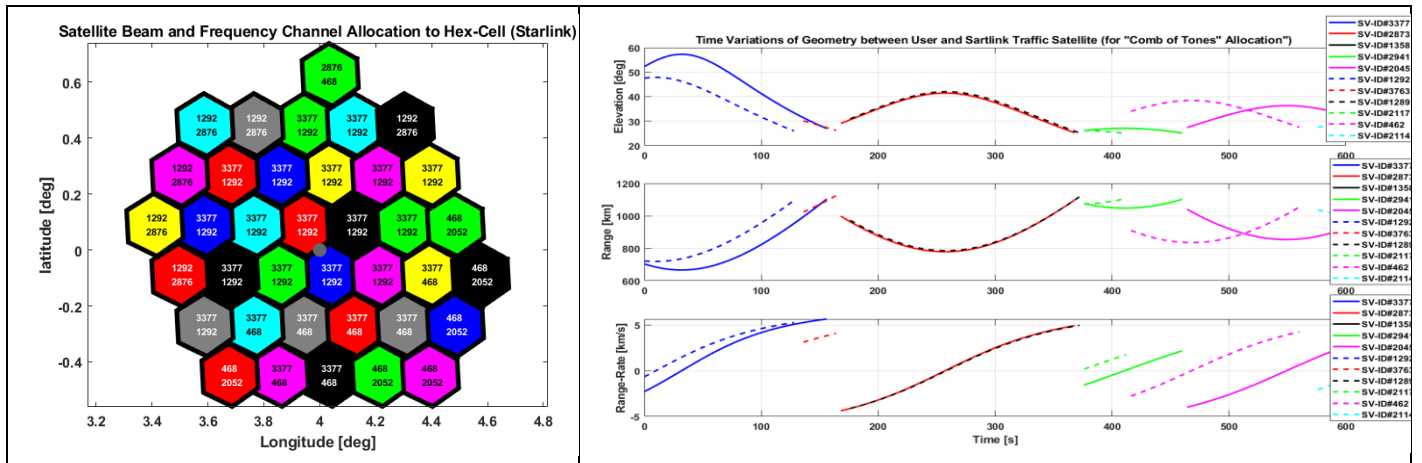
FIGURE 6: Illustrative allocation of beams to hexa-cells for the tone combs transmitted by Starlink satellites

- **Payload and System Capabilities to support PNT service:**

As stated, the transmitted signal tones seem to support the network entry, and could also offer the required position accuracy for the UT to initiate the communication exchange. However, according to Pressrelease. (2022) and Pressrelease. (2020) attempts to deny communication service with L-Band jammers located in the vicinity of the terminal still permit identifying some GNSS dependency, and thereof a non-fully standalone PNT solution (which could have been exercised with the comb of tones). Beyond the PNT needs to support the communication service, no enhanced and decoupled PNT service has been officially declared by the Starlink operator.

2.4 5G NTN and TN

The 5G standard, standing for Fifth Generation mobile network, is the successor technology to the 4G (LTE) technology for both terrestrial infrastructures (e.g. networks) and user terminals. The 3rd generation partnership project (3GPP) is the standardization body (see 3GPPPortal) in charge of defining the main physical, data link and network layers, as well as services and system aspects among others. The outcomes of this standardization activity are captured over so-called releases, published every 1-2 years, the most recent being the Release-19 (Rel-19). Besides terrestrial networks (5G TN) for communication, the 3GPP also considers non-terrestrial network (NTN), comprising uncrewed aircraft systems (UAS), high altitude platforms (HAPs) or satellites, as a mean to enhance quality of service (QoS) especially in regions without terrestrial infrastructures (white zones). Release-17 (2021) has been the first to introduce and define NTN systems. Atop the provision of communication services, the standardization could support positioning and timing services through NTN in the upcoming releases, yielding to a so-called fused communication and navigation service as existing in terrestrial networks (see Wang et al., (2020)) and expected in LEO deployments (see Wang et al., (2023) and Iannucci et al., (2022)). In the HybPNT study, a tailoring of the main NTN system building-blocks and components is applied, considering that the outcomes of this (re-) design activity shall not be too invasive in the original NTN architecture to avoid a strong impact on LEO-COM system and a reduction of the communication capacity. Several notes presenting technical specifications have been issued and provide detailed information supporting PNT capabilities for terrestrial deployments. This concerns the description of the physical layer based on orthogonal frequency division multiplexing (OFDM) and including dedicated positioning reference signals (PRS), the typical constellation topology but also the system resource allocation to the UT. In the recent years several initiatives for LEO-COM demonstrators hosting 5G NTN re-generative or transparent payloads have been launched. However, to the best knowledge of the authors, no complete LEO-COM system, implementing 5G NTN standards, is currently operational to support fused COM/NAV services. Therefore, decision was made to exploit available information originating from 3GPP framework to provide initial quantitative assessments for PNT performances based on 5G NTN systems.

- **Constellation:**

The reference constellation defined as "Set-2" in 3GPP TSG RAN (2019), with a Walker-Star topology constituted of 10 planes inclined with 87.5° and comprising each 17 Satellites at 1200 km in altitude, has been selected (see **FIGURE 8**).

• **Physical Layer:**

5G signals apply an OFDM modulation offering high spectral efficiency. Each OFDM symbol with duration T_{symb} comprises N_{sc} sub-carriers uniformly spaced within an OFDM channel, with a subcarrier spacing Δf_{sc} equal to the inverse of the symbol period to preserve orthogonality between subcarriers. N_{RB} sub-carriers constitute a resource block (RB). Each sub-carrier can be modulated with pilot or data resource elements, using for example QPSK or quadrature amplitude modulation (QAM) symbols. Sub-carriers can also be left unmodulated yielding to empty sub-carriers. The OFDM (radio) frame represents the highest hierarchical level in the OFDM layout. It is constituted of N_{sf} sub-frames each fragmented into N_s slots. Guard intervals, also called cyclic prefix, are introduced between symbols to improve immunity to multipath. Guard bands are introduced between OFDM channels for spectral isolation. The quantitative setting of the former parametrization is called numerology. As a disruptive evolution of 4G LTE standard, the 5G offers enhanced diversity and flexibility in the numerology yielding to numerous configurations.

The synchronization signal block (SSB), formed by primary and secondary synchronization signals (i.e., PSS and SSS) disclosed in the 3GPP TS 38.211 standard (and defined differently from those included in the Starlink signal structure) are used by the receiver for cell acquisition and synchronization. Those sequences are however not sufficient to support precise ranging, due to a limited bandwidth depending on the numerology. Therefore, the PRS is here introduced as a key enabler supporting ranging and positioning, and is expected to play the role of the PSP in the current study. Different candidate variants are proposed for the allocation of the PRS sub-carriers per and over the symbols. Hence, 3GPP standardisations authorise different distributions, also called PRS occasions, of the PRS symbols within the 5G signals. Two working assumptions are considered, with a sparse distribution, also called low PRS occurrence rate, corresponding to one modulated PRS symbol every 320ms, and a more frequent PRS distribution, named high PRS occurrence rate, with one PRS symbol every OFDM frame. As far as the distribution of the modulated sub-carriers for the PRS symbol are concerned, the comb-2 allocation is retained (one PRS sub-carrier every other) as per Graff et al., (2021). It is noted that besides the PRS symbols additional pilot subcarriers enable to estimate the channel state information (CSI) to figure the equalizer (see Tufvesson et al., (1997)). However, as stated in the frame of the activity focus was only given on the PRS exploitation.

Following 3GPP working assumptions, two main candidate frequency regions and associated bands are considered in this study for the 5G NTN with the FR1 in the S-Band at 2.1GHz and an overall bandwidth of 30MHz, and the FR2 comprising both the Ku at Ka-Band and with a bandwidth of 400MHz. A sub-carrier spacing of 30kHz (resp. 120kHz) was selected in FR1 (resp. FR2) and with one modulated PRS symbol among 280 (resp. 1120) symbols per radio frame of 10ms (for the high PRS occurrence rate option).

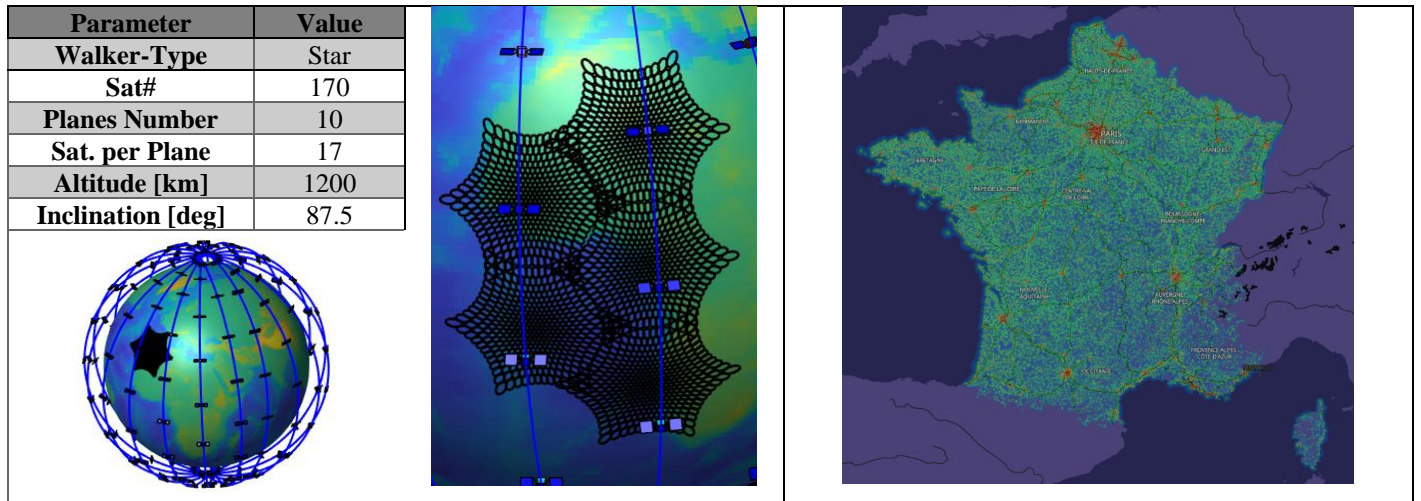| Parameter	Value
Walker-Type	Star
Sat#	170
Planes Number	10
Sat. per Plane	17
Altitude [km]	1200
Inclination [deg]	87.5

FIGURE 7: Left: Representative 5G NTN constellation and earth projection of 5 satellite beam layouts (FR2), Right: Location of 5G gNBs in France from DataGouvFR., (2024)
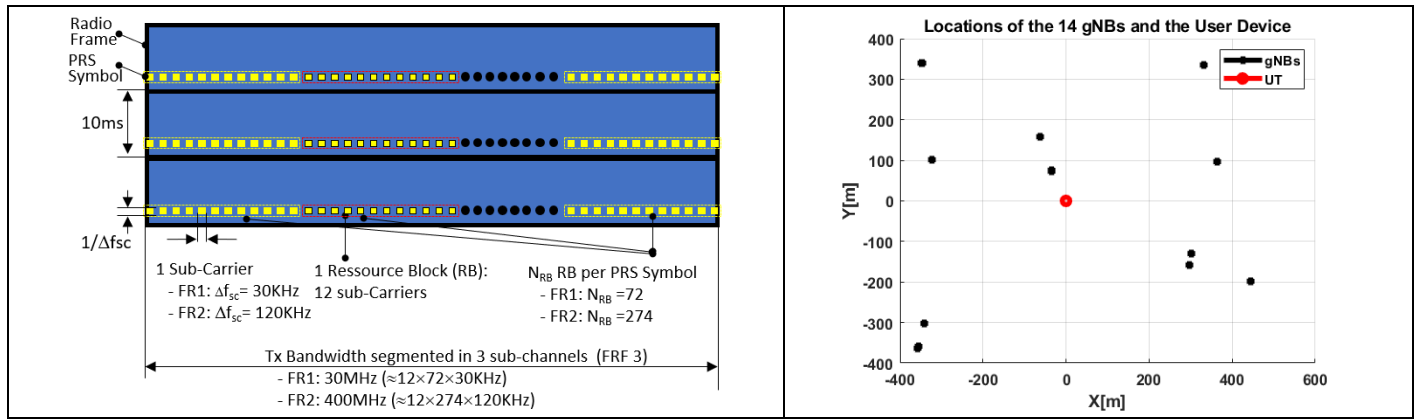
FIGURE 8: Left: 5G NTN signal Structure, Right: example of gNB distribution in Paris area from DataGouvFR., (2024)

- **Payload:**

Different Study Cases (SCs) covering different constellation topologies, carrier frequencies (S-Band or Ka-Band) and frequency re-use factor (FRF) are defined in 3GPP TSG RAN (2019) for link budget analysis. Among those different configurations explored in 3GPP TSG RAN (2019) and 3GPP TR 38.821. (2023), the ones corresponding to the SC 30 and 27 have been retained, respectively for the FR1 and FR2, to illustrate PNT capabilities. Because the current 3GPP release does not propose complete information for a Ku-Band configuration in FR2, and which might correspond to a candidate frequency plan of the future European communication system IRIS², some adaptations and scaling of the Ka-Band configurations have been applied. For example, the required EIRP levels in Ku-Band have been reduced from the Ka-Band with 5.5dB to account for the smaller space losses. Furthermore, a FRF set to 3 is applied (option 2 in 3GPP TR 38.821. (2023)), yielding to the actual available bandwidth for communication and ranging of 10MHz in S-Band and 133 MHz in Ku/Ka-Band. Finally, a regenerative payload has been proposed to facilitate implementation of a PNT service, and a fixed beam layout to the satellite frame, corresponding to the *Moving Tracking Area* option defined in 3GPP TR 38.821. (2023), has been retained.

TABLE 2 synthetises the main configuration parameters applied, as example, for the 5G NTN in FR1 (S-Band) and FR2 (Ku-Band).

TABLE 2: Retained exemplary configurations for 5G NTN in FR1 (S-Band) and FR2 (Ku-/Ka-Band)

Parameter	Value for FR1	Justification	Value for FR2	Justification
N_{beam}	91	Set-2[2]	397	Set-2[2]
HPBW	8.83°	Set-2[1]	4.4127°	Set-2[1]
Channel Bandwidth	10MHz (FRF=3)	SC 30[1]	133MHz (FRF=3)	SC 27[1]
EIRP	74dBm	SC30, End of Coverage[1]	53.2dBm in Ka-Band 48.5dBm in Ku-Band	SC27, End of Coverage[1] $20\log_{10}(20/11.7)$ reduction
Cut-Off Angle	30°	Set-2[1]	30°	Set-2[1]
Notes	(1): see 3GPP TR 38.821. (2023) (2): see 3GPP TSG RAN (2019)			

- **Additional 5G Transmitters:**

For completeness of the analyses, a terrestrial network constituted of 5G base stations, called gNB (Next Generation Node B), is also considered besides the 5G NTN transmitters. To gain representativeness, the gNB locations in the vicinity of Paris are selected from a real 5G gNB coverage map, extracted from DataGouvFR., (2024), see **FIGURE 7**. To determine the number of terrestrial ranging sources, only stations located less than 500m from the UT are retained. The high number of 5G base stations (i.e., 14 gNBs) is representative of an urban area with typical dense network deployments, as shown on **FIGURE 8**. Along the simulations the corresponding local network of 14 gNBs will "accompany" the UT for each evaluated latitude. Obstructions between gNB and UT have however not be considered (only considering favorable LoS situations).

Finally, it is also proposed to include a HAPS 5G (NTN) transmitter located at zenith of UT in the scenarios, to understand the benefit on the positioning performance and especially in the vertical direction.

For both 5G gNB TN and HAPS NTN, the assumption is made that the same signal structure is applied as the 5G NTN and the EIRP is set to ensure a received power aligned to the 3GPP study in 3GPP TSG RAN (2019), resulting in 81.3 dB-Hz in (C/N_0).

- **Payload and System Capabilities to support PNT service:**

The future adoption of PNT services in 5G/6G NTN still needs to be initiated within the 3GPP standardization, but a target of at least 50m position accuracy can be assumed as baseline. To achieve this level, one of the most elegant and efficient architectural solutions is to implement the same building blocks as a LEO-PNT payload on board the 5G NTN satellites, with a precision orbit determination (POD) unit coupled with a GNSS receiver (see section 2.5) and whose grade will depend on the target performance levels. Furthermore, the regenerative payload will ease direct dissemination of the navigation message (i.e., ephemeris and system time offset), generated on-board, in a potential upgrade of so-called System Information Block 19 (SIB-19), introduced in the Release 17.

2.5 Dedicated LEO-PNT Systems

The introduction of the commercial positioning service STL, based on the Iridium system, brought a positive impulse for the development of commercial and fully dedicated LEO-PNT systems. Several initiatives can be contemplated worldwide with the Xona and Trustpoint systems (US private Companies) or the Geely and Centispace ones (Chinese companies).

- **Payload:**

Such upcoming systems are characterized by a LEO-PNT payload offering more responsibility to the satellite for the ranging signal generation thanks to three main building blocks (BB):
- An on-board POD estimating very accurately the LEO orbit position thanks to the GNSS signals and further precise point positioning (PPP) corrections to reach decimetric or even centimetric accuracy. This receiver also enables LEO clock steering to relax long-term stability requirements, relying thus on GNSS time scale for time synchronization.
- A LEO-PNT signal generation BB in charge of producing the navigation message comprising ephemeris and clock prediction models, modulated onto the ranging signals.
- A LEO-PNT signal transmission BB comprising the analogue and digital signal conditioning, the amplification stage and the transmit antenna, as for typical GNSS systems.
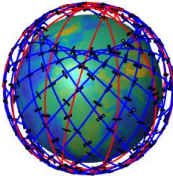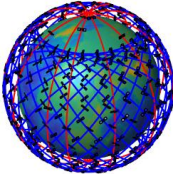
One of the main benefits of the LEO-PNT is that the monitoring, the ODTS and the navigation message generation functions, usually implemented on-ground for GNSSs, take place on-board, besides the PNT signal generation and transmission. This architectural specificity certainly impacts positively both capital and operational expenditures (Capex/Opex) of the system, facilitating thus financial viability. Even if the dedicated LEO-PNT system costs can be noticeably reduced with the implementation of a LEO-PNT payload, a (new) space infrastructure and the accompanying system operations still needs to be supported. Such encumbers do not apply for LEO-PNT initiatives building on the fused communication and navigation paradigm (see Iannucci et al., (2022)), for which a major part of the system expenditures (launch, space infrastructure, …) are already backed. Furthermore, the access to the filing needs to pass through several rounds of discussions with already-in-place GNSSs operators at ITU levels, while frequency access for the PNT service builds on the filing of the communication systems.

Another common characteristic between LEO-PNT initiatives is the application of CDMA-like signals, certainly to ensure compatibility with GNSS to facilitate UT implementation (e.g. fast PPP convergence). Nevertheless, some variants, developed in more details hereafter will still permit differentiating those LEO-PNT systems according to the main emphasize given to their mission (e.g. improved accuracy, resilience or robustness).

- **Constellation:**

In the following, choice was taken to retain the Trustpoint and Xona systems for performance evaluation considering the richness of already available publications related to those systems (see for example Anderson, (2023) for Trustpoint and Reid, (2022) for Xona). For missing information in the public domain, some working assumptions have been proposed, yielding to the appellation of "Trustpoint-like" and "Xona-like" for both systems. Their main characteristics are summarized in the **TABLE 3**.

TABLE 3: Xona-like and Trustpoint-like main characteristics

LEO-PNT	Trustpoint-like		Xona-like	
User Freq.	C-Band[1]		L-Band[2],[4] C-Band[2],[4]	
Signal Characteristics	CDMA		CDMA[4] 10MHz (L-Band)[2] 20MHz (C-Band)[2]	
Satellite#	288[1]		492[3]	
Const. Shell	1	2	1	2
Delta-Type	Delta	Star	Delta	Star
Planes Number	16	6	24	6
Sat. per Plane	15	8	18	10
Altitude [km]	1000[1]	1000	1200	1200
Inclination [deg]	50	80	60	90
Notes:	(1): From Shannon., (2022) (2): From ICG (2022) and eoPoral., (2024) (3): From Reid (2023) for final deployment phase (alt. 1200 km) (4): From ICG (2022). Discontinuous/Pulsed Transmission of CDMA signal described in Reid et al., (2023) also to support compatibility with on-board- GNSS Receiver.			

- **Physical Layer:**

Scarce information regarding the EIRP, the received PoG, or the exact signal waveforms is available, certainly to preserve confidentiality. Although one of the main argument advertising advantages of LEO-PNT w.r.t GNSS is the 20 to 30 dB higher PoG, as a consequence of the reduced space losses (see Eissfeller, B. et al., (2024)), ITU regulations might impose a limit to ensure compatibility with other systems (see ITU-R M.1831 (2015) and ITU-R M.1642 (2007)). As far as the Xona-like system is concerned, a PoG value of -136dBW in the E5-band was announced in Marathe et al., (2024) and has been applied and distributed equally to both Pilot and Data components for later analyses. For the Trustpoint-like system, operating in the C-band, still "immaculate" from GNSS, a PoG for both pilot and data components of -152 dBW (i.e. 3dB higher than GNSS) at a 0dBci circular polarised antenna has been proposed as working assumption. As for the L-Band, it is still worth mentioning that a regulatory framework has been initiated with GNSS providers in C-band (see ITU-R M.2219 (2011)) and could also be applied for the Trustpoint system. It is finally reminded that the proposed received PoGs have to be considered as working points based on available information. Those proposed values might be modified according to regulatory discussions, but their order of magnitudes (and especially compared to typically GNSS levels) can be considered as representative of the future operational LEO-PNTs.

Regarding the adopted signal waveforms, it is proposed to consider for the Trustpoint-like system operating in C-Band a BOC(5,5) standing for Binary Offset Carrier with a chip rate of 5MCps and a sub-carrier of 5.115MHz, based on an earlier study for navigation in C-band, Schmitz-Peiffer (2009), while a BPSK(2) is proposed in L-Band for the Xona-Like system. Finally, for the later quantitative analyses, it is assumed that the PRN sequences modulated with the aforementioned waveforms are continuously transmitted, as for GNSSs, (i.e. no discontinuities between PSP as for Starlink or 5G NTN).

- **Payload and System Capabilities to support PNT service:**

GNSS independency, for improved resilience, is also advertised by Xona either for the on-board ODTS exploiting inter-satellite and ground links, or for the positioning signals also broadcast in C-Band. Trustpoint promotes a fully GNSS independent solution by transmitting signals in C-Band to enhance resilience to jammers with frequency diversity.

2.6 Taxonomy of PNT Systems

Based on the former survey, a taxonomy of the PNT systems has been derived by considering two main axes of discrimination. The first one deals with the GNSS dependency either at UT or at system level. From the user perspective, alternative PNT positioning services are supported by signals transmitted in other frequencies than the GNSS L-band. Multi-tier architectures assume that the satellite ODTS is achieved with an on-board PoD function combined with a precise GNSS receiver for the production of clock and ephemeris data (CED). Full alternative PNT considers that neither the user nor the satellite position relies on GNSSs, while multi-tier GNSS considers a full dependency at both UT and system (ODTS) sides. The second discrimination axis addresses the commitments of the LEO system provider to sustain a PNT service, ranging from the pure opportunistic up to dedicated approaches. From this taxonomy several use cases (UC) presented in the **TABLE 4** have been identified:

TABLE 4: Identified use cases from the PNT system taxonomy

GNSS Dependency [1]	ODTS	Multi-Tier ODTS		Fully Alternative ODTS	
		ODTS based on PoD GNSS Rx, Navigation message production performed on board		ODTS independent of GNSS	
	UT-Link	**Multi-tier GNSS**	**Alternative PNT**	**Multi-tier GNSS**	**(Fully) Alternative PNT**
		Augmenting/Interoperable with GNSS (same Band)	Non-Interoperable with GNSS (diff. Band)	Interoperable/Compatible with GNSS (same Band)	Non-Interoperable with GNSS (diff. Band)
Operator Commitment to sustain PNT Service	Cooperative	• UC#1: dedicated LEO PNT • System : Xona-like[4]	• UC#2: dedicated LEO PNT • System: Trustpoint-like		
	Fused	N/A[2]	• UC#3: fused for tailored narrowband and broadband LEO-COM. • System: 5G NTN in FR1 and FR2		
				• UC#4: Alt-fused for tailored narrowband LEO-COM. • System: Globalstar[3]	• UC#5: Alt-fused for Tailored narrowband LEO-COM. • System: Iridium
	Opportunistic	• UC#6: non-authorised exploitation of restricted PNT Services	• UC#6: non-authorised exploitation of restricted PNT Services		• UC#7: non-cooperative SoOP on broadband LEO-COM. • System: Starlink
Notes	(1): Dependency to GNSS applies for the provision of a PNT service, and not to UT Localization required for communication service ("Network Entry"). (2): From regulatory body, no spectral overall between RNSS/RDSS and MSS in L-Band (3): Globalstar transmits in S-Band [2483.5-2500] MHz allotted for both RDSS and MSS. (4): According to Xona Patent, measured ISRs will support the integrity monitoring rather than support and independent GNSS ODTS.				

To complete this taxonomy, further definitions are then provided:

• **A PNT solution with a standalone system** is characterised by the ability to exploit the sole radio frequency (RF) signals and information of a system to determine the UT position and time under specific operational conditions (multipath and radio frequency interference (RFI) environment, dynamic, …). Standalone PNT systems or solutions will share same meaning. A UT exploiting a standalone PNT system is called a **standalone PNT UT**.

• **PNT solution with hybridised systems** is characterised by the ability to exploit the combination of two or more PNT systems to determine the UT position and time typically with improved performance w.r.t. the ones achieved with the individual standalone PNT systems. Hybridized systems or solutions will share the same meaning. A UT exploiting hybridized PNT systems is called a **hybrid PNT UT**, also called **Hybrid Navigation Terminal (HNT)**.

• **An opportunistic solution based on a PNT system** is characterised by the ability to divert the original mission of a system (typically communication), by exploiting transmitted SoOP to estimate UT position and time and without consent of the system operator. Opportunistic PNT systems or solutions share same meaning, and **SoOP** will also be abusively used here.

• **A cooperative solution based on a PNT system** is characterised by the ability to exploit additional information related to the RF signals and system, shared with consent by the system provider to permit improved estimation of UT position and time. Cooperative PNT systems or solutions share the same meaning and **Coop** will also be abusively used here.

Sensors such as barometers, inertial measurement unit (IMU) are rather considered as ancillary technologies, implemented in UT platform, but are not properly spoken as a PNT systems. Nevertheless, a standalone UT does not comprise any sensors.

Opportunistic PNT usually requires minimal information, such as two-line elements (TLE). Such information, not accessible through the SIS, are typically made available to the UT via a (terrestrial) communication channel, requiring a communication module. This interface will represent a deviation to the pure and strict definition of the standalone UT, but could also be explained by considering a concept of operation (CONOPS) where a standalone UT estimates its position and time, once disconnected, with pre-downloaded and pre-recorded TLEs. Another deviation applies for opportunistic PNT terminals which, not only estimate their own states, but also the states of the LEO satellites involved in the position solution. Here a satellite tracking and navigation (STAN) filter described in details in Kassas et al., (2024) is applied. The initiation of the STAN typically requires the accurate UT position, which can be, for example, obtained with the GNSS technology. For such UTs, the standalone opportunistic PNT will only cover the steady state phase, once GNSS is no more available (for example due to obstruction, RFI, or simply because the GNSS module has been deactivated).

Finally, in the context of the Hybrid PNT study, the analysed LEO PNT initiatives will essentially refer to space infrastructures comprising satellites transmitting RF signals to support communication or navigation services. However, an exception is made in the specific case of the 5G systems, as terrestrial network (5G TN) communication systems also completed with HAPS (5G NTN) will also be considered in addition to the 5G Non-Terrestrial Network (5G NTN).

3 HYBRID NAVIGATION TERMINAL AND ASSOCIATED PERFORMANCE

3.1 Hybrid Navigation Terminal Architecture

3.1.1 Generic Architecture

The former review highlighted a strong diversity of the LEO-COM or PNT signal characteristics (carrier frequency, signal modulation, multiple-access scheme, PSP) and protocols for the resource allocation. This richness will also be reflected into the UT architecture, the ranging and positioning processing algorithms. Despite this diversity, it is still possible to propose a generic architecture, shown on **FIGURE 9**, applicable for standalone UT and expandable for a hybrid PNT UT.
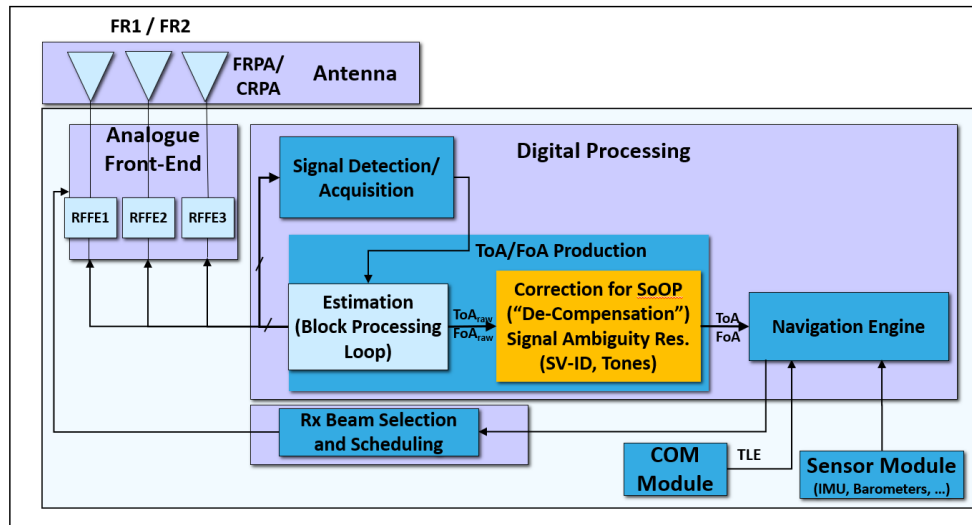

FIGURE 9: Generic architecture of a standalone and hybrid PNT user terminal

Two main categories of hybrid PNT user terminals can be distinguished:
- The first category comprises terminals only offering positioning and timing as main products. Here the analogy to multi-GNSS receivers can be proposed, extended to multi-GNSS/Dedicated LEO-PNT terminals (exploiting GNSS and dedicated LEO-PNT signals), or multi-LEO-PNT terminals (exploiting, opportunistically or cooperatively, communication signals and (dedicated) LEO-PNT signals both for unique PNT purpose). Terminals only exploiting SoOP, and whose performance have been described in Kassas et al., (2023), belong to this first category.
- The second category comprises terminals offering positioning and timing information besides the communication capability, and are called enhanced fused COM terminals (e-FCT). This corresponds to terminals exploiting 5G NTN signals for both position and communication, following the fused approach, and expandable to other communication signals (e.g. Iridium or Globalstar in FR1,

Starlink, OneWeb or Kuiper, etc.. in FR2), to enhance position performance such as observability (but without traffic). For use cases involving 5G NTN signals, this second type of terminal will be referred. One of the key constraints will be to still ensure continuous communication, besides the PNT one by exploiting SoOP and CooP signals.
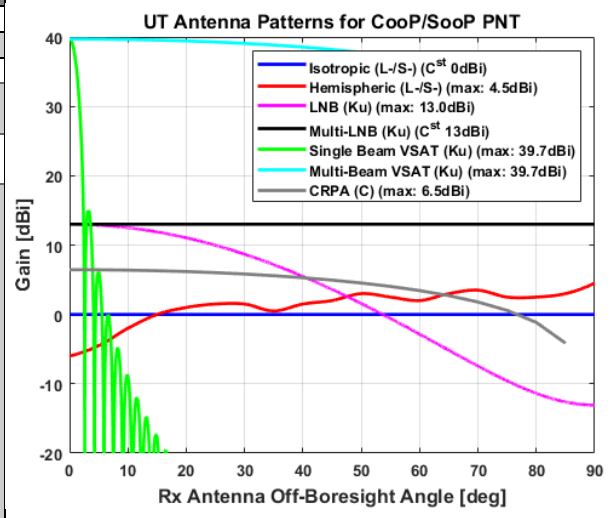
The four main building blocks highlighted in the former figure are described hereafter.

3.1.2 UT Antenna Building Block

The antenna unit transforms electromagnetic waves transmitted by the LEO satellites into an electric current with sufficient strength. It is an essential component permitting "closing the link" to satisfy minimal Signal-to-Noise Ratio (SNR). The main KPIs associated to this BB are the antenna gains, power consumption and the encumberment function of the aperture. If the directivity offered by the fixed radiation pattern antenna (FRPA) is usually sufficient in FR1, steerable dish or controlled radiation pattern antenna (CRPA) are typically applied in FR2 to ensure sufficient gain in satellite direction. CRPA technology can also be required in C-Band, as explained by Shannon, (2022). **TABLE 5** describes the typical technologies and antenna gains as function of off-boresight angle (OBA) for three main user grades. For antenna phase array technologies, such as ESA, cosine losses, are applied to compute the gain for increasing OBA.

TABLE 5: Antenna technologies proposed for the Hybrid PNT UTs

Freq. Band	Grade		
	Low	Medium	High
L-Band	Microstrip[(F)]	Microstrip[(F)]	Chock Ring[(1) (F)]
S-Band	Microstrip[(F)]	Single-Beam Array[(2)(C)]	Multi-Beam Array[(C)]
C-Band	Microstrip[(F)]	Multi-Beam Array[(4)(C)]	Multi-Beam Array[(4) (C)]
Ku-Band (SoOP)	LNB[(F)]	Multi-LNB[(6)] (M-LNB)	Multi-Beam-VSAT[(6)(C)] (MB-VSAT)
Ku-Band (Coop)	N/A	Single Beam-VSAT[(3)(D)(C)] (SB-VSAT)	Multi-Beam-VSAT[(5)(C)]
Notes:	(1): Geodetic Antenna (2): Single beam sufficient for communication (3): Mechanically steered dish (SatCom for "on the Move") or CRPA with 34.2dBi peak gain for Starlink (see FCC (2021b)), and 39.7dBi for 5G (3GPP TR 38.821. (2023)) (4): a low cost CRPA with 4 (resp. 7) elements for the medium (resp. high) grade, as per Shannon., (2022), yields to a gain of 4dBi (resp. 6.5dBi) at zenith when applying a 70% antenna efficiency. (5): Electronically steerable antenna (ESA) (6): The Multi-LNB comprises 5 LNBs assembled in a "*frustrum pyramid*" topology. Signals showing the largest received power from all 5 elements is retained for later processing. If the peak gain of an individual LNB can reach 15dBi at boresight a conservative flat value of 13dBi is considered over the full OBA span to account for OBA losses. The M-LNB permits anticipating performance achieved with a small form factor Multi-Beam-VSAT		
Legend	Legend: (F): FRPA, (C): CRPA, (D): Dish		

UT Antenna Patterns for CooP/SooP PNT

Legend:
- Isotropic (L-/S-) (C^{st} 0dBi)
- Hemispheric (L-/S-) (max: 4.5dBi)
- LNB (Ku) (max: 13.0dBi)
- Multi-LNB (Ku) (C^{st} 13dBi)
- Single Beam VSAT (Ku) (max: 39.7dBi)
- Multi-Beam VSAT (Ku) (max: 39.7dBi)
- CRPA (C) (max: 6.5dBi)

Gain [dBi] vs. Rx Antenna Off-Boresight Angle [deg]

3.1.3 Analogue Section

The analogue section, also called radio frequency front-end (RFFE), comprises the typical functions necessary for RF signal conditioning. This concerns the amplification (such as the low noise amplifier (LNA), if not part of the antenna building-block, and eventually an automatic gain control AGC), the down-conversion from RF to intermediate frequency (IF) or to baseband (BB), the filtering and finally the analogue-to-digital conversion (ADC). Each function might not appear once, but can be distributed along the analogue front-end. Hence, it is common to implement different amplification stages, interleaved with filtering and down-conversing stages, and the exact implementation meets the typical compromise between performance (noise figure, spectral excision, signal purity) and cost. As an example, a LNB converter comprises an LNA and a first (analogue) down-converter from RF-to-IF. The LNB is then followed by other amplification and down-conversion stages.

3.1.4 Digital Section

The digital section can typically be split into the high- and low-rate sub-sections.

• In a typical GNSS receiver the high-rate sub-section will take over the computationally intensive tasks, carried-out at sample rate, such as the digital down-conversion (if any), but also the processing steps specific to the LEO signal characteristics and modulation scheme. Here correlations for CDMA and fast Fourier transform (FFT) for OFDM signals can be cited.

Three functions have been identified with:
- the detection and acquisition of the PSP (see Lichtenberger et al., (2024))
- the estimation of the raw ToA and FoA either based on block processing or tracking loop techniques.
- the necessary correction of the raw ToA and FoA to produce exploitable ToA and FoA for the navigation engine, and is especially relevant in the case of LEO-COM systems. This concerns for example the wipe-off of any contamination due to Doppler or delay compensation (see Neinavaie et al., (2021)). Furthermore, as no information can be demodulated from the SIS in an opportunistic approach, some ambiguities related to the transmitting satellite identifier (Sat-ID), or the PSS identification (no PSS counter available) in the Starlink case need also to be solved. Other ambiguities such as the identification of the tone identifier out of 9 still in the Starlink case will also have to be fixed (see also section 3.2.7). If this additional function has been placed the raw ToA and FoA estimation and the navigation engine, its physical implementation can also take place within the ToA and FoA estimation or in the navigation engine modules. For example, ambiguity fixing could be implemented in the navigation engine, following some techniques developed in a GNSS context.

• The low-rate sub-section hosts operations which are carried-out at symbol rate or even lower. This concerns for example the navigation engine implementing either a weighted least square (WLS) algorithm for SPP, or a sequential filter, such as an Extended Kalman Filter (EKF).

• One trade-off especially relevant for the wideband signals (such as the one transmitted in FR2) relates to the location in the analogue or digital front-end of the channel selection. Two options are identified. The first proposes a digitization of the complete analogue bandwidth (e.g. 30 MHz for 5G NTN in FR1, 400MHz for 5G NTN in FR2, 2 GHz for Starlink) followed by a digital bandpass filtering for the channel selection. The second one carries-out channel selection with an analogue filter (e.g. 10MHz for 5G NTN in FR1, 133 MHz for 5G NTN in FR2, 250MHz for Starlink), followed by a down-conversion before ADC. The adopted strategy will have an important impact on the positioning performance and especially on the observability, and on the power consumption (see also section 6.1.1). Indeed, a digitization of the full band permits selecting several channels (corresponding to different LoS directions) separately in the digital domain, assuming the corresponding SNR is sufficient. In FR1, digitization of the complete band permits processing of different signals received simultaneously. This is also true at FR2 when considering a UT equipped with M-LNB antenna.

3.1.5 Beam Scheduler

The beam-scheduler is a function specific to the FR2 (and possibly to C-Band) and provides to the antenna BB the steering angles to be applied over time to point the antenna boresight direction towards the LEO satellite. Two situations are distinguished.
• In a cooperative context, the communication protocol informs the UT about the channel ID (among 3, FRF3) allotted to the SV-beam illuminating the UT area. This channel switching over successive SV-beams ensures optimal received power levels to permit demodulation, but also ranging performance based on the PRS processing. For a medium grade UT equipped with a SB-VSAT, observables produced by a single "traffic" SV are available at each epoch and can support synchronization, but not SPP. To improve positioning availability and performance, a high-grade UT comprises a multi-beam antenna able to form additional beams towards "non-traffic" satellites transmitted in the other channels. Considering a limited number of beams formed at UT, the algorithm selecting the SV beams among all in view satellites needs to account for figures of merit (FoM) such as optimal dilution of precision (DOP), but also hardware constraints starting with the number of frequency channels which can be simultaneously processed (atop the traffic one).
• In a non-cooperative context, the SV beam-to-channel scheduling is unknown. A high-end equipment capable to simultaneously form multiple beams towards all satellites in views, and feeding the three channels with the intention to detect the "active" beam and channel for optimal SoOP positioning could be envisaged. However, such an equipment cost might become too prohibitive, and simpler configurations based on a single or a multiple LNB feeding appear more affordable.

In both cases, not only the antenna shall consider the SV-beam directly illuminating the cell the UT belongs to, but might also have to point towards the satellites illuminating adjacent cells to exploit antenna spill-overs and to enhance thereof observability (see Iannucci et al., (2022)). For a single LNB, the achieved sensitivity in acquisition and tracking place a detrimental role to receive as many signals as possible thereby achieving low cost and high observability.

The following addresses the importance of the analogue bandwidth in combination to the antenna and digital signal processing capability. For LEO-COM systems providing traffic in different channels (e.g. up to 8 for Starlink) a UT showing a large spectral aperture can theoretically process a number of LEO-COM satellites illuminating the cell the UT belongs to, as large as the channel number (assuming an orchestration supporting multi-channel illumination to the same cell). A UT equipped with a multi-beam antenna in FR2, and combining a sufficient number of digital chains capable of processing the signals simultaneously captured, will definitively improve observability and facilitate availability of the SPP solution. This enhanced capability will obviously impact the UT cost, which might be of importance for opportunistic positioning. In the frame of the activity, an opportunistic UT processing of a single Starlink channel of 250MHz has been considered as working assumption.

It is finally noticed that the proposed HNT architecture is not only tailored to the reception and processing of LEO signals, but can also exploits GNSS LoSs, assuming that the Antenna and RFFE can receive and process L-Band signals (for example in conjunction to dedicated LEO-PNT signals).

3.2 Retained Ranging Techniques

3.2.1 Time-of-Arrival and Frequency-of-Arrival Estimation

Two main measurement categories can be extracted from the received LEO signals to support UT position estimation either based on multilateration techniques, or when hybridized with other measurement types, for example produced by sensors.

• The first category, called time-of-arrival (ToA), reflects the propagation time between the antenna phase centres of the satellite and UT. It can be estimated from the time offset, or phasing, of the PSP modulated on the transmitted signal. Alternatively, the ToA can be estimated from the carrier phase directly accessible for unmodulated signals, i.e. tones, or after PSP wipe-off (e.g. through the correlation process). Depending on the exact mission of the LEO-system, the modulated PSP for ToA estimation can take several forms. For positioning systems (GNSS, LEO-PNT), the most encountered form is a PRN sequence repeated continuously over the transmission. For communication systems, it can also take the form of PRN sequences, as for Globalstar, but the pattern can also serve signal acquisition or data frame synchronization in which case its time occurrence appears more sporadic, as for Iridium. Finally, the PRS introduced for 5G NTN is another example of PSP.

• The second category is the frequency of arrival (FoA) corresponding to a frequency offset of the nominal carrier frequency and caused by the Doppler effect due to the relative motion between satellite and UT. Besides, the Doppler also creates a contraction or dilatation of the apparent waveform modulated onto the carrier frequency, as shown in Neinavaie et al., (2021).

The knowledge of the PSP permits applying matched filter (MF) techniques which consists in correlating the received signal with a (noise-free) replica built with the pattern. MF approach is known to offer better ToA estimation accuracy w.r.t. other blind ranging techniques, more agnostic w.r.t. the transmitted signal features. One can cite time difference of arrival (TDoA) techniques, also used in RFI localization and which consist in correlating the received signal captured at a first user platform with the received signal captured at a second reference platform, and serving as "noisy" replica. Thereof, in the current work, the prerequisite on an a-priori PSP knowledge is assumed to support the MF techniques.

The exact MF implementation approach for ToA estimation will depend on the repetitiveness of the pattern within the received signal, but also on the UT grade and especially on its power consumption regime. Here two main techniques can be distinguished.

• Block processing or snapshot ranging techniques aim at estimating the ToA with a single signal snapshot. Such techniques are typically applied for signals comprising intermittently the pattern, in which case a detection step needs to precede the estimation one, as the snapshot might not contain the complete pattern (Lichtenberger et al., (2024)). Those techniques offer a more precise time tagging of the ToA measurements, and are also more power consumption-friendly, for those devices asking for longer autonomy. Finally, specific block processing techniques such as FFT typically used for OFDM data demodulation, can also be adopted for ToA estimation to simplify implementation of the position capability besides the communication one.

• Tracking loops techniques help refining the ToA estimation by continuously processing the received signals. One of the most encountered implementations is the delay locked loop (DLL) which has been extensively applied for ToA estimation of the CDMA signals transmitted by GNSS satellites. The generic architecture implementing such a technique comprises three main blocks with a discriminator producing an output proportional to tracking error, a filter which helps sustaining link dynamic and finally a numerically control oscillator (NCO) for the shifted replica generation. This ToA estimation technique is now further extended to other signal types such as OFDM (Graff et al., (2024) for 4G-LTE). Alternative implementations replace the loop

filter with a Kalman filter (see Won et al. 2012) which essentially differentiates in the variable Kalman gain, contrarily to the fixed loop filter coefficients.

If block processing techniques could theoretically also be envisaged to extract ToA information from the carrier phase, the most encountered implementation relies on tracking loops, and especially phase locked loops (PLL), widely applied for PPP and real-time kinematic (RTK) GNSS applications.

As far as the FoA estimation is concerned, FFT-based techniques represent the most usual implementations for the block processing option, while frequency locked loop (FLL) or PLL are the most common for the tracking loop option. FLL or PLL can be directly fed with the unmodulated tones, or with the output of the matched filter used for ToA estimation, in which case post-correlation FoA appellation is applied.

The following sub-sections identify and describe the most encountered techniques in the literature for ToA or FoA estimations applied to the signals transmitted by the four main LEO system categories, either for SoOP or Coop PNT.

3.2.2 Iridium

The more than 25 years of Iridium system exploitation and signal transmission, definitively supported numerous research groups to explore opportunistic positioning, a shown hereafter. A first inspection of Iridium signal attributes with a small bandwidth per channel, and the presence of tones preceding each burst, and directly accessible, favours application of FoA rather than ToA techniques for opportunistic positioning. Furthermore, due to the sporadic but periodic reception of the broadcast bursts in the simplex channels (alert ring, paging), block processing techniques are preferred when compared to tracking loop ones for Doppler estimation. Finally, if not fully excluded, exploitation of duplex bursts appears less appealing due to stronger traffic dependency, and reduced steadiness. Typical Doppler extraction techniques from Iridium signals, apply a two-step approach starting with a coarse determination with FFT (see Lichtenberger et al., (2024)), followed by a finer maximum likelihood estimation (MLE) (see the work of Tan et al., (2019)). Further works propose to enhance Doppler estimation by processing the residual phase after estimated (fine) frequency wipe-off (see Huang et al., (2022)), or by exploiting so-called implicit pilots as part of the data chunk of the burst (see Wie et al., (2020)), or by extending coherent integration interval (CPI) by demodulating the QPSK data serving as "flying" replica to access the tone (see Leng et al., (2015)). Finally, still with the intention to exploit the complete burst duration, the work performed by Orabi et al., (2021) and Tan et al., (2020) raises the snapshot signal at a power M (corresponding to M-PSK burst modulation), to suppress modulated data. The capability to apply tracking loop techniques, as proposed in Farhangian et al., (2013) to further improve the Doppler estimation accuracy highly depends on the burst revisit time. This one can be as large as 4.32s for single beam/simplex channel reception (as shown in Leng et al., (2015) and Orabi et al., (2021)), and can be reduced with the reception of signal transmitted by adjacent beams, or from multiple simplex channels. Besides FoA, Leng et al., (2015) also proposes extracting a ToA observable by applying the demodulated QPSK data as replica to exploit the 31.5KHz bandwidth. It is worthwhile noting that the commercial service, satellite time and location (STL), also exploits ToA obtained from the simplex burst (see DecodeSystem. (2017)).

3.2.3 Globalstar

Despite contemporaneity of the Iridium and Globalstar systems, opportunistic exploitation of signals transmitted by the later one seems less fruitful, which could be explained by the following reasons. The absence of unmodulated tones in the signal structure prevents direct FoA positioning techniques. Rather, ToA and post-correlation FoA, both estimated from the pilot CDMA channel, appears more suited. Two main hurdles however hinder direct application of pseudo-range (PR) estimation techniques currently applied in GNSS. Firstly, the PRN sequences (or parameters permitting their generation) are not publicly available, issue which can be overwhelmed with adequate reverse engineering techniques also supported with signal captures from high-directive antennas. Secondly, the bent-pipe nature of the Globalstar forward link coupled with the delay and Doppler compensation, introduces inconsistencies between the measured code and carrier Doppler. If the corresponding compensations can be estimated and subtracted from the apparent delay and Doppler, the corresponding residuals will contribute to the user ranging error. In Neinavaie et al., (2021), the capability to estimate the actual down-link Doppler causing the compression or dilatation of the modulated chip is demonstrated, with the further possibility to deduce the Doppler compensation law, based on a hybridized PLL and DLL architecture, yielding to an average PR error of 100m.

3.2.4 Starlink Signals

Processing techniques applied to Starlink signals for observable extraction combine both FoA estimation exploiting tones, and/or ToA and post-correlation FoA estimation with the synchronization sequence processing. They represent, in a way, a synthetize of ToA and FoA estimation techniques applied to the Iridium and Globalstar systems. Some differences are still worth mentioning:

• Contrarily to Iridium tones, Starlink tones are transmitted continuously, which will obviously favour FLL or PLL techniques.

• As far as the permanent and occasional sequence are concerned, first attempts to track the corresponding signals with delay lock loop (DLL) fail when exploiting only permanent sequences, while DLL keeps tracking once impermanent are present, see Neinavaie et al., (2023). In the current work, it is however proposed to consider that both types of permanent and occasional sequences can be processed for ToA production, for example by considering that a scheme is developed in the "SoOP correction" module (**FIGURE 9**). Thereof, the following analyses assume full exploitation of the PSS to benefit of the large Gabor bandwidth.

3.2.5 5G NTN

Contrarily to aforementioned systems, the exploitation of 5G/6G signals and especially the PRS shall support cooperative PNT services. The implications are the availability and accessibility of information regarding PRS transmission (SV-beam to Channel orchestration, applied numerology etc…), but also the provision of satellite ephemeris and clock information, for example derived from an on-board PoD receiver, as part of an upgrade of the SIB-19 or another dedicated PNT message. Both ToA and FoA observables obtained from PRS processing will feed the UT navigation engine. Decision regarding block processing or tracking loop estimation techniques will essentially depend on the PRS repetition rate. For the low PRS rate, block processing techniques are more suited, while a high PRS rate would favour application of tracking loop techniques. Finally, it is recalled that only PRS modulated symbols are exploited but no other PSP candidates such as PSS, SSS and pilot sub-carriers.

3.2.6 Dedicated LEO-PNT Systems

Considering the main mission requirement to ensure compatibility and interoperability between GNSS and LEO-PNT systems, both transmitting CDMA signals, tracking loop techniques are proposed as the most suited solutions to estimate ToA with DLL and post-correlation FoA with PLL or FLL.

3.2.7 Ambiguity resolution for opportunistic signal processing

Raw ToA and FoA extracted from SoOP might be affected by ambiguities which materialised at different levels.

• In the Starlink case, this ambiguity appears thrice. Considering the comb of tones, the probability to detect, and lock on all 9 tones simultaneously is minimal (see Jardak et al., (2023)), especially because they rarely show similar power (as a consequence of the possible amplitude modulation). Considering that only a sub-set of FoA derived from tones is obtained (in the minimal situation, only one tone is tracked), results in an ambiguity related to the tone identifier. In case the UT tracks the same tone ID among all received satellites, will yield to an error in the user clock frequency estimation. However, in case the tracked tone IDs are different among received satellites, this non-consistency will propagate into a positioning error. The ToA derived from the PSS will also suffer from an ambiguity of T_{OFDM} (e.q. ~400km) as no PSS counter permits identifying the frame in an opportunistic way and thereof its absolute transmission time (expressed in the Starlink time scale). It is noted that this second ambiguity shares strong analogies with the pseudo-range ambiguity encountered in snapshot GNSS positioning, and similar solutions could be proposed to solve it (for example with the introduction of the time of transmission, see **APPENDIX A.1**). The last ambiguity is related to the satellite identifier, SV-ID, as the same PSS is transmitted over the constellation. Combining the information of TLEs associated to the SV-ID and the estimated Doppler represents an efficient candidate method to solve this ambiguity.

• In the Globalstar case, this ambiguity applies to the spreading sequences which, as for the Starlink PSS, cannot be distinguished.

In the following, working assumption is made that the aforementioned ambiguities have been solved as part of the "Correction for SoOP" function, so that absolute and unambiguous ToA or FoA are fed to the position engine.

3.2.8 Summary

Based on the former assessments, **TABLE 6** synthetises, for each PNT system, the retained ToA and FoA estimation techniques applied to the related PSP.

TABLE 6: Summary of proposed signal processing techniques for ToA / FoA estimation

PNT System	Positioning Signal Pattern	Purpose	Observable Type	Signal Processing Technique
Iridium	Tone (Burst header)	Signal Acquisition	FoA	Block Processing (FFT, MLE)
	Unique Code (Burst Header)	Signal Acquisition and Frame Sync.	ToA	Block Processing (MLE)
Globalstar	Pilot Channel	Signal Acquisition, Phase Estimation	ToA	Adapted DLL[1]
Starlink	PSS, SSS	Frame Sync	ToA	DLL
	PSS, SSS	Frame Sync	FoA	Post-PSS Correlation FLL/PLL[1]
	Tones	Signal/Beam Acquisition	FoA	FLL/PLL
5G NTN	PRS (Low Occurrence Rate)	Ranging	ToA	Block Processing
	PRS (Low Occurrence Rate)	Ranging	FoA	Block Processing
	PRS (High Occurrence Rate)	Ranging	ToA	DLL
	PRS (High Occurrence Rate)	Ranging	FoA	Post-PRS Correlation FLL/PLL[1]
Trustpoint / Xona-Like	PRN sequence	Ranging	ToA	DLL
	PRN sequence	Ranging	FoA	Post-PRN Correlation FLL/PLL
Notes:	(1) The FLL/PLL is fed with the matched filter output for optimal ToA estimation exploiting PSS (Starlink) or PRS (5G NTN) (2) The "contamination" of the forward link Doppler compensation into down-link signal prevents direct exploitation of down-link FoA. The accuracy of the down-link FoA estimated from the Doppler stretch is not provided in Neinavaie et al., (2021). (3) See Neinavaie et al., (2021) for the tailored DLL/PLL architecture			

3.3 Retained Positioning Techniques for standalone positioning

For standalone positioning performance a WLS positioning algorithm, widely exercised for SPP with GNSS, has been retained and is described in **APPENDIX A.1**. The motivation for the WLS selection for a moving UT is to identify the limitations of each PNT system, and especially when considering observability conditions imposed by the generalized position equation, but also to propose mitigations taken at system and UT level to partially reduce such limitations.

3.4 Main Performance and associated Key Performance Indicators

Different categories of KPI can be identified and are evaluated with SVS campaign.

 • The first encompasses KPIs related to the single link. It comprises the link-budget KPIs including the received PSP power (also considering that the PSP component might be transmitted simultaneously with other non-PSP components) and the (C/N_0) applicable to the PSP, called $(C/N_0)_{PSP}$. The accuracy levels for the ToA and FoA are also important, together with the ToA or FoA availability during a specific window, considering that those estimators will fail for $(C/N_0)_{PSP}$ levels below a $(C/N_0)_{PSP,th}$ thresholds which is signal processing dependent. The difference between the actual $(C/N_0)_{PSP}$ and $(C/N_0)_{PSP,th}$ is defined as a robustness margin applicable at link level against intentional or non-intentional RFI, but also against additional power attenuations due to obstacles.

 • The second one encompasses KPIs related to the geometry. This concerns the number of visible satellites or lines-of-sight (LoS), but also the number of exploitable LoS, as not all visible (communication) satellites actually transmit signals to the UT. Another well-spread KPI at the fringe between geometry and position category is the DOP based on ToA (see Equation (4)) or FoA (Doppler DOP, see Equation (6)) either expressed in the vertical, horizontal, isotropic (3D) directions, or for Timing.

 • The third one encompasses KPIs representative to the position and timing performance, which are derived when combining DOP (resp. DDOP) and ToA (resp. FoA) accuracy. Here as well, position performance is declined in the vertical, horizontal, isotropic (3D) directions, or for timing. Those KPIs will be completed with the availability of the position solution. Another useful KPI is derived from the difference between the actual number of exploited satellites, and the minimal number of satellite necessary to solve the position equation, $(N_{sat,min,obs})$ (see **APPENDIX A.1**). This observability margin informs about the number of LoSs which could be lost, for example due to obstructions or RFI, but still ensure an acceptable position solution even degraded. In that sense it is representative of the robustness of the PNT system in the position domain.

4 SVS FRAMEWORK

4.1 Supporting SVS Tool

As stated in the introduction, PNT performance will be assessed with two runs of SVS campaigns. For this purpose, a tailored version of the Airbus **LEON-Tool** has been applied, and is depicted on **FIGURE 10**. This figure firstly shows the standard modules in charge of the satellite orbit and link geometry generation, the link budget calculation and the ranging accuracy and position accuracy, as for any legacy "σ×DOP" analyses. Atop those legacy modules, another specific module is required to support the studied use cases. This one called orchestration module models the resource allocations to the UT or more precisely the cell it belongs to. Typical resources for LEO-COM satellites comprise the SV-beams and channels which have been described for the Starlink, 3GPP NTN, Iridium and Globalstar systems. Examples of the output for this module are shown on **FIGURE 5** and **FIGURE 6** in the case of Starlink. Other more minor adaptations w.r.t. standard SVS tools concern the inclusion of the FoA measurements, the extension of the design matrix and finally the ability to process PSP which are not transmitted continuously.
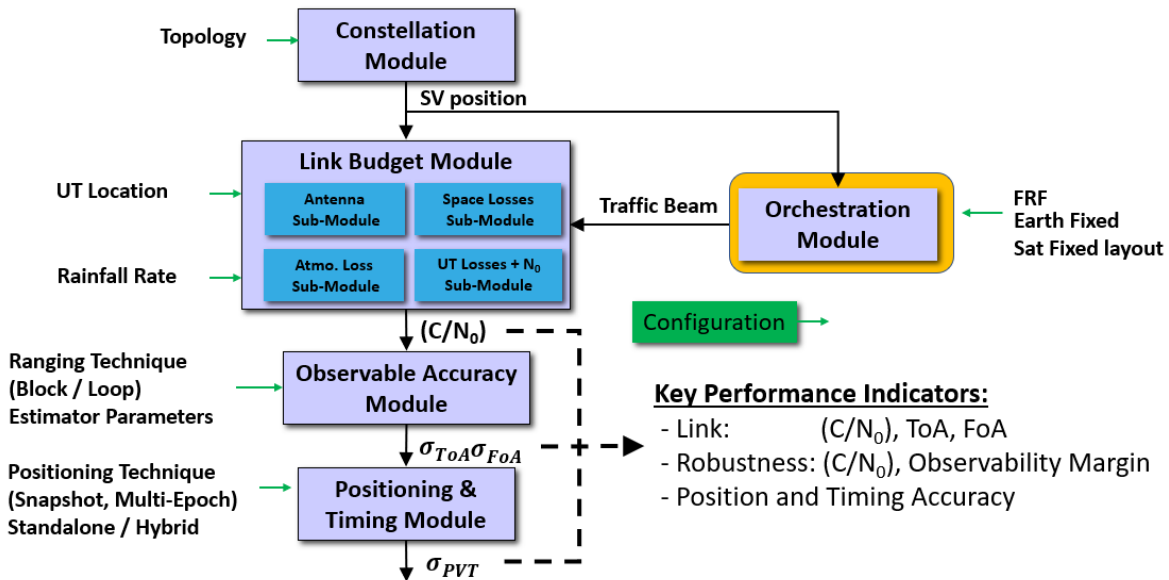

FIGURE 10: System Volume Simulation Frame Work

The following working assumptions have been applied for the SVS campaigns conducted in this work:

• The thermal noise is considered as the main contribution to the measurement error, considering that it firstly drives the (ranging) link availability, and also informs about the minimal achievable PNT performance, as all other error sources (such as propagation channel, radio frequency interference environment or satellite orbit and clock corrections) can only worsen PNT accuracy and availability. Inclusion of other contributions in the user equivalent range (UERE) and user equivalent range rate (UERRE) budget are foreseen in later works.

• Furthermore, it is considered that the signal acquisition and initialisation of the positioning filter have already taken place. In the case of opportunistic PNT, the STAN approach could be for example cited. Therefore PNT performance are evaluated in a steady-state mode.

• As explained in section 3.3, a SPP filter will be applied in the navigation engine. No sequential positioning filter also fed with measurements from sensors (IMU, barometers) is considered. It is still noticed that the application of a sequential filter (EKF) combining IMU measurements and ToA/FoA observables is an efficient technique to palliate for the non-simultaneously of ToA/FoA measurements over time (relevant for the Starlink SB-VSAT or Iridium use cases). Furthermore, initialization of the EKF solution with sparse ToA/FoA derived from LEO satellites, and IMU might still represent a challenge for moving platforms.

From the SVS, KPI addressing accuracy performance, robustness and resilience at link and position solution levels, and defined in section 3.4, have been extracted.

4.2 Generic Configuration

In the section 5, configurations related to the signal processing and beam exploitation and suitable to each LEO-PNT initiative evaluated in a standalone way will be discussed. Nevertheless, generic configuration parameters are transverse to the different standalone or hybridized scenarios. Those ones are summarized in the following **TABLE 7**

TABLE 7: Generic Parameters for SVS campaign

Parameter	Value	Comment	Reference
User Latitude	• 10° • 30° • 45°	• Flat rural • European peri-urban • Deep urban	**Inline (2018)**
User Masking Angle	• 0° • 30° • 45°	• Most severe atmospheric losses • Most populated latitude • Averaged latitude for US, European and south China	
Simulation Time	• 10mn • 20mn	• "Snapshot" duration offering sufficient readability of curves • Period providing representative geometry for SVS campaign	
Simulation Step	• 4 seconds • 1 second • 1 second	• Simulations without IMU hybridization • Simulations involving Starlink system • Simulations with IMU hybridization	

In order to better illustrate and justify SPP performance, so-called snapshot simulations will show the time variations of the main KPIs over a 10-minute interval. Statistics (min, median and maximum of individual KPIs) are then derived with more systematic SVSs covering a longer time period (20mn), and are available in **APPENDIX A.4**.

5   PERFORMANCE EVALUATION FOR STANDALONE SYSTEMS

This section presents the results for the different steps leading to the SPP performance and for the standalone PNT use cases. This concerns the link budget analysis conducted in section 5.1, the evaluation of the range and range-rate accuracies presented in section 5.2, the visibility analyses proposed in section 5.3, the SPP performance shown in section 5.4 and finally the gap analyses presented in section 5.5.

5.1 Link Budget Analyses

User link budget analyses are now derived for the aforementioned systems to evaluate the $(C/N_0)_{PSP}$. **TABLE 8** provides the main link budget contributions for a UT at 30° in latitude. For the Starlink system, the link budget exercise is carried-out for both OFDM and tone signals, and for three main UT grades, essentially distinguishing with the antenna technology. For the other systems a low UT grade is usually considered. The $(C/N_0)_{PSP}$ determination does not account for the PSP duty cycle, v_{PSP} (see Equation (14)), which is ranging technique dependent (loop processing), but only considers the losses to extract the power allocated to PSP component from the other data components (e.g. Globalstar or LEO-PNT case). Finally, no RFI is considered for the power spectral density, N_0.

TABLE 8: Snapshot link budget comparison for different LEO-PNT initiatives and for a user at 30° in latitude

UT-Grade (Antenna)	Starlink OFDM Frame[3]			Starlink Tone Comb[3][6]			Iridium	Globalstar	Trustpoint-like	Xona-like	5G NTN (FR1)	5G NTN (FR2)
	LNB	M-LNB	SB-VSAT	LNB	M-LNB	SB-VSAT	Omni.	Omni.	CRPA (7 el^{ts})	Isotrop.	Isotrop.	SB-VSAT
f_{carr} [GHz]	11.325	11.325	11.325	11.325	11.325	11.325	1.610	2.491	5,020	1.2	2.19	11.325
OFA [deg]	27,6	27,6	27,6	27,6	27,6	27,6	56,8	28,73	41,6	27,3	31,07	30,92
OBA_{Tx} [deg]	0,5	0,5	0,5	0,5	0,5	0,5	11,9	11,16	41,6	27,3	1,06	2,00
EIRP [dBW]	28,2	28,2	28,2	-5,5	-5,5	-5,5	19,4	16,36	18,1	21,4[7]	41,02	12,97
Range [km]	626,9	626,9	626,9	626,9	626,9	626,9	1728,5	1660,53	1433,8	1386,4	1452,59	1449,70
FSL [dB]	169,5	169,5	169,5	169,5	169,5	169,5	161,3	164,78	169,6	156,9	162,50	176,75
Rain Att.[9] [dB]	0,9	0,9	0,9	0,9	0,9	0,9	0,0	0,00	0,0	0,0	0,10[4]	0,50[4]
Gaz Abs.[9] [dB]	0,1	0,1	0,1	0,1	0,1	0,1	0,1	0,04	0,1	0,0	-	-
Scintillation[9] [dB]	0,3	0,3	0,3	0,3	0,3	0,3	0,3	0,13	0,3	0,1	2,20	0,30
Shadowing [dB]	N/A	N/A	N/A	N/A	N/A	N/A	N/A	N/A	N/A	N/A	3[1]	0,00[1]
Elev. [deg]	60,0	60,0	60,0	60,0	60,0	60,0	20,1	54,08	39,8	57,0	52,18	52,37
OBA_{Rx}[8] [deg]	30,0	30,0	0,0	30,0	30,0	0,0	20,1	54,08	0	57,0	52,18	0,00
Rx Gain [dBi]	7,7	12,0	34,2	7,7	12,0	34,2	0,0	0,00	4,5	0,0	0,00	39,70
Pol. Loss. [dB]	3,0	3,0	0,0	3,0	3,0	0,0	0,0	0,00	0,0	0,0	0,00	0,00
Rx Power [dB]	-137,8	-133,5	-108,3	-171,5	-167,2	-142,0	-142,3	-148,60	-147,4	-135,6	-126,78	-124,89
Proc. Loss. dB	3,0	3,0	3,0	3,0	3,0	3,0	2,0	23,07[2]	5,0[2]	5,0[2]	0,00	0,00
N_0 [dBW/Hz]	-203,0	-203,0	-203,0	-203,0	-203,0	-203,0	-201,6[5]	-202,86	-203,0	-203,0	-196,98	-204,76
$(C/N_0)_{PSP}$ [dB-Hz]	62,2	66,5	91,7	28,5	32,8	58,0	57,3	31,19	50,6	62,4	70,19	79,87

Notes
(1): Shadowing considered as additional contribution in 3GPP
(2): Comprises 3dB (Trustpoint/Xona-Like) and $10\log_{10}(128) \approx 21$dB (Globalstar) of Pilot/Data extraction losses atop 2dB digital processing losses
(3): Two distinct link budgets are applied for Starlink OFDM frames and tone combs.
(4): Atmospheric (rain and Gaz) losses are combined and fixed according to 3GPP TR 38.821. (2023)
(5): According to Gaffney et al., (1994)
(6): Applies for a single tone (among 9)
(7): E5-Band link budget according to Marathe et al., (2024)
(8): For FRPA (LNB, hemispheric and isotropic antenna), but also M-LNB (as constant gain), the OBA_{Rx} is referenced to Zenith direction. For CRPA and SB-VSAT the OBA_{Rx} is null (assuming no pointing error).
(9): Except for the 3GPP case where rain attenuation and Gaz absorption are provided in the link budgets from standardizations, ITU-models described in **APPENDIX A.2** are applied to evaluate the contribution of the atmospheric losses.

The former table highlights that the received $(C/N_0)_{PSP}$ of broadband LEO-COM systems significantly exceeds the ones of the GNSSs, which optimistically culminates at around 50 dB-Hz, considering a PoG of -155dBW, a noise floor of -203dB-Hz, a maximal receiver antenna gain of 4dBi and 2dB of processing losses. It also dominates the $(C/N_0)_{PSP}$ levels of the dedicated LEO-PNT systems, even if in the Xona-like case, those ones still benefit from a larger advertised PoG. The $(C/N_0)_{PSP}$ range for the Iridium system, 50 to 60dB-Hz, also matches the one of the dedicated LEO-PNT systems, while in the Globalstar case, the ~21dB of pilot extraction losses penalize the achieved $(C/N_0)_{PSP}$ levels. It is noted that the relatively low $(C/N_0)_{PSP}$ levels in the Globalstar case are obtained due to the uniform power reparation between all 128 channels. However a power imbalance advantaging the pilot component could improve situation. It is finally interesting to note that in the Starlink OFDM case, even for a UT equipped with a M-LNB antenna offering moderate directivity, the $(C/N_0)_{PSP}$ reaches 60dB-Hz, and which appears sufficient for ToA or FoA estimation.

To complete the former tabulated snapshot link budgets, **FIGURE 11** represents the time variations of $(C/N_0)_{PSP}$ for both 5G NTN and Starlink systems operating in Ku-Band, and for a UT at 30° in latitude applying different SoOP or CooP configurations. Sensitivity analyses focussing on the way to improve the observability margin with the inclusion of additional LoSs obtained either with alternative SV-beam activation schemes, or with antenna spill-overs are also conducted.

FIGURE 11 (left) firstly highlights the $(C/N_0)_{PSP}$ variations for the 5G NTN "traffic" satellites with ID 40, 41, 56 and 57, for a UT equipped either with a SB-VSAT (e.g. parabolic dish), or with a MB-VSAT (e.g. ESA). Furthermore, the model for the SV-beam pattern is either limited to the main lobe or also comprises all secondary lobes of the Bessel function (3GPP TR 38.821. (2023)). The figure shows that the $(C/N_0)_{PSP}$ is stable over the successive traffic satellites transmitting through the main lobe, and with similar orders of magnitude for both SB and MB-VSAT. The difference of roughly 2dB resides in the application of cosine losses for the MB-VSAT and increasing with lower elevations. Concentrating on Sat-ID 57 during the 2nd to 5th minutes, ripples are observed and correspond to the successive "cuts" of the main lobe for each beam over the 12 rings. After handover to Sat-ID 40, the $(C/N_0)_{PSP}$ for the Sat-ID 57, now observed with an elevation lower than the cut-off-angle of 30°, experiences an abrupt collapse for the SB-VSAT due to the large OBA_{Rx} between both satellite directions, while it reduces gradually for 1 or 2 more minutes of 10dB for the MB-

VSAT, as this one can further "pursue" with an additional receiver beam the transmitting main beam after handover. The MB-VSAT later scans the following secondary lobes of the beam pattern mainly belonging to the 12th ring. This example shows that even after handover from one to another traffic satellite, the passing one could still continue transmitting PRS symbols to the UT through the main (non-traffic) lobe for enhanced PNT availability and performance, assuming orchestration and actual traffic authorise it. A similar principle applies for the transmission of PRS symbols before handover. This example also illustrates that a proper design of an extended beam antenna pattern could further permit prolonging PRS availability to the UT with an appreciable $(C/N_0)_{PSP}$ thanks to the secondary lobes. From UT perspective, only a dual or multiple beam antenna permits simultaneous reception of the traffic signal without discontinuity, and of the PRS symbols belonging to signals received from non-traffic SV-beams and transmitted in other channels than the traffic satellite.

FIGURE 11 (right) represents the $(C/N_0)_{PSP}$ variations of the received Starlink signals (OFDM frames) for a UT equipped with a SB-VSAT, a MB-VSAT or a M-LNB antenna (each colour corresponds to a different Sat-ID). As working assumption the UT only exploits opportunistically beam illuminations in a single channel (no multi-channel), highlighted with the blue colour on **FIGURE 5**. Three scenarios for the Starlink signals reception are considered with, the sole reception of the traffic satellite beam illuminating the hexa-cell collocating the UT, or the additional reception of the spillovers from other satellite beams illuminating one of the first ring of 6 adjacent hexa-cells, or the further additional reception of other satellite beam spillovers illuminating the second ring of 12 further adjacent hexa-cells (see **FIGURE 5**). It is still noted that, those results have been obtained with an adaptation of the HPBW in the along pointing direction necessary to avoid ICI, according to (FCC (2016)) description. Similar ripples corresponding to the successive beam handovers from the same satellite are observed. For the SB-VSAT (dotted line), only the traffic satellite illuminating the hexa-cell collocating the UT is observed. The $(C/N_0)_{PSP}$ decreases over the satellite pass due to larger atmospheric losses for lower elevations. For the MB-VSAT (plain line), the additional cosine losses amplify this $(C/N_0)_{PSP}$ decrease over the satellite pass. As anticipated from **TABLE 8**, the $(C/N_0)_{PSP}$ for OFDM frames and obtained with the SB or MB-VSAT reaches 90dB-Hz. This high value applies to the complete OFDM frame, and shall be reduced with $10\log_{10}(T_{symb}/T_{OFDM})$ when accounting for the PSP duty cycle for DLL-based ToA or post correlation FLL-based FoA estimation (see Equations (9) and (13)). The MB-VSAT scenario also permits identifying with different linewidths the additional received signals originating from the illuminated adjacent cells. In particular, the $(C/N_0)_{PSP}$ coming from the 1st ring (resp. 2nd ring) of illuminated adjacent cells is roughly 10 dB lower (resp. 30dB), on average. Furthermore, the furthest the illuminated cells, the larger the $(C/N_0)_{PSP}$ dynamic, property which will impact the capability to keep lock for loop processing techniques. Comparing the $(C/N_0)_{PSP}$ levels with the ones of 5G NTN FR2, it can be verified that they are about 10dB larger. The atmospheric losses (rain attenuation and Gaz absorption) derived from ITU models, applied for the Starlink, are indeed still mild at 30° in latitude. For an equatorial user, atmospheric losses would become more severe (~10dB), which is shown with SVS campaign (see **FIGURE 21**), while still kept constant to a fraction of dB according to 3GPP TR 38.821., (2023).

Similar statements can be made when applying a Multi-LNB, now observing $(C/N_0)_{PSP}$ levels roughly 25dB lower due to the lower directivity (only the illumination to the collocating hexa-cell is shown here). Similar observations (not shown on **FIGURE 11**) can be made for the tone combs, with the main difference that two satellites (see **FIGURE 6**) now illuminate the collocating hexa-cell and a ~30dB lower $(C/N_0)_{PSP}$ levels are obtained as consequence of the lower transmit power.

For both Ku-Band systems, a legacy commercial communication terminal equipped with a SB-VSAT, would only perceive illuminations from the traffic satellite to the collocating hexa-cell, while a terminal equipped with a dual beam would only point towards the next traffic satellite for handover, so not suffering from ICI caused by adjacent cell illuminations. Therefore, the former $(C/N_0)_{PSP}$ assessments, and especially the capability to exploit spill-overs is specific to a tailored communication and PNT terminal, called e-FCT, equipped with a dual or MB-VSAT pointing to the "non-traffic" SV-beams for cooperative PNT, or to any "active" SV-beam for opportunistic PNT. In the subsequent quantitative assessments, the following conservative assumptions have been applied w.r.t exploitation of the spillovers:
   • For the Starlink system, illuminations to the collocating hexa-cell and to the first ring of adjacent cells have been considered.
   • For 5G NTN, only the main beam and the first secondary lobes (achievable with proper antenna design) are considered.

Finally, it is worth insisting that in an opportunistic context, exploitation of communication signals can be achieved only under the obvious and mandatory condition that communication traffic is demanded by the subscribers belonging to the cell the (PNT) UT belongs to, or their adjacent cells (case of OFDM for Starlink, but not for the tones combs supporting network entry).
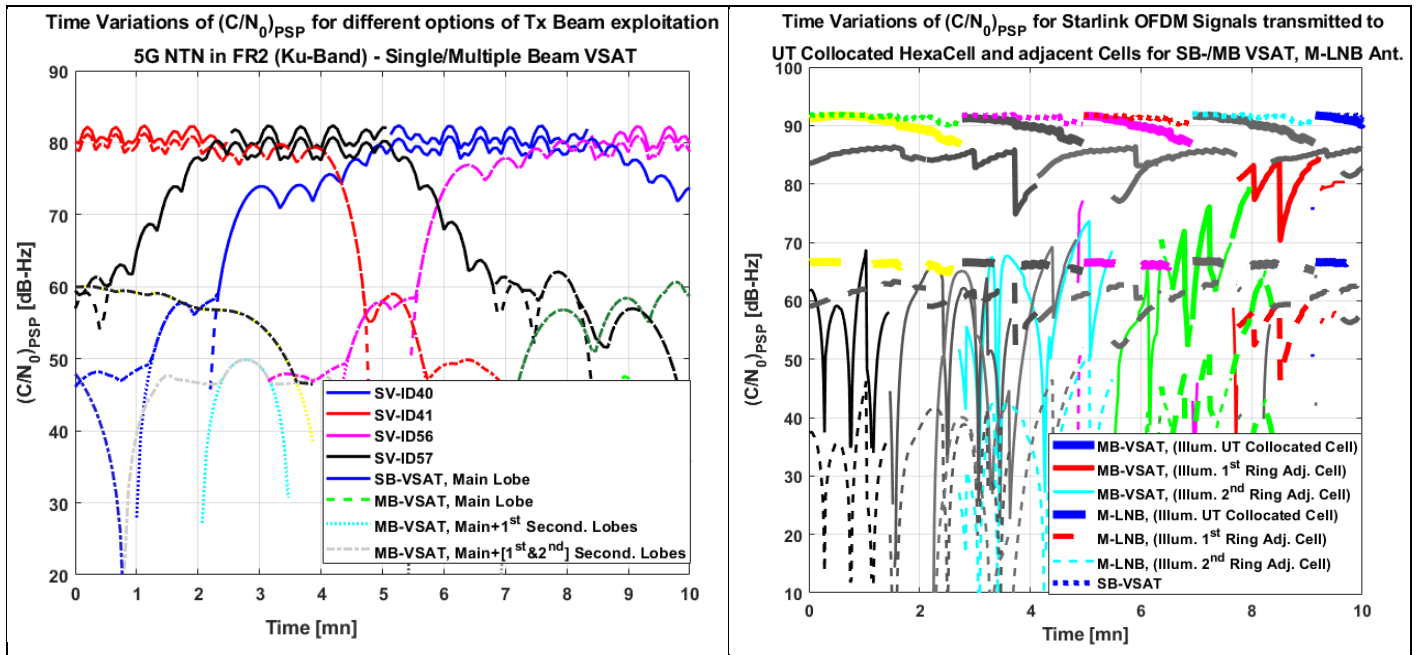
FIGURE 11: Time variations of the $(C/N_0)_{PSP}$. Left: 5G NTN in Ku-band – Right: Starlink– UT at 30° in latitude, 10° in UMA

FIGURE 12 represents the $(C/N_0)_{PSP}$ for the systems operating in FR1 (L-/S-Band). In all cases, the UT is equipped with a low directive antenna (isotropic or hemispherical). Starting with the 5G NTN scenario, it is shown that the $(C/N_0)_{PSP}$ with low directive antenna reaches maxima levels around 70 dB-Hz, 10 dB below the ones achieved for a MB-VSAT antenna in FR2. For some epochs, PRS originating from 2 to 3 satellites can be received, assuming that orchestration still ensures transmission through the main and first secondary lobes, before or after handover. The $(C/N_0)_{PSP}$ for the Iridium simplex signals range between 50 and 60dB-Hz, while the ones for the Globalstar vary between 20 and 33dB-Hz (due to the pilot extraction losses) which is close to the values given in Rabinowitz et al., (1998). Regarding the LEO-PNT scenario, $(C/N_0)_{PSP}$ levels range between 44 and 52dB-Hz for a Trustpoint-like system (assuming a UT equipped with a CRPA composed of 7 elements), yielding to a link margin of ~19dB for a tracking threshold $(C/N_0)_{PSP,Thr}$ set to 25dB-Hz, see section 5.2, for example to mitigate RFIs. The $(C/N_0)_{PSP}$ levels range between 60 and 66 dB-Hz for a Xona-like system, yielding to a larger link margin of ~35dB. The difference of ~14dB can be attributed to the relatively high PoG levels announced by Xona, in Marathe et al., (2024).
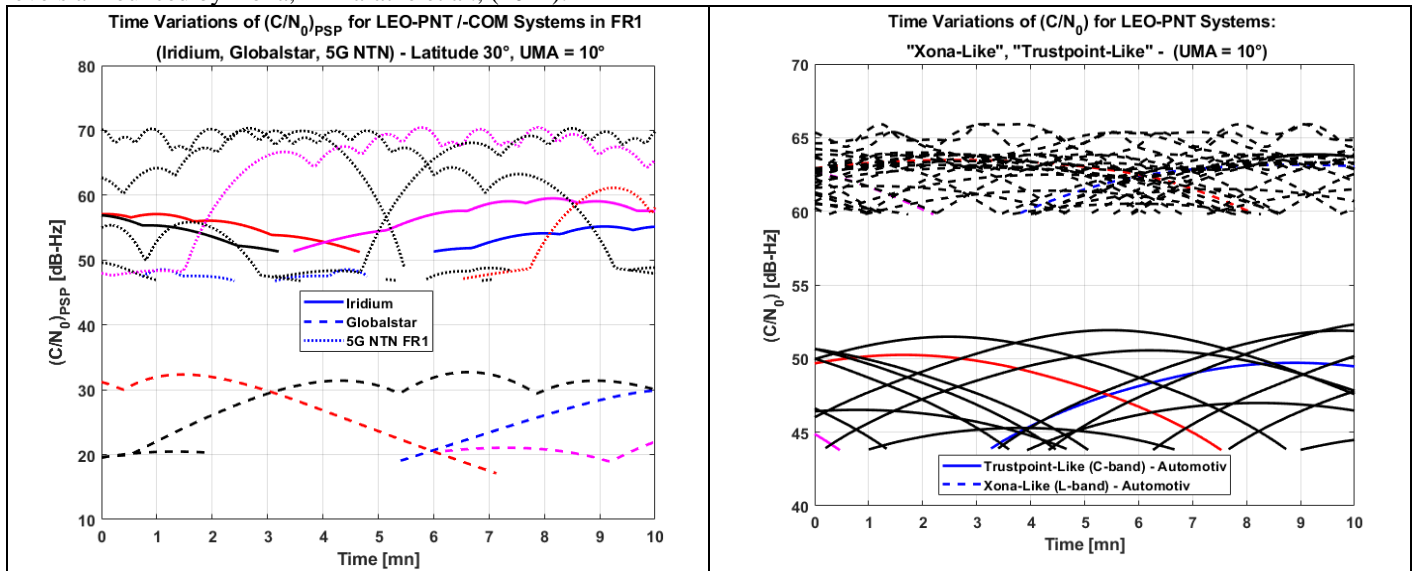

FIGURE 12: Time Variations of the $(C/N_0)_{PSP}$ for Iridium, Globalstar and 5G NTN in FR1 (left) or Dedicated LEO-PNT, Trustpoint/Xona- Like (right) – UT at 30° in latitude, 10° in UMA

5.2 Ranging Performance Analyses

In **APPENDIX A.3**, the closed-form expressions for the ToA and FoA estimation accuracy, either based on tracking loops or block processing techniques have been provided. **TABLE 9** summarises the parameter setting, for the retained expressions for each of the different LEO-PNT initiatives, according to **TABLE 6**. This setting is derived and justified from references having demonstrated ToA and FoA estimations based on real signals.

TABLE 9: Signal processing configurations for ToA and FoA estimation with tracking loop or block processing techniques

| Signal Processing Technique	Loop Processing						Block Processing			
	DLL				FLL		MLE for ToA		MLE for FoA	
	ν_{PSP}	ELS [Chip]	B_{DLL}[Hz]	T_{int} [ms]	B_{FLL}[Hz]	T_{int}[ms]	f_{samp}[Ksps]	T_{int}[ms]	f_{samp}[Ksps]	T_{int}[ms]
Starlink (OFDM)	0.33%[4]	1[1]	1[2]	20[3]	10[1]	20[3]	N/A	N/A	2.5E3	20
Starlink (Tone)	N/A	N/A	N/A	N/A	10[1]	10[1]	N/A[7]	N/A[7]	N/A[7]	N/A[7]
Iridium	N/A	0.5[1]	1[2]	4[5]	10	4[5]	41.667	4[5]	41.667	4[5]
Globalstar	N/A	0.5[1]	1[2]	10[2]	10[1]	10[1]	N/A[7]	N/A[7]	N/A[7]	N/A[7]
5G NTN FR1	1/280[4]	0.5[1]	1[2]	10[2]	10[1]	10[1]	30E3[8]	T_{symb}=10/280[6]	30E3	T_{symb}=10/280[6]
5G NTN FR2	1/1120[4]	1[1]	1[2]	10[2]	10[1]	10[1]	400E3[8]	T_{symb}=10/1120[6]	400E3	T_{symb}=10/1120[6]
Xona-Like	N/A	0.5[1]	1	20	10	20	N/A[7]	N/A[7]	N/A[7]	N/A[7]
Trustpoint-Like	N/A	0.1[1]	1	20	10	20	N/A[7]	N/A[7]	N/A[7]	N/A[7]
Notes:	(1): For very wideband signals (Ku-band), an ELS set to one equivalent chip is sufficient to ensure satisfactory ToA performance, also to not penalize the sampling frequency. For lower band signals (FR1), a smaller ELS of half an equivalent chip is applied. Exception is made for Trustpoint-like for which a narrow ELS is required for a BOC(5,5). (2): A B_{DLL} is set to 0.5Hz in Neinavaie et al., (2021) for Globalstar (at 1400km). It is proposed to consider a slightly more conservative value B_{DLL}=1Hz. This larger value is applied to all DLLs for LEO tracking, also considering lower orbits and thus higher dynamic. (3): The setting proposed in Jardak et al., (2023) for the PLL and FLL tracking the tones have been reused for the FLL fed with "post-PSS correlation" tone, considering that the loop bandwidth and coherent integration time are essentially driven by link dynamic. (4): Starlink case: corresponds to T_{Symb}/T_{OFDM}, 5G NTN/TN case: corresponds to PRS "density" per radio frame (5): Extended coherent time of 4ms exploits unique word and part of simplex data, after decoding (Huang et al., (2022)) or with implicit Pilot (see Wie et al., (2020)) (6): From 3GPP, one frame comprises 280 (resp. 1120) symbols with 30kHz (resp. 120 kHz) sub-carrier spacing in FR1 (resp. FR2) (7): For signal received continuously (dedicated LEO-PNT, Globalstar, Starlink's tone) loop processing techniques are applied. (8): Assumes digitization over the complete communication bandwidth (i.e. not reduced to sub-channel)									

To account for the sensitivity of the ToA or FoA estimator, a lower limit for $(C/N_0)_{PSP}$ depending on the adopted processing technique has been set. For tracking loop techniques a hard threshold of 25dB-Hz has been applied to the effective $(C/N_0)_{eff}$ (defined by Equation (14)) considering that the probability of loss of lock (LoL) cannot be neglected below this value (based on GNSS receiver experiments). For block processing techniques, a lower limit of 2dB is set conservatively to the SNR_{PSP} defined by Equation (15).This lower limit is derived from Zhang et al., (2024) which shows the applicability interval of the Cramer-Rao Lower Bound (CRLB) as function of SNR. **TABLE 10** synthesises the threshold applicable to the $(C/N_0)_{PSP}$ for the studied LEO-PNT systems

TABLE 10: Sensitivity threshold for loop and block processing techniques

Signal Processing Technique	Loop Processing			Block Processing		
	ν_{PSP}[%]	$(C/N_0)_{eff,Thr}$ [dB-Hz]	$(C/N_0)_{PSP,Thr}$ [dB-Hz]	T_{PSP} [ms]	$SNR_{PSP,Thr}$[dB]	$(C/N_0)_{PSP,Thr}$ [dB-Hz]
Starlink (OFDM)+	0.33%	25	49.7	4.4 10^-3	2	55.5
Starlink (Tone)	100%	25	25	N/A[1]	N/A[1]	N/A[1]
Iridium	N/A	25	25	2.56	2	27
Globalstar	100%	25	25	N/A[1]	N/A[1]	N/A[1]
5G NTN FR1	1/280	25	49.5	10/280	2	46.5
5G NTN FR2	1/1120	25	55	10/1120	2	52.5
Xona-Like	100%	25	25	N/A[1]	N/A[1]	N/A[1]
Trustpoint-Like	100%	25	25	N/A[7]	N/A[7]	N/A[7]
Notes	(1): For signal received continuously (dedicated LEO-PNT, Globalstar, Starlink's tone) loop processing techniques are applied.					

The former table highlights that for each signal type and LEO-PNT initiative, the tracking threshold, $(C/N_0)_{PSP,Thr}$, can differ with up to 5 dB between both loop or block processing techniques.

From the derived $(C/N_0)_{PSP}$, the corresponding ToA and FoA accuracies estimated for the different benchmarked PNT systems are depicted on **FIGURE 13**. The upper left part shows the estimation performance for both 5G NTN scenarios in FR1 and FR2, when considering either low PRS occurrence rate (asking for block processing techniques) or high PRS occurrence rate (applying loops) and for a UT equipped with an isotropic antenna in FR1 and a MB-VSAT in FR2. The upper right part shows performance for both Starlink OFDM and tones, both processed with loops, for a UT equipped either with a MB-VSAT or M-LNB antenna. The lower part shows estimation performance for both Iridium and Globalstar systems on the left, and on the right part equivalent curves for the dedicated LEO-PNT systems.
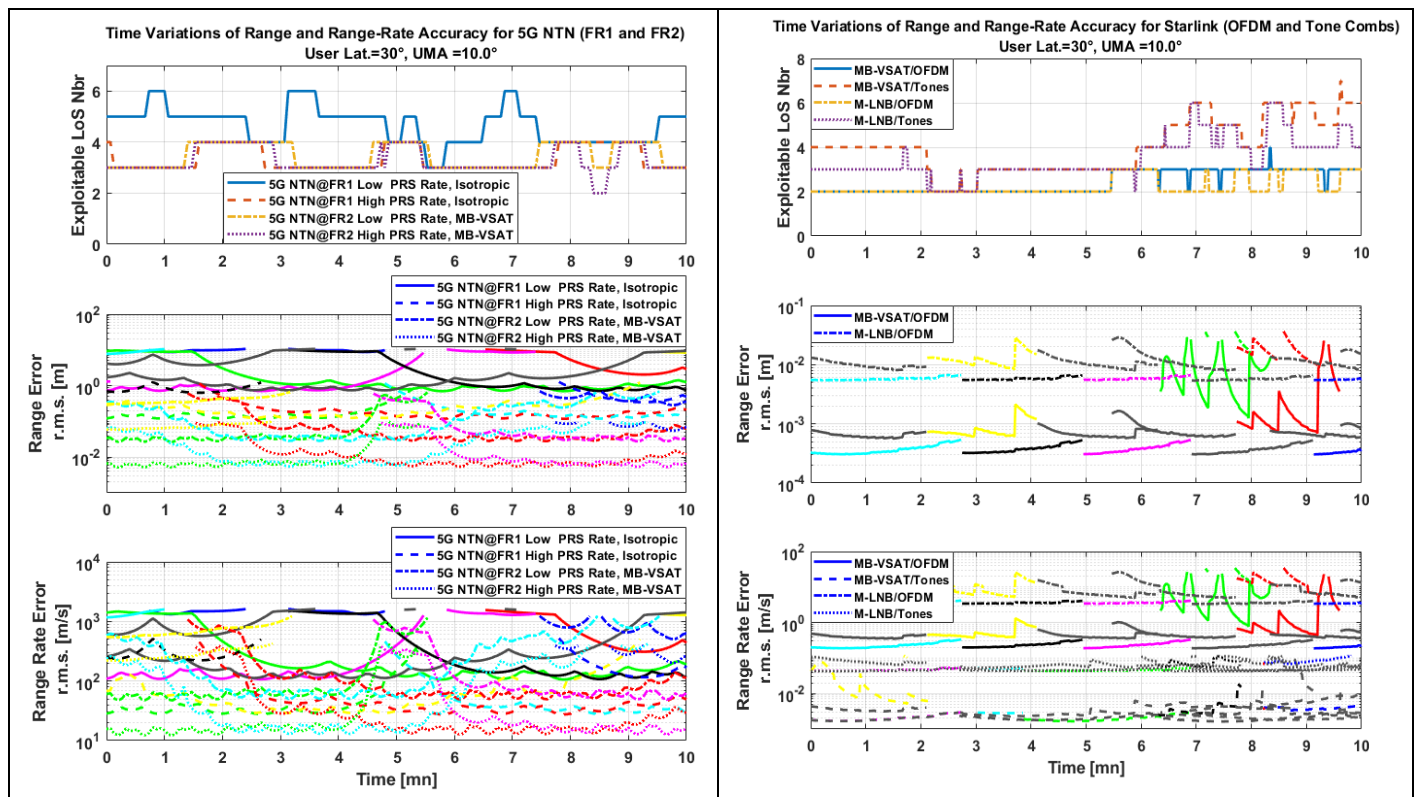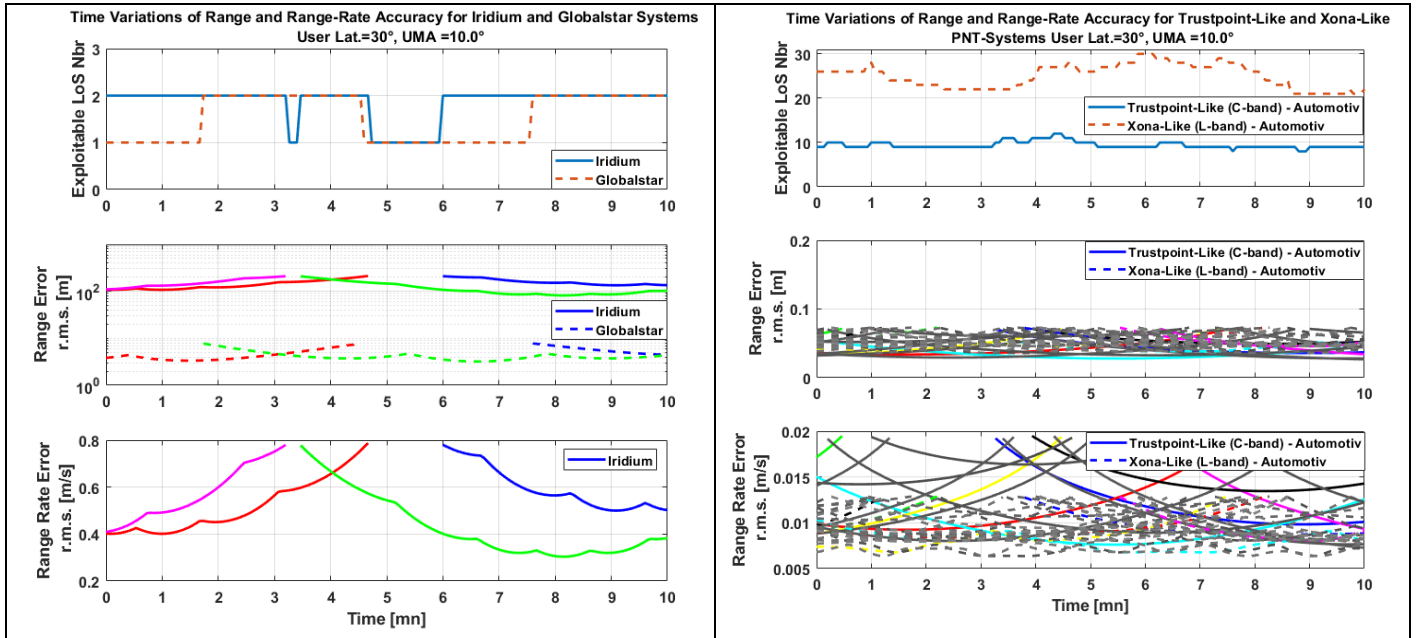
FIGURE 13: ToA and FoA accuracy. Upper Left: 5G NTN, Upper Right: Starlink, Lower Left: Globalstar, Iridium, Lower Right: Xona-Like, Trustpoint-Like – UT at 30° in latitude, 10° in UMA

Following outcomes can be proposed:

• For the 5G NTN technology, ToA accuracy is typically at sub-meter level, even when exploiting the main and secondary lobes of the passing or future traffic satellites. Exception applies for ToA derived with block processing techniques for 5G NTN at FR1 in which case ToA accuracy lies at 10m level. FoA accuracy is at 10m/s (resp. 100m/s) level for 5G NTN in FR1 (resp. FR2) when applying loop techniques. Closer analyses for this relatively weak performance (typical range-rate levels are below 1m/s for continuously received signals, see Lehtinen (2002)), show that the presence of the PSP duty cycle, ν_{PSP}, upfront the coherent integration time T_{int} in the CRLB Equation (13) degrades the FoA accuracy. The FoA accuracy obtained with block processing techniques (for low PRS rate) become one or two orders of magnitude even worse, especially at FR1 penalized by the lower carrier frequency. Generally, application of an antenna capable of exploiting all received communication signals (omnidirectional in FR1, MB-VSAT in FR2) permits providing measurements from 3 or more satellites to the positioning module. It is worthwhile noticing that applying a $(C/N_0)_{PSP,Thr}$ of 49.5dB-Hz (loop proc.) instead of 46.5 (block proc.) can yield rejecting 1 or 2 exploitable LoSs for the 5G NTN in FR1 use case. This can be visually verified from **FIGURE 12**.

• For Starlink transmitting PSP OFDM frames the ranging performance levels are outperforming the ones of the 5G NTN in FR2, as a consequence of the larger $(C/N_0)_{PSP}$ for the same antenna technology and higher PSP duty cycle. Exploitation of signals from illuminations to adjacent cells also appears promising for enhanced positioning availability and performance. It is recalled that those very promising ToA performance assume full exploitation of PSS without the burden identified in Neinavaie et al., (2023), and which still need to be resolved in the "Correction for SoOP" function depicted on **FIGURE 9**. As for 5G NTN, the FoA accuracy obtained with the post-PSS correlation is penalized by the non-continuously transmitted PSS. However, the FoA accuracy corresponding to the continuous tone exploitation reaches sub-meter per seconds levels which appears prone to support Doppler positioning (both with UT equipped with MB-VSAT or M-LNB).

• For Iridium and Globalstar scenario, the number of exploitable LoSs per system lies between 1 and 2 as a direct consequence of the relatively low number satellites populating the big LEO constellations, and satellite communication CONOPS (2 satellites required for traffic handover). Ranging performance are around 100m for Iridium (due to the low bandwidth). The ranging performance lying between 5 and 10m for Globalstar is one order of magnitude better than the ones reported in Neinavaie et al., (2021), also applying a $(C/N_0)_{PSP}$ in the same range. A reasonable explanation for the discrepancy is related to the tailored DLL/PLL architecture necessary to strip-off the Doppler compensation, while the closed-form expression used for Globalstar ToA performance are based on a more standard GNSS receiver architecture.

• For the dedicated LEO-PNT system (Xona-like, Trustpoint-like), the ranging performance are outstanding (decimetre), certainly explained by the combination of loop processing techniques, to continuously received ranging signals at a high $(C/N_0)_{PSP}$. Furthermore, the large number of exploitable LoSs per constellation permits direct implementation of SPP algorithms. Finally, it is worthwhile noticing that the 14dB of higher (C/N_0) between the Xona and Trustpoint-like systems does not reflect in the ranging performance. The main reason is the smaller Gabor bandwidth of the Xona-like waveform when compared to the Truspoint-like one (see Equation (10)).

5.3 Visibility Performance

In a GNSS context, the satellite visibility is usually the first quantitative KPI used to anticipate early positioning and timing performance, as any visible GNSS LoS is exploitable for positioning (with exception of cyphered GNSS signals). In an opportunistic or fused PNT context, this principle has to be revised as only a part or even a small fraction of the visible LoSs can actually participate to the UT position, the most striking example being provided by Starlink. More particularly, two conditions have to be met beyond the simple "optical access" above a specific UMA: the first one obviously requests that the satellite transmits (communication) signals directly to the UT or in its vicinity (e.g. adjacent cells), and the second one asks for sufficient $(C/N_0)_{PSP}$ to ensure detection and ToA/FoA estimation. As a matter of fact, as KPI, the number of exploitable LoSs supersedes the simple satellite visibility, and this KPI becomes signal processing dependent, as the $(C/N_0)_{PSP,Thr}$ threshold might not be identical for tracking loop techniques or block processing ones (see **TABLE 10**). This (new) KPI is compared to the minimal number of required LoS ($N_{Sat,min,obs}$) to solve the SPP equation, and introduced in **APPENDIX A.1**, providing thus insight onto the observability margin. It is depicted in all figures showing ranging but also positioning performance (also on the so-called KPI board in **APPENDIX A.4**).

5.4 Positioning Performance Analyses for Standalone UT with SVS

5.4.1 Identification of the most promising Standalone PNT scenarios

APPENDIX A.1 presents the generalized position equation developed for SPP algorithms fed with different combinations of ToA and/or FoA either for standalone or hybridized PNT systems and exploited either in a cooperative or an opportunistic way. Furthermore, **TABLE 15** synthetised the minimum number of satellites ($N_{Sat,min,obs}$) providing each ToA, FoA or both, to permit solving position equation. **TABLE 11** presents the list of candidate standalone PNT scenarios for moving platforms which will be down-selected based on the quantitative assessments regarding the first link KPIs ($(C/N_0)_{PSP}$, range and range-rate estimation performance, number of exploitable LoSs).

TABLE 11: Suitability of different PNT systems for standalone SPP for moving UT

LEO-System	Coop/ SoOP	UT Config. (Antenna /Channel)	Standalone SPP Suitability	Comment
Iridium	SoOP	Hemispheric	• Poor/Medium	• 2 Satellites in view for 8°, 1 for UMA > 20° • Medium/Low ToA Accuracy[4] • Long Inter-Simplex illumination interval, 4.32s (no simultaneous ring alert Illumination)[5]
Globalstar	SoOP	Hemispheric	• Poor	• Only ToA proposed due to Doppler compensation contamination (no FoA)
5G NTN FR1	Coop	Hemispheric	• Medium/Good	• Orchestration dependent (PRS transmission before/after handover) • Tx antenna design required to ensure stability of secondary lobe with azimuth
5G NTN FR2	Coop	SB-VSAT	• None	• No SB switch to "non-traffic" satellites possible to preserve traffic continuity
		MB-VSAT	• Medium/Good	• Orchestration dependent (PRS transmission before/after handover) • Tx antenna design required to ensure stability of secondary lobe with azimuth
Starlink	SoOP	SB-VSAT[1] Mono/Multi-Channel	• None (OFDM/Tone)	• SB-VSAT switch does not authorize simultaneous ToA/FoA measurements. Re-synchronization of measurements required with EKF, asking for UT velocity model.

		MB-LNB Mono-Channel	• Poor/Medium[2] for OFDM-PSS	• PSS: Depends on Spillovers from adjacent cells
			• Poor/Medium for Tones	• At least twice more FoA derived from tones (but no ToA) • Strongly dependent of (C/N_0)[3]
		MB-LNB Multi-Channel[2]	• Good (OFDM-PSS/Tones)	• Illumination from other satellites in different (250MHz) channels[2] improves observability (simultaneous ToA/FoA) but strongly impact (SoOP) PNT terminal costs.
LEO-PNT	Coop	Hemi, Low CRPA	• Very High	• LEO-PNT System Design for Standalone PNT
Notes	(1): Starlink: For SoOP, high-rate SB switch to satellite possible as no traffic (continuity constraint is not applicable) (2): Starlink: OFDM Frame (PSS) strongly dependent on Traffic (3): Starlink: Observed decrease of Tone (C/N_0) in 2024 might jeopardize SooP with Tones (Lichtenberger et al., (2024)) (4): Iridium: ToA accuracy limited by small (31KHz) simplex bandwidth. (5): Iridium: FoA/ToA measurements availability can however be improved with 1) Exploitation of additional simplex channels illumination from same satellite, 2) spill over from adjacent beams, 3) exploitation of Header Burst from Duplex channels (asks for larger RFFE covering traffic channels) and is traffic dependent.			

It is recalled that the statement regarding the position capability consider a SPP algorithm, as at this stage no hybridization with IMU is considered.
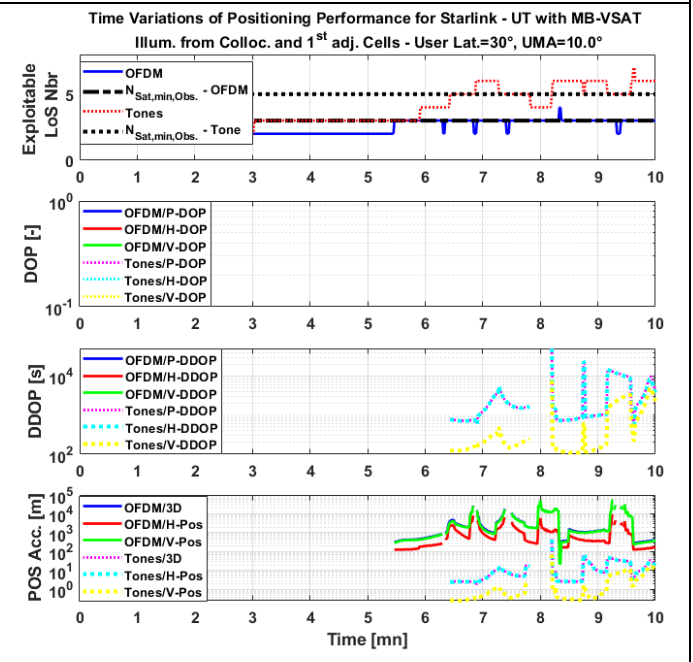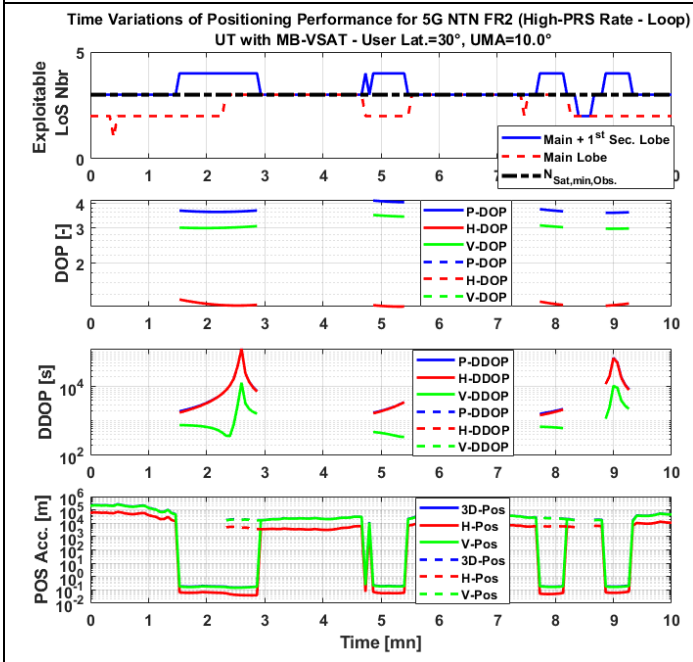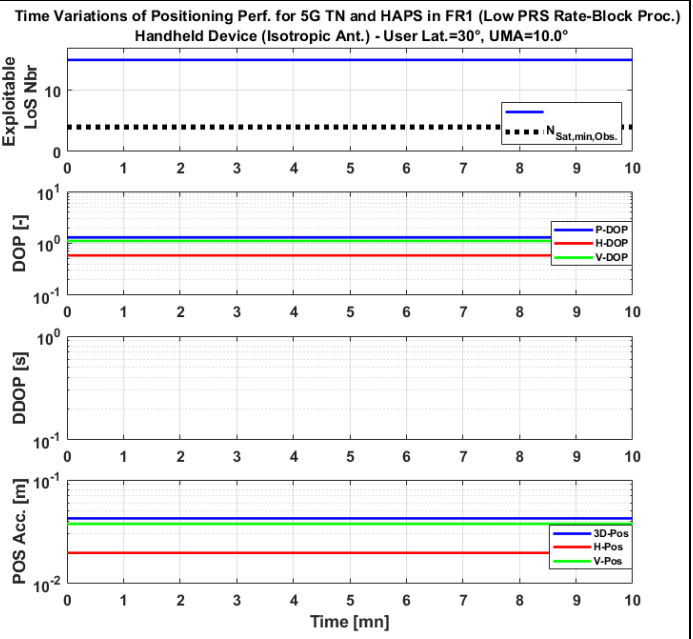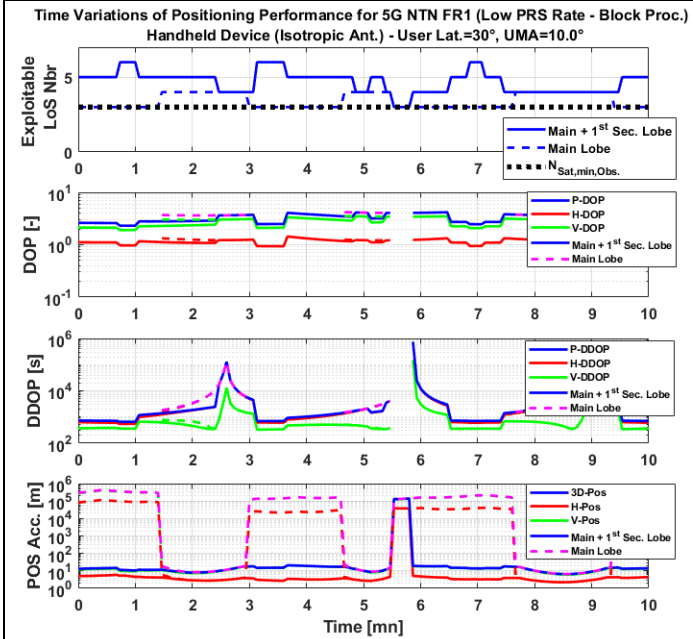
From the former evaluation, **TABLE 12** summarises the standalone PNT system scenarios that have been retained for the SVS simulation campaigns.

TABLE 12: Retained standalone PNT scenarios

Standalone PNT Scenario	UT Configuration	Space Segment Configuration
5G NTN in FR1	Handheld device with isotropic antenna pattern.	• PRS transmission before and after handover through main and 1st secondary antenna beam lobe. • PRS transmission before and after handover through main beam lobe (for comparison)
5G TN and HAPS in FR1	Handheld device with hemispherical antenna	• PRS transmission before and after handover through main and 1st secondary antenna beam lobe.
5G NTN in FR2 (Ku-Band)	UT equipped with MB-VSAT antenna	• PRS Transmission before and after handover through main and 1st secondary antenna beam lobe.
Starlink	UT equipped with M-LNB and a MB-VSAT antenna	• Exploitation of direct illumination to the collocating hexa-cell and 1st ring of hexa-cells.
LEO-PNT	Handheld device with hemispherical antenna	• Isoflux, broadcast CDMA scheme

5.4.2 Evaluation of the Snapshot Simulations

Evaluations of the time variations for main identified KPIs are conducted first with the so-called snapshot simulations. **FIGURE 14** represents for each scenario the number of exploitable LoS, the DOP and DDOP and finally the position accuracy derived with a joint exploitation of both ToA and FoA, when available.
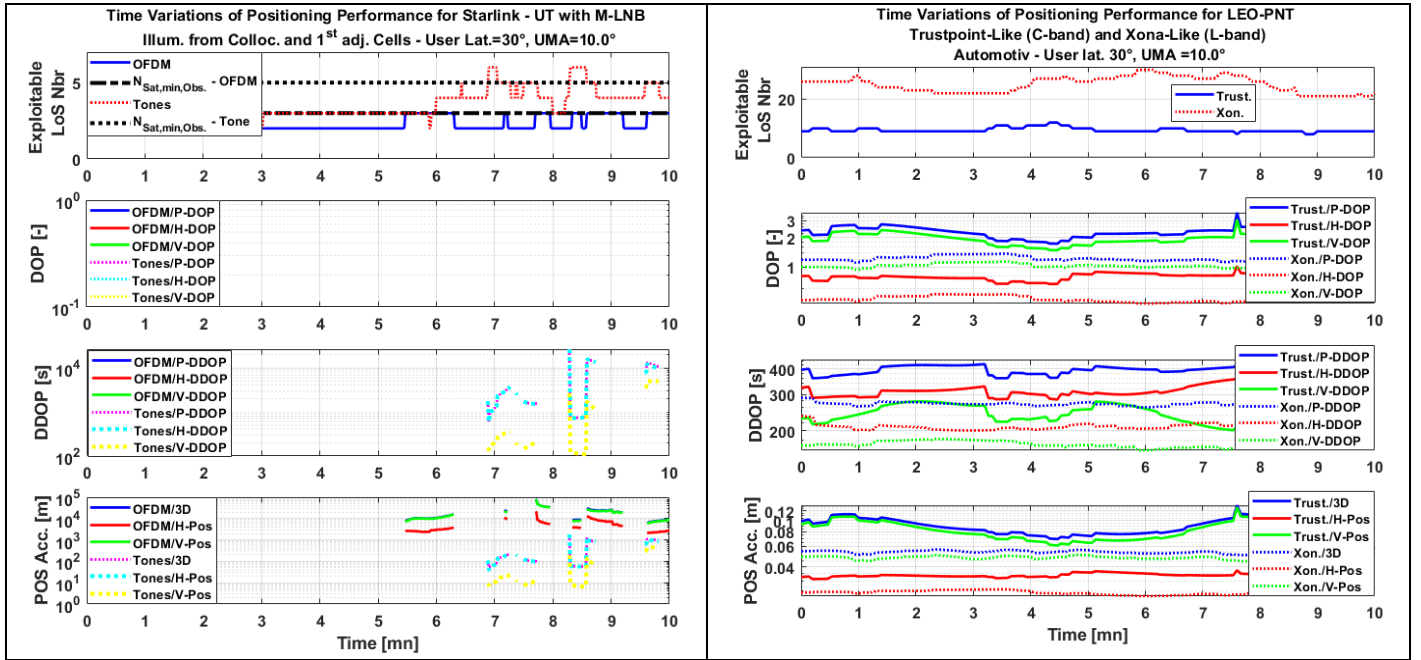
Time Variations of Positioning Performance for 5G NTN FR1 (Low PRS Rate - Block Proc.) Handheld Device (Isotropic Ant.) - User Lat.=30°, UMA=10.0°

Time Variations of Positioning Perf. for 5G TN and HAPS in FR1 (Low PRS Rate-Block Proc.) Handheld Device (Isotropic Ant.) - User Lat.=30°, UMA=10.0°

Time Variations of Positioning Performance for 5G NTN FR2 (High-PRS Rate - Loop) UT with MB-VSAT - User Lat.=30°, UMA=10.0°

Time Variations of Positioning Performance for Starlink - UT with MB-VSAT Illum. from Colloc. and 1st adj. Cells - User Lat.=30°, UMA=10.0°

FIGURE 14: Standalone SPP performance. Upper left: 5G NTN FR1, Upper right: 5G TN and HAPS in FR1: Middle left, 5G NTN FR2: Middle right: Starlink with PSS, Lower Left: Starlink with Tones, Lower right: Xona-Like/Trustpoint-Like – UT at 30° in latitude, 10° in UMA

From those results, the following outcomes can be proposed:

• The 5G NTN technology permits a SPP solution, without interruption, assuming transmission of PRS before and after traffic handover. When compared to LEO-PNT systems the relatively low number of exploitable LoS requires combination of both ToA and FoA to ensure solvability of position equation (OWR or OWD alone would not permit SPP as periods with only 3 exploitable satellites exist). Furthermore, only considering transmission of PRS through the main lobe reduces the average number of exploitable satellites to a level close or equal to $N_{Sat,min,obs}$ (equal to 3, as cooperative) for 5G NTN in FR1. For the 5G NTN in FR2, observability conditions are worse even when the orchestration and antenna design ensure PRS transmission through the secondary lobes. Position performance are at meter level (without accounting for other contributions such as residual of ephemeris and clock, multipath and atmospheric delays) when observability margin exists. Still for the 5G NTN scenario in FR2, the poor FoA accuracy does not permit a stabilisation of position accuracy (when the number of exploitable LoSs just equal $N_{Sat,min,obs}$ =3) which degrades with several orders of magnitudes. Finally, horizontal performance is usually better than vertical one due to non-uniform spatial distribution of LEO satellites. This statement also applies for the other LEO-PNT initiatives.

• The 5G TN technology augmented with a single HAPS (5G NTN) also permits SPP solution, assuming a sufficient number of gNB, which shall be satisfied in urban environment. As outlined earlier, the favourable assumption was made that no obstruction occulted access to the gNB. Due to the static configuration between gNB and user, $N_{Sat,min,obs}$ equal to 4 LoSs rather than 3 as in the case of 5G NTN are needed as Doppler cannot be exploited (considering user dynamic not sufficient for FoA).

• Starlink offers occasional SPP solutions with a UT equipped with a MB-VSAT. Exploitation of OFDM for joint ToA and FoA yields to a solution at kilometre level, as the actual number of exploitable LoSs (also originating from adjacent cell illuminations) just reaches the minimum required ($N_{Sat,min,obs}$=4, as opportunistic). Tone exploitation (rather than OFDM frames) improves the situation even when only one observable type (FoA) feeds positioning engine. The two reasons are an enhanced FoA accuracy (as tones are continuously received) on a one side, and on the other side a doubling of the FoA measurement number per epoch, and which can compensate the increase of $N_{Sat,min,obs}$ ($N_{Sat,min,obs}$=5). When a M-LNB antenna is applied positioning performance are one order of magnitude worse due to lower antenna directivity. Furthermore, larger gaps of position availability have to be declared, when compared to the opportunistic UT equipped with a MB-VSAT.

• Dedicated LEO-PNT systems offer the best performance (at decimetre level, still without accounting other contributions to the ranging error), together with the larger number of exploitable LoS.

5.4.3 Evaluation of the first SVS Campaign Results

The second type of analyses is based on SVS conducted over different latitudes and elevation masking angles. Here statistics (minimal, maximal, median values) regarding the retained KPIs are depicted. The corresponding "KPI performance boards" are placed in **APPENDIX A.4**. From those boards the following additional statements can be proposed for each standalone PNT scenario.

- **Standalone Performance for 5G NTN in FR1:**

The performance of the standalone 5G NTN scenario presented in **APPENDIX A.4.2** are firstly analysed (see **FIGURE 19**). The minimal value for the $(C/N_0)_{PSP}$ is approximately 10dB smaller for a UMA of 10° than 30°. The reason is that according to 3GPP TR 38.821. (2023) the EIRP and antenna beam directivity are guaranteed for a cut-off angle of 30° for the considered study-cases. Below this value (e.g. 10°), the received power will suffer from higher space losses and lower directivity (through secondary lobes). The UMA of 30° prevent accessing such LoSs with reduced PoG. For an automotive 3GPP terminal the difference becomes even larger due to the larger dynamic of the receiver antenna gain (see **TABLE 5**). Maximal values corresponding to the zenithal link keep unchanged for 10° or 30° in UMA. The corollary is that a lower number of exploirable LoSs has to be declared for an UMA if 30° than 10°. Link margin measured between $(C/N_0)_{PSP,Thr}$ and median $(C/N_0)_{PSP}$ is approximately 15dB for both block processing (low occurrence PRS rate) and loop (high occurrence PRS rate) estimation techniques. The number of exploitable LoSs is just sufficient to ensure UT position with SPP for a 10° UMA. As just stated, for a 30° UMA, the additional PRS illuminations before or after handover are occulted from UT yielding to negative observability margins. For higher latitudes (e.g. 45°), observability conditions improve for a 10° UMA, as a consequence of the Walker star topology proposed for the "Set-2" (see **FIGURE 7**). This improvement is however not perceptible for a UMA of 30°. ToA accuracy obtained with tracking loop techniques is one order of magnitude better than with block processing, since taking advantage of the averaging or smoothing effect. As formerly highlighted, the FoA accuracy is not sufficient, even when applying tracking loop techniques, due to the too short duration of the PRS modulate symbol. An exploitable FoA for positioning would certainly ask for more energy dedicated to the PRS within the radio-frame. Comparison of positioning performance and availability obtained with block processing or tracking loops show the strong influence of the threshold $(C/N_0)_{PSP,Thr}$. For the scenario applying block processing, the threshold is roughly 3 dB lower than for scenario applying loops. As previously explained and also shown on **FIGURE 12**, those 3 dB are sufficient to exclude one LoS on average, so that the probability to have at least one exploitable LoS more than the bear minimum $N_{Sat,min,obs}$ is higher with block rather than loop processing techniques. This margin can be directly reflected in the median position accuracy around 20m for low PRS rate, while it is close to 100km for high PRS rate, while ranging accuracy is worse with block processing techniques than with loop ones. This important result regarding benchmarking between loop or block processing techniques demonstrates that it is preferable to ensure a larger number of exploitable LoS for the position equation (higher observability margin) than a higher ToA (or FoA) accuracy. In general, similar statements can be proposed for both handheld and automotive users.

FIGURE 19 also highlights the need to improve PRS symbol distribution to bring FoA accuracy below the 10cm/s. To identify a first working point regarding the required PRS density per radio frame, i.e. PRS duty cycle for high PRS occurrence rate scenario, and which would permit a 10cm/s FoA accuracy, **TABLE 13** provides the FOA accuracy, using Equation (13), as function of the number of PRS symbols per frame for two $(C/N_0)_{PSP}$. The first one corresponds to the $(C/N_0)_{PSP}$ level achieved when exploiting main lobes (also with PRS transmission before and after handover) and the second one corresponds to the $(C/N_0)_{PSP}$ level achieved when exploiting the secondary lobes (see **FIGURE 12**).

TABLE 13: Preliminary estimation of the PRS duty cycle to support FoA accuracy at decimetre level (for 5G NTN FR1/ FR2)

	5G NTN in FR1 (λ=13.70cm)				5G NTN in FR2 (λ=2.65cm)		
	v_{PRS}	σ_{FOA} for 45dB-Hz (2ndary Lobe)	σ_{FOA} for 60dB-Hz Main Lobe		v_{PRS}	σ_{FOA} for 50 dB-Hz (2ndary Lobe)	σ_{FOA} for 60dB-Hz Main Lobe
1 PRS Symb./Frame	1/280 (0.35%)	500m/s	65 m/s	**1 PRS Symb./Frame**	1/1120 (0.09%)	460 m/s	105m/s
75 PRS Symb./Frame	75/280 (26%)	56cm/s	**10cm/s**	**100 PRS Symb./Frame**	100/1120 (9%)	31cm/s	**10cm/s**
230 PRS Symb./Frame	230/280 (82%)	**10cm/s**	2cm/s	**230 PRS Symb./Frame**	220/1120 (20%)	**10cm/s**	3cm/s

It can be verified that to achieve an exploitable FoA accuracy for the position engine, 25% (resp. 80%) of the radio frame would have to be populated with PRS when exploiting received power from the main (resp. secondary lobes). Those ratios show that a PRS-based FoA estimation would be too "invasive" w.r.t. communication traffic modulated in the remaining part of the radio frame. In order to achieve sufficient FoA accuracy with a more negligible footprint on the communication mission the following alternatives are proposed:

- The first proposes to exploit the phase with a PLL to deduce the frequency, rather than the FLL. It is shown that PLL offer higher performance but are less robust at lower (C/N_0) (high cycle slip and loss of lock probabilities).
- The second proposes to exploit other components of the 5G frames such as PSS, SSS or pilot sub-carriers, considering that those ones are transmitted with less interruption, or ideally continuously. In that case the PNT service would be ensured with the PRS for ToA, and other components of the 5G physical layer for the FoA.

• PNT Performance for Standalone 5G NTN in FR2:

Regarding the standalone scenario for 5G NTN in FR2 (see **FIGURE 20** in **APPENDIX A.4.3**) similar conclusions to FR1can be hold, but with the following deviations. Due to the larger $(C/N_0)_{PSP}$, both FoA and ToA accuracy are one order of magnitude better in 5G NTN FR2 than in FR1 as already shown on **FIGURE 13**. This larger $(C/N_0)_{PSP}$ levels is however not reflected in the number of exploitable LoS. Hence, the observability margin is still worse for 5G NTN FR2 than FR1, and therefore the positioning performance are expressed in 10s of km, both for the high PRS rate (i.e. Loop) or low PRS rate (i.e. block processing use cases). Even if the $(C/N_0)_{PSP,thr}$ is 3dB lower for a low PRS than a high PRS rate, it does not neither offer a significant increase of the number of exploitable LoSs.

A similar exercise has been carried-out to evaluate the required PRS duty cycle to reach FoA accuracy at decimetre level (see **TABLE 13**), now in FR2. It can be verified that comparatively to the 5G NTN in FR1 the required duty cycles become smaller. The main reason is the smaller wavelength with 2.65cm rather than 13cm in FR1. However, and even if smaller, the corresponding PRS duty cycles still appear too high (at least 10%) to not reduce attractiveness of a fused COM-NAV system, as it could jeopardize financial viability of the main communication service.

• PNT Performance for Standalone Starlink:

Regarding the standalone scenario for the Starlink system (see **FIGURE 21** in **APPENDIX A.4.4**), the following statements hold, independently to the sub-scenario configuration (OFDM vs. tone exploitation, or the UT equipped with a MB-VSAT vs. a M-LNB). First, it is shown that by applying the actual atmospheric loss models (rain attenuation, Gaz absorption, see **APPENDIX A.2**) the $(C/N_0)_{PSP}$ levels are 10dB lower on average for an equatorial user w.r.t. a user at 30° (or more) in latitude. FoA accuracy levels derived from post-PSS correlation are better than the ones derived from post-PRS correlation of 5G NTN, but still not sufficient to really influence favourably position accuracy. FoA derived from tones reach levels at sub-meter per second which permit exploitation for positioning. The sub-scenarios are now analysed separately. First, it can be verified that the observability is not sufficient when exploiting PSS as part of OFDM frames, even when including illuminations from adjacent cells. This is different when exploiting the tones which offer sufficient positive margin. Use of an M-LNB permit positioning either with tones or OFDM but only at 30° in latitude, and with an availability ranging between 20 % and 60%. Even for a UMA of 30°, it is possible to have a position fix with a 20% availability while availability is close to 0% for 5G NTN in FR2. One justification is the lower cut-off angle of 25° declared by Starlink (while it is equal to 30° for 3GPP). The scenario involving a UT equipped with a MB-VSAT and exploiting tones represents the most favourable one for a standalone and opportunistic solution. It is reminded that those performance are obtained for a UT exploiting only one Starlink channel of 250MHz (MB-LNB Mono-Channel). Exploitation of two or more Starlink channels will definitely improve observability margin and thus performance, but will also be penalised with a higher equipment cost.

• PNT Performance for Standalone Dedicated LEO-PNT:

Finally, SVS confirms results of snapshot simulations for the dedicated LEO-PNT systems (see **FIGURE 22** in **APPENDIX A.4.5**). A Xona-like system permit a standalone PNT solution for all three investigated latitudes and for almost all UMA. The sole identified pain point regards the availability issue for UT placed in a deep-urban environments (UMA = 45°) and for a UT at 30° in latitude. The smaller number of satellites of the Trustpoint-like system yields to a lower availability already for UMA larger or equal to 30°.

5.5 Gap Analysis for Standalone PNT

From the first SVS campaign applied to each LEO-PNT initiative individually, the following strengths and weaknesses could be identified:

• The received $(C/N_0)_{PSP}$ are usually 10 to 20 dB larger for the broadband LEO communication systems than for the dedicated LEO-PNT or for the "big LEOs" systems Iridium and Globalstar, as a direct consequence of higher data rate. However as the PSP (PSS for Starlink, PRS for 5G NTN) are not transmitted continuously only a fraction of the integrated signal energy can actually be exploited, yielding to higher lower limit for the $(C/N_0)_{PSP,Thr}$ threshold. On average this lower limit is 25 dB larger than for the dedicated LEO-PNT systems, transmitting continuously PSP (PRN sequences) as shown in **TABLE 10**. Thereof the link margin which can be either used for enhanced robustness or resilience to e.g. jammer is aligned between both families of LEO-PNT systems. This assessment needs however to tempered when considering the following additional aspects:

- Broadband systems operating at higher frequencies, FR2, offer an additional immunity to jammers on a one side thanks to the high directivity offering a native spatial notching to towards the RFI sources, and on the other side thanks to larger free space losses affecting the jamming power.
- For the 5G NTN use case (in both FR1 and FR2), the assessments have been carried-out for a specific working point within the large configuration space, i.e. numerology, authorised by 3GPP. Especially only one PRS symbol was introduced per radio frame, in the high PRS occurrence rate. It is possible to improve ToA but also FoA by increasing PRS density at the price of the communication capacity. This represents one of the key trade-offs, atop the architectural ones, which are intensively discussed at 3GPP standardization level, to introduce a positioning service as part of 5G NTN.
- Exploitation of Starlink tones, transmitted continuously, offers a strong link margin, further magnified for UT equipped with MB-VSAT
- Finally, a possible reduction of the applied and claimed received PoG level for Xona(-like) and possibly Trustpoint (-like) dedicated LEO-PNT systems could be expected in the future after final agreements from the radio frequency compatibility and interoperability discussions taken place at ITU level. This would have a direct consequence onto the link margin.

• Once the "$(C/N_0)_{PSP,Thr}$ barrier" passed successfully, the large (FR1) or very large (FR2) bandwidth of the communication signals permit reaching ToA accuracy levels at sub-meter level. The non-continuous nature of the PSP transmitted by Starlink (PSS) or by 5G NTN satellites (PRS) yields to a strong degradation of the FoA accuracy which appears detrimental for further Doppler positioning. As just discussed, this situation might evolve for the 5G NTN case with an adaptation of physical layer for which early working points were presented. For the dedicated LEO-PNT systems both ToA and FoA accuracies are sufficient to offer the required levels supporting standalone positioning.

• Placing the discussion at positioning domain, one of the main differentiators between opportunistic or cooperative exploitation of LEO-communication systems, compared to the dedicated LEO-PNT system one, is the low observability margin. Sole usage of traffic SV-beams does not permit SPP. This specificity permits anticipating application of sequential positioning filters absorbing IMU measurements atop the ToA and FoA ones, such as a hybrid LEO-IMU engine implementing an EKF for cooperative, or the STAN for opportunistic PNT. It is noted that the observability margin in the position domain represents one additional mean to sustain RFI or jammers, by authorising the loss of few exploited LoSs, with an acceptable degradation of position solution. To partially solve observability issue for LEO-COM-based PNT, mitigations taking place at UT or system side have been proposed, either by exploiting additional LoSs corresponding to non-traffic satellites, or by increasing the PRS availability by transmitting through main and secondary lobes before and after handovers.

SVSs also show that aforementioned mitigations to enhance Los number for a fused navigation are annihilated for a UMA at least equal to the cut-off-angle introduced for the design of the communication service (set to 30° in the 3GPP framework).

If the dedicated LEO-PNT systems offers best performance up to urban, and in a lower extend, deep urban environments, SVS show that for deep urban environments (UMA=45°), observability margin gets negative for UT at 30° in latitude for the Xona-Like system. For a Trustpoint-like system the availability of performance is guaranteed only for UMA below 30°.

• Finally, former analyses showed that the architecture of a legacy communication UT might not be sufficient to support a SPP solution without adaptation, especially for systems operating in FR2, and this already for a standalone positioning. As just explained, the need to improve observability requires a UT antenna offering additional beams in reception, to the one supporting the traffic. In FR1 the large opening angle of the (isotropic, hemispheric) antenna, appears sufficient for a navigation enable terminal. Nevertheless, as for FR2 additional analogue or digital channels (i.e. correlators) have to be implemented to exploit

other received signals than the traffic one and to produce ToA and FoA. Here improvement of the observability will have to be accompanied with an increase of analogue bandwidth to permit capture of additional ranging signals transmitted in all channels.

6 PERFORMANCE EVALUATION FOR HYBRIDIZED SYSTEMS

6.1 Hybridization strategy

The former gap analysis showed that in the case of LEO-COM based PNT, mitigation strategies can be proposed at system and UT levels to improve standalone positioning, up to the limit of the cut-off-angle. However, those ones might not be sufficient for a robust solution which would require additional LoSs, and especially for large UMA. Furthermore, if dedicated LEO-PNT systems appears as the most suited one for standalone positioning, some limitations still apply in deep-urban environments. To palliate those caveats or to further improve performance, hybridization between different LEO-PNT initiatives appears as a promising solution. Two different directions are explored for the hybridization strategy:

• The first approach searches for synergies at each processing step of the user CONOPS yielding to the position solution, and is thus more driven from a chipset manufacturers perspective. A first candidate combination exploits signals sharing same physical layer characteristics, yielding to an HNT exclusively processing CDMA or OFDM signals. Another case combines systems transmitting signals (having possible different waveforms) in the same or neighboured frequency band(s) to communalize the receiver front-end.

• The second one, more application driven, hybridizes systems for enhanced performances. For example, fast and high accuracy with PPP is achieved by jointly processing GNSS and LEO signals received in L-band to minimize biases. Alternatively, improved resilience asks for processing GNSS and LEO signals transmitted in different frequencies to escape the band contaminated by a jammer. Observable (range, Doppler) diversity also improves resilience by ensuring minimal service availability under jamming attack. Technology complementarity can also serve robustness enhancement. For example, the joint exploitation of GNSS and/or LEO observables with IMU measurements enables bridging at short term satellite link scarcity in urban environments.

For the first hybridization process, priority has been placed on the first approach and especially by combining systems operating in the same frequency region, or using similar waveforms. In the following, different hybridization scenarios are identified.

6.1.1 Hybridization in FR2

The first hybridization scenario proposes to combine broadband systems operating in the FR2, such as Starlink and a future communication system applying the recommendations from the 3GPP NTN standardization. This hybridization currently proposes clustering an opportunistic PNT system with a cooperative one, which yields to additional burden (e.g. estimation of time of transmission). This burden can be obviously solved if the hybridization combines two cooperative PNT systems.

The following statements justify the first hybridization in FR2:

• Firstly, even if the current analyses essentially concentrated on the steady state regime (i.e. once signal acquisition achieved and positioning engine initiated), it is important to highlight that a pure opportunistic initialisation appears challenging. As an example, the STAN requires coarse-to-accurate UT positioning, currently ensured by the GNSS technology. This constraint to involve a GNSS module for initiation can be released once steady state achieved with opportunistic exploitation of SAT-COM signals only. This GNSS dependency of the opportunistic positioning filter creates again some vulnerabilities. Therefore, replacing the GNSS technology with the 5G NTN one, as "Pivot" enabler would not only simplify UT architecture and cost by suppressing the GNSS module but also provides a more resilient solution. The challenge then obviously resides in demonstrating the capability for a 5G NTN only initialisation, without having recourse to GNSS (else the issue regarding GNSS dependency would have just been "transferred"). Here requirements related to the time-to-first fix (TTFF) and time transfer will have a strong impact onto the designed solution. Candidate schemes similar to the ones developed in the frame of the next GNSS systems for broadcast signals, and detailed in García-Molina et al., (2022) could be adapted for communication systems. Another solution would consist in applying two-way ranging (TWR), which represents one of the main enabler and differentiator of communication systems w.r.t. dedicated LEO-PNT systems.

• The former statement regarding a GNSS independent solution when hybridizing a cooperative and an opportunistic system, becomes even more valuable when hybridizing two cooperative (SAT-COM) systems, to support UT state vector initialisation

and ease entry to the network. Here, interoperability of the two SAT-COM systems would be strongly beneficial to facilitate UT CONOPS to initiate communication.

• Having solved initialisation, the combination of both broadband systems shall offer a higher number of exploitable LoSs, which will certainly enhance observability. It will have to be shown through simulations, that the additional unknowns (LLTO, LLFO, ..) introduced in the state vector and required to support to the hybridization will however not degrade the observability.

• It was explained that improved PNT performance can be gained if the analogue front-end embraces all communication channels, offering thus higher occasions to exploit other LoSs, especially for opportunistic navigation. When combining two systems, possibly with different frequency and channel plans, the decision regarding the relative position of the respective channels and especially the inter-system channel overlap, will have to solve the trade-off between ranging accuracy and observability. To illustrate this aspect, Figure 15 shows one candidate frequency plan allocation between the (up to) 8 Starlink channels and one channel of 400MHz for a future 5G NTN broadband communication system both operating in Ku-Band. Here, it is assumed that the commercial modem can digitized the signals from the complete 400MHz band, and that sub-channel (i.e. 133MHz) selection is performed in digital domain. In this example, the central carrier frequency has been selected so that the 400MHz span can cover the maximal number of Starlink channels for improved geometrical diversity. For example, by aligning the third carrier frequency of the Starlink systems (1325MHz) with the central carrier frequency of the 5G NTN one, it is possible overlap with up to 3 Starlink channels: both lateral sub-channels will be able to capture 74.5MHz (=133+133/2-125) so about 30% of a Starlink channel of 250MHz, while the combination of both lateral sub-channels and the central one permits capturing a complete Starlink channel of 250MHz. Hence, by getting simultaneous access to up to 3 Starlink channels, it is possible to extend the number of LoS whose signals can be exploited opportunistically with a factor up to 3, which will definitively favour DOP and SPP performance. An alternative optimization would consist in maximizing the captured bandwidths of the Starlink channels overlapping with the 400MHz of 5G NTN, with the intention to improve the ToA ranging quality (the wider the Gabor bandwidth, the better the performance). This alternative strategy would have conducted to select the central carrier of the 5G NTN system at 11200MHz, yielding to capture two Starlink channels with 199.5MHz (=133+133/2 MHz). It is noted that such discussions essentially focus on the trade-off between ranging, observability and position accuracy and do not account for radio frequency compatibility aspects between the existing Starlink/OneWeb systems and a future 5G NTN system operating in Ku-Band.
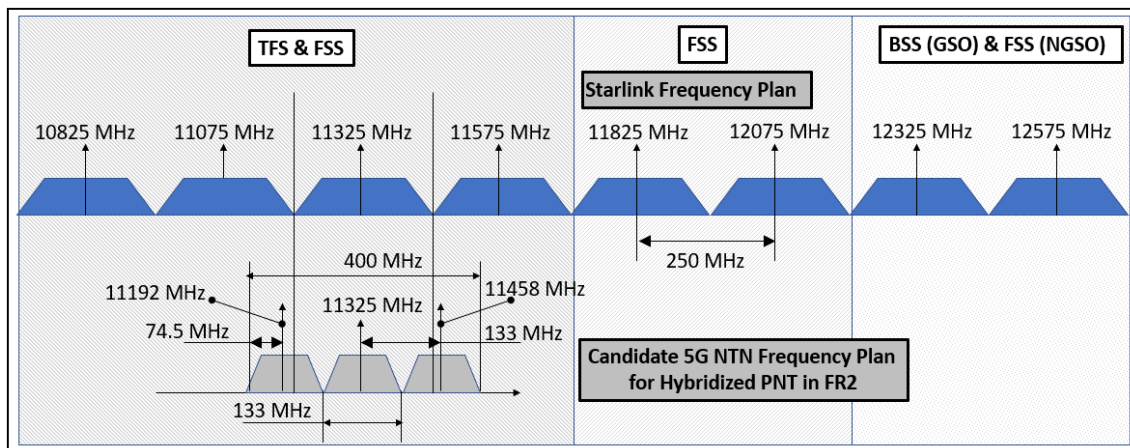

FIGURE 15: Exemplary frequency plans between existing LEO-COM and a future 5G NTN in FR2 (Ku-Band) for enhanced observability

6.1.2 Hybridization of 5G NTN/TN in FR1

The second hybridization scenario proposes to combine all sources transmitting 5G signals in the FR1. This concerns the 5G NTN satellite, but also the 5G gNBs and finally the HAPS transmitter. This solution has the advantage to capitalize on the work performed at 3GPP standardization level, ensuring compatibility and interoperability between those different elements of the 5G landscape. Furthermore, the hybrid 5G NTN terminal will definitely benefit of the commonalities between 5G technologies, considering the same signal processing techniques based on OFDM signals, and also an antenna showing a large opening angle in FR1. Here limitations of the observability observed with the standalone 5G NTN scenario shall be compensated by introducing additional

sources, also exploiting the geometrical complementarity between 5G components fostering horizontal position performance (5G gNBs) and other ones (5G NTN satellites and HAPS) favouring vertical position performance.

6.1.3 Hybridization of Iridium and Globalstar

The third hybridization scenario aims at improving the observability limitations of both Iridium and Globalstar systems. Considering that both systems operate in the FR1 could thus ease the design of a hybrid PNT terminal, by exploiting some communalities. As an example, the same L-Band antenna, followed by a circulator, could be used for both systems, by noticing that the Globalstar up-link signals are transmitted in the 1610-1618.725MHz band, close to the Iridium simplex band, but sufficiently distant to permit spectral excision between Globalstar up-link and Iridium down-link signals.

6.1.4 Hybridization of LEO-PNT

The fourth and final investigated hybridization is proposed to palliate the observability weaknesses of each single dedicated LEO-PNT system and observed for large UMA in deep urban canyons.

6.2 Positioning Performance Analyses for Hybridized UT with SVS

6.2.1 Evaluation of the Snapshot Simulations

● **PNT Performance for Hybridized 5G NTN, TN and HAPS in FR1:**

FIGURE 16 represents the time variations of the positioning performance for a hybridized PNT system exploiting 5G signals transmitted by terrestrial and non-terrestrial sources, either when combining 5G NTN and TN (left figure) or by including one additional HAPS (right figure). Atop showing the number of exploitable LoSs (LEO, gNBs and HAPS), the upper part of the figures provides the number of measurements (considering that no FoA can be derived from the gNB and HAPS static sources), to be compared to the number of unknowns, set equal to 5 (UT coordinate, clock offset and drift for a cooperative scenario). It can be verified that the system for the position solution is largely overdetermined, yielding to position at sub-meter level (again without considering any other contribution to the UERE/UERRE).
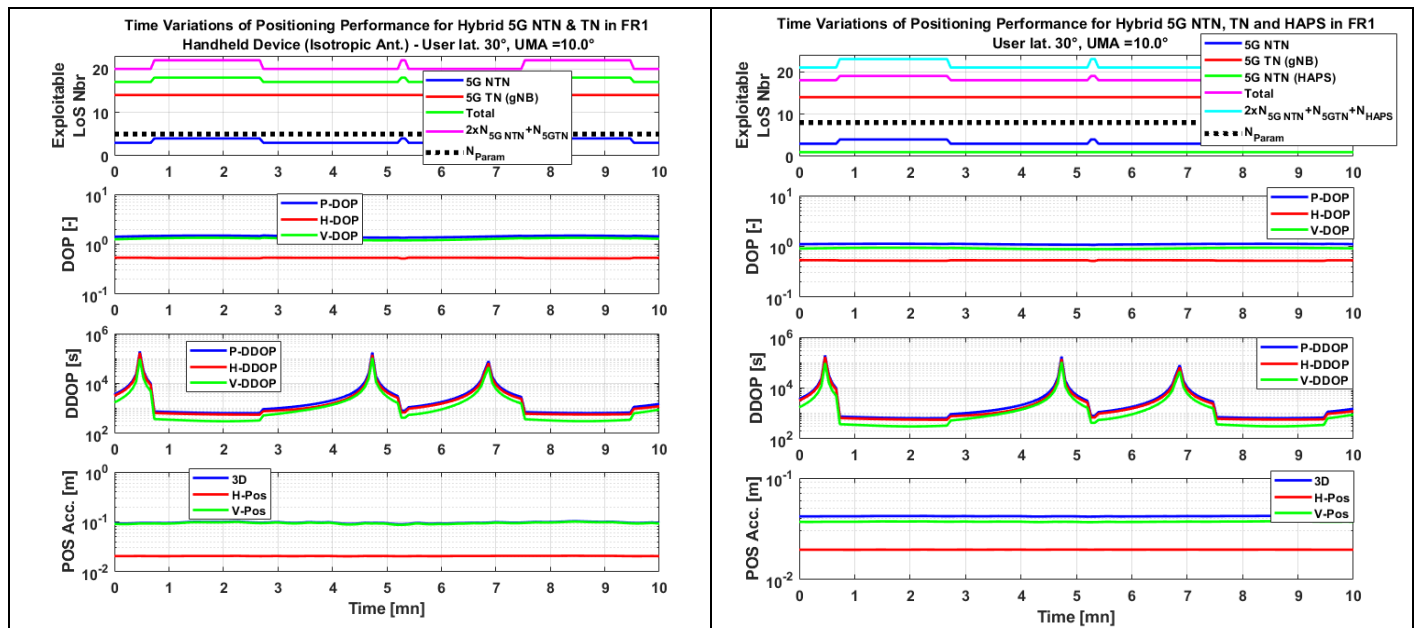

FIGURE 16: Hybridized SPP. Left: 5G NTN/TN, Right: 5G NTN/TN/ HAPS in FR1 – UT at 30° in latitude, 10° in UMA

● **PNT Performance for Hybridized 5G NTN and Starlink in FR2:**

FIGURE 17 represents the time variations for positioning performance when hybridizing the Starlink and 5G NTN in FR2 systems. Furthermore, two configurations have been considered for the air interface of the UT exploiting the Starlink signals. In the first one a M-LNB antenna was applied, while in the second one the same MB-VSAT as the one used for the reception of the 5G NTN signals was considered. Result analysis shows that the significant number of exploitable LoSs, compensates for the increase of the minimal required number of satellites, $N_{Sat,min,obs}$, from 3 (standalone) to 4 (hybridized). When comparing **FIGURE 17** to **FIGURE 14**, it is shown that the availability of sub-meter position accuracy improves. Nevertheless, position accuracy well beyond the kilometer level still remains. A closer look shows that those situations occur during time intervals when observability margin is one (i.e. 1 more LoS than the required $N_{Sat,min,obs}$). As soon as the margin equals two (yielding to 6 LOS), OWR positioning is possible (see **TABLE 15**) yielding to outstanding performances. This result also confirms that FoA accuracy levels are not sufficient to significantly improve positioning solution accuracy. Still during intervals showing 6 LoSs the comparison of the positioning performance between the scenarios for a UT equipped with a M-LNB or with a MB-VSAT reveals that no significant improvement is achieved, although the ranging error obtained with the MB-VSAT is one or two orders of magnitude larger. Closer investigations show that not only the aggregate number of LoSs has to be larger than $N_{Sat,min,obs}$ but also that the number of LoSs from the Starlink system has to be equal or larger than the number of additional unknowns cause by the hybridization, so two (T_{SoOP} and LLTO). If it is just equal, the quality of the corresponding two additional ToAs will not substantially benefit to the position accuracy. Hence, because FoA does not (currently) influence performance, it is highlighted that the additional opportunistic constellation will have a beneficial impact on the position estimation only when at least three ToAs are available.
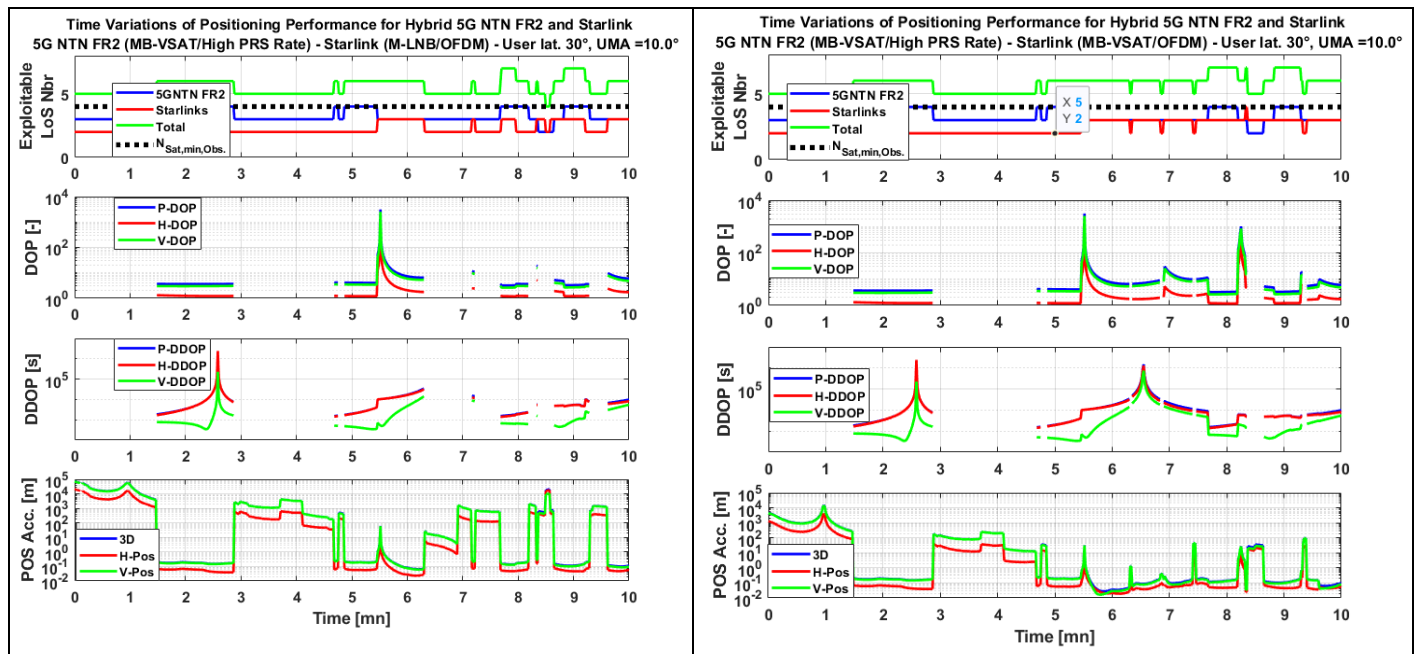

FIGURE 17: Hybridized Starlink/5G NTN FR2. Left: MB-VSat (5G) with M-LNB (Starlink) configuration, Right: MB-VSat (5G) with (same) MB-VSAT (Starlink) configuration – UT at 30° in latitude, 10° in UMA

● **PNT Performance for Hybridized Iridium and Globalstar:**

FIGURE 18 represents the time variations for the aggregated number of exploitable LoS when hybridizing both Iridium and Globalstar systems, together with the number of availability measurements (considering that ToA and FoA can be estimated from Iridium burst, while only ToA can be derived from the Globalstar signals, after "decompensation"). This number has to be compared with the 8 parameters to be estimated (as shown on **TABLE 15**). Because not enough measurements are available, no position in the SPP sense can be derived.
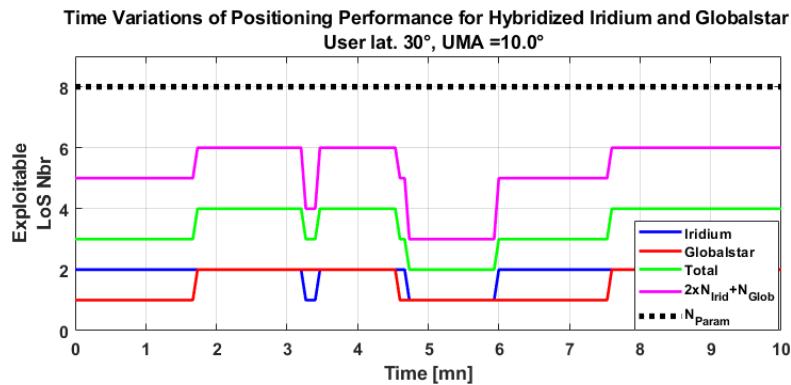
FIGURE 18: Time Variations of the aggregated number of LoS for both Iridium and Globalstar Systems

- **PNT Performance for Hybridized Dedicated LEO-PNT systems**

The PNT performance corresponding to the hybridized Dedicated LEO-PNT scenario are only shown on the performance boards (**FIGURE 25** in **APPENDIX A.4.8).**

6.2.2 Evaluation of the Second SVS Campaign Results

- **Hybridized Performance for 5G NTN, TN and HAPS in FR1:**

The results of SVS simulations shown on **FIGURE 23** in **APPENDIX A.4.6** confirm that the hybridization of non-terrestrial and terrestrial sources for 5G signal transmission provides outstanding performance and availability. It is still outlined that such performance can be achieved in locations offering a dense gNB network. In areas with poor coverage (so called "white areas") or over oceans such outstanding performance cannot be maintained, and performance will essentially rely on the 5G NTN component.

- **PNT Performance for Hybridized 5G NTN and Starlink in FR2:**

The analysis of **FIGURE 24** in **APPENDIX A.4.7** brings a further proof regarding the minimal number of LoSs from the Starlink systems necessary to take advantage from the improved ToA achieved with a MB-VSAT. For a UT at 30° in latitude and with a masking angle of 10°, it can be shown that the number of LoSs significantly exceeds $N_{Sat,min,obs}$. Therefore at least 3 or more Starlink LoSs can be exploited atop the 5G NTN ones. Under those conditions, the larger ToA accuracy levels obtained for a UT equipped with a MB-VSAT are then effectively reflected into the position accuracy (~10m max. for MB-VSAT w.r.t. ~100m for M-LNB). Still considering results from SVS, it can be verified that the hybridization between the Starlink and 5G NTN systems significantly improve availability of positioning, and also positioning performance for all latitudes. Nevertheless, the 100% availability is only achieved for latitudes equals or above 30° and for a UT equipped with a MB-VSAT.

- **PNT Performance for Hybridized Dedicated-LEO-PNT (Xona-like and Trustpoint-like):**

FIGURE 25 in **APPENDIX A.4.8** obtained with SVS simulations shows that despite the larger number of LoSs, it was still not possible to improve position availability for the 30° latitude and for deep urban environment. The main reason is that by combining both Xona- and Trustpoint-like systems one additional satellite is required to compensate for the two newly introduced parameters related to the LEO-system time offset (LLTO and LLFO). This early result highlights the benefit to align time scales from different systems (for example on a common GNSS system), or to provide to the UT the LLTO and LLFO parameters through the navigation message (similar principal as GGTO broadcast in GNSS navigation messages).

6.3 Gap Analysis for Hybridized PNT

The second SVS campaign, covering three main hybridized scenarios, showed that the limitations identified for each of the LEO-PNT initiatives, exploited individually could effectively be reduced, but not fully mitigated. Hybridization of the different 5G NTN and TN components in the FR1 still show very promising performance. Regarding the two other hybridization use cases

(hybridization between LEO-COM systems in FR2, and hybridization between dedicated LEO-PNT systems), the two following directions of improvement are proposed:

- Combine additional LEO-PNT initiatives of the same type and operating in the same frequency. As example, in the FR2 it would imply hybridizing OneWeb, exploited opportunistically, atop the Starlink and the 5G NTN systems. For the hybridization use case between dedicated LEO-PNT systems, this would mean integrating a third system, such as Centispace or Geely. It is noted that an activate cooperation between operators of the hybridized systems, for example with the determination and transmission of inter-system biases (LLTO/LLFO), would also yield to a performance improvement.

- Hybridize LEO-PNT initiatives operated in different frequencies, as shown on **FIGURE 1**. Here the dedicated LEO-PNT systems, would represent the common socle between two inter-frequency hybridization scenarios. The first one proposes hybridizing LEO-PNT initiatives in the FR2 (5G NTN, Starlink, OneWeb) with the dedicated LEO-PNT systems, while the second proposes hybridizing 5G NTN systems operating in FR1 with dedicated LEO-PNT systems. Both scenarios would ensure accuracy and availability brought by the dedicated LEO-PNT systems, and resilience with the cooperative or opportunistic exploitation of the LEO-COM systems.

7 CONCLUSION

The work carried-out during the first phase of the HybPNT project, and presented in this paper, represents one of the first comprehensive studies having benchmarked with a same SVS platform the three main categories of LEO-PNT initiatives, not only when considered individually but also once hybridized. For this purpose, the SVS platform typically used to assess GNSS performance had to be adapted to model the specificities of LEO-PNT based positioning. This concerns the inclusion of a module for the ressource allocation (orchestration) of LEO-COM systems. Furthermore, the position equation has been actualised to account for the FoA measurements besides the ToA ones, and also for the new components of the user state vector, essentially related to timing (time of transmission for opportunistically processed signals, LEO-LEO Time and Frequency Offsets (LLTO/LLFO) for hybridized LEO-PNT systems). The resulting generalized position equation helped defining conditions related to the minimal number of exploitable LoSs ensuring sufficient observability for SPP estimation. The statements regarding the system observability and proposed for a SPP solution will also be of importance when relaxing the condition of synchronicity of the ToA or FoA measurements between different LoSs, and fed to a sequential positioning filter.

The following summarises the main outcomes of the corresponding work:

- Dedicated LEO-PNT systems offer the best performance in terms of accuracy and availability for a standalone position, which is certainly part of their mission requirements. Strong observability margins could be confirmed at position level, taking advantage from the large number of LoSs, for both rural and urban environments. For deep urban (i.e. UMA equal or larger than $45°$), observability gaps can significantly reduce position availability. The announced high received PoG levels for the Xona system also authorise anticipating high robustnes margins at link level. However, those PoG levels might be revised according to the discussions taking place at ITU level. Even if the core topic of the current work is mainly focussed on SVS performance and less on the architectural cost benefit comparisons between the different LEO-PNT initiatives, it is still worth mentioning that dedicated LEO-PNT systems require to set-up a complete space infrastructure, while alternative paradigms are based on communication systems, and especially the fused one, build on existing infrastructures and already in-place filings.

- 5G NTN systems can offer a standalone SPP solution when implementing schemes to guarantee a sufficient number of exploitable LoSs, else the sole exploitation of the traffic satellite signals does not fulfill observability criterion. In the current work, such schemes propose to transmit PRS before and after traffic handover, but also to enhance the operated antenna directivity beyond the main lobe. Such schemes can however only be exploited if the user masking angle is lower than the cut-off-angle applied for the definition of the constellation topology and the design of the communication antenna. Once those conditions fulfilled, the large Gabor bandwidth of the communication signals, combined with the very high $(C/N_0)_{PSP}$ allowing to compensate for the non-continuous transmission of the positioning reference signal (PRS), offer sub-meter ranging performance. Link budget margins at 15 dB can also be confirmed thanks to the large available (C/N_0) (up to 80 dB-Hz) required to support high data rates. However the value for the minimal threshold $(C/N_0)_{PSP,Thr}$, below which ToA and FoA estimation can not be performed, is significantly increased due to the non-continuous transmission nature of the PRS. Hence it reaches levels around 50dB-Hz (with a working assumption of a PRS duration equal to 1 symbol), while it lies around 25dB-Hz for GNSS or dedicated LEO-PNT systems. This threshold increase directly reduces the potential link margin which could be gained if PSP could be exploited continuously. The case of the Starlink tones transmitted continuously demonstrates, for example, a link margin of 45dB for a UT

equipped with a MB-VSAT. In FR2, the link margin against RFIs and especially jammers, is further improved as higher frequencies increase the (local) free space losses and reduce the side lobe envelop of the receiver antenna, which both attenuate the RFI power.

• Exploitation of the signals transmitted by the Starlink system in a single channel and processed in an opportunistic manner does not satisfy at all epochs the observability condition. Still, SPP solution based on the tone exploitation can be obtained during time intervals assuming sufficient directivity of the UT antenna for example achieved with a MB-VSAT, but also by exploiting illuminations to adjacent hexa-cells. The main identified reason for the promising SPP performance with Starlink tones is that several satellites can illuminate the same hexa-cell with the tones, which improves spatial diversity, while only one traffic satellite serves the hexacell with the OFDM signals. It is also noticed that works, contemporary to this article, have demonstrated some volatility in the Starlink signal characteristics and especially w.r.t. tone properties. Furthermore, achieved performance in the current work assumed implementation of specific techniques, some being to be consolidated, to allow full exploitation of the PSS and thereof of the large communication bandwidth. It is finally outlined that those statements will have to be revised when processing simultaneously 2 or more Starlink channels, to improve the observability margin.

• In a general manner, SVSs show that observability prevails on ToA or FoA accuracies, and therefore highlights the importance to minimize the lower $(C/N_0)_{PSP,thr}$ to authorise processing signals at lower PoG. In the example of 5G NTN systems, an increase of the PSP duty cycle per frame could allow reducing this threshold, so improving the link margin. Having a larger duty cylce or equivalently a longer PSP duration is also beneficial for the FoA accuracy, whose level currently obtained for the proposed configuration (1 PRS symbol per frame for 5G NTN) or with the processing of the PSS (Starlink) will not influence significantly the position solution accuracy. Now, this increase of the PSP duration has to be limited to not degrade the communication service.

• Hybridization between two or more LEO-COM systems, such as a cooperative 5G NTN system combined with Starlink (opportunistically exploited) both operating in FR2 represents another solution to paliate for the observability shortage. If hybrid CoOP/SoOP already showed the benefit for such a combination, the opportunistic nature of the Starlink signals forces to inject additional components (e.g. transmission time) in the user state vectors which again impacts unfavourably observability, and also limits full exploitation of accurate ToA. Hybridization between two cooperative LEO-PNT initiatives (LEO-COM systems or Dedicated LEO-PNT) would permit reducing the number of unknowns, especially if the inter-system biases (LLTO and LLFO) are computed and distributed to the UT in the navigation message, as already in place for multi-GNSS scenarios.

• Performance obtained for a UT exploiting all LoSs transmitted by 5G TN or NTN sources in FR1 can level the ones obtained by dedicated LEO-PNT, or GNSS (only accounting for thermal noise impact), but those outstanding performance can be guaranteed only in regions showing a dense gNBs terrestrial network, and obviously not over maritime areas.

• Finally, this work also enabled to define the architecture and predesign for a Hybrid PNT terminal, or hybrid navigation terminal (HNT) processing both main categories of signals either transmitted by (dedicated) LEO-PNT or by communication systems. One generic recommendation for an HNT exploiting communication signals is to expand the analogue and possibly the digital bandwidth to the full bandwidth of the communication system, as it enables simultaneous reception of additional LoS possibly transmitted in other channels to the traffic one (case of e-FCT). This capability will participate to an improvement of the system observability. When hybridizing two communication systems having different channel bandwidths, the frequency plan will have to account for this HNT design constraint, as part of the ranging accuracy/observability trade-off. A further and obvious design requirement asks for the simultaneous processing of the different received PNT signals to estimate ToA and FoA observables, and which will impact the HNT computational capacity. In the concrete example of 5G NTN signals it means that the processing of the non-traffic radio frames to estimate ToA and FoA from the PRS symbols will have to be supported by the hardware and/or firmware. When processing communication signals in an opportunistic manner, additional tasks to produce exploitable measurements for the navigation engine will have to be implemented. This concerns for example the removal of any delay or Doppler compensation, but also the different ambiguity resolutions. Another and final design aspect refers to the antenna technology implemented in the HNT. If the wide opening angle of the conventional antennas in FR1 allow simultaneous receptions of different LoSs, in FR2 alternative technologies to the ones typically implemented by the legacy communication terminals (e.g. single beam VSAT) will have to considered. Here multi-beam antenna (one beam continuously dedicated to the traffic link and another or more beam(s) to capture other non-traffic signals) or multi-LNB technologies have, for example, been investigated, and the resulting PNT performance quantified. Based on those high-level statements, it can be stated that enabling PNT for a communication terminal requires mild modification in FR1, while those modifications are more constraining in FR2.

Based on those outcomes the following future tasks have been identified in the continuity of the current work:
- Explore alternative schemes to improve FoA accuracy obtained from 5G NTN PRS and Starlink PSS, for example by enhancing PRS density in the radio frame (relevant for 5G NTN), or by exploiting the carrier phase estimated with a PLL.
- Extend SVS when considering sequential positioning filters, either fed only with ToA and FoA measurements received from several satellites at different epochs, or when including additional measurements from sensors (barometers, IMU).
- Include other contributions (ODTS, propagation channel, RFI environment, etc.) to the UERE and UERRE budgets, also considering the architectural solution implemented for the ODTS function (e.g. LEO-PNT payload, STAN, etc.)
- Cover the signal acquisition and initiation of the filter, preferably without the support of the GNSS technology.

In parallel to those further investigations, the second phase of the HybPNT project will consist in verifying the corresponding assessments with synthetic, or real signals, processed with a SDR-based implementation of the HNT, derived from the Multi-Sensor Navigation Analysis Tool (MuSNAT).

CONFLICTS OF INTEREST

The authors declare no conflict of interest. Furthermore, the view expressed herein can in no way be taken to reflect the official opinion of the European Commission.

REFERENCES

3GPPPortal. The 3GPP Groups. (https://www.3gpp.org/)

3GPP TSG RAN WG1 Meeting #99. (2019). Discussion on performance evaluation for NTN. R1-1911858. Reno, USA, November 18 – 22, 2019

3GPP TR 38.821. (2023). 3rd Generation Partnership Project; Technical Specification Group Radio Access Network; Solutions for NR to support non-terrestrial networks (NTN) (Release 16). V16.2.0 (2023-03)

Anderson, P. (2023). TrustPoint System/Service Overview. *Workshop on Low Earth Orbit PNT Systems supporting International Committee on GNSS (ICG)*. 09 June 2023.

Benzerrouk, H., Nguyen, Q., Xiaoxing, F., Amrhar, A., Nebylov A. V., & R. Landry. (2019). Alternative PNT based on Iridium Next LEO Satellites Doppler/INS Integrated Navigation System. *2019 26th Saint Petersburg International Conference on Integrated Navigation Systems (ICINS)*, St. Petersburg, Russia, 2019, pp. 1-10, doi: 10.23919/ICINS.2019.8769440.

Betz, J.W., & Kolodziejski, K. R. (2009). Generalized theory of code tracking with an early-late discriminator part I: Lower bound and coherent processing. *IEEE Transactions on Aerospace and Electronic Systems*, 45(4), 1538–1550. https://doi.org/10.1109/TAES.2009.5310316.

Blázquez-García, R., Cristallini D., Seidel, V., Heckenbach1, J., Slavov, A., & O'Hagan, D. (2022). Experimental acquisition of Starlink satellite transmissions for passive radar applications. *In: 2022 International Conference on Radar Systems*, 2022, pp. 1–6

Blázquez-García, R., Cristallini D., Unmenhofer, M., Seidel, V., Heckenbachl, J., & O'Hagan, D. (2023). Experimental comparison of Starlink and OneWeb signals for passive radar. *in Proccedings of IEEE Radar Conference, 2023, pp. 1–6.*

Borio, D., Sokolova, N., & Lachapelle, G. (2011). Doppler measurement accuracy in standard and high-sensitivity global navigation satellite system receivers. *IET Radar, Sonar & Navigation, vol. 5, no. 6, pp. 657-665, July 2011.*

Cakaj, S. (2021). The Parameters Comparison of the Starlink LEO Satellites Constellation for Different Orbital Shells. *Front. Comms. Net., 07 May 2021, Sec. Aerial and Space Networks*

Chang, D. D., & De Weck, O. L. (2005). Basic capacity calculation methods and benchmarking for MF-TDMA and MF-CDMA communication satellites. *International Journal of Satellite Communications and Networking, 2005, 23, pp. 153-171. doi.org/10.1002/sat.812*

Claybrook, J R. (2013). Feasibility Analysis on the Utilization of the Iridium Satellite Communications Network for Resident Space Objects in Low Earth Orbit. *Theses and Dissertations*. Air Force Institute of Technology. 819. https://scholar.afit.edu/etd/819.

DataGouvFR. (2024). Carte des réseaux mobile en France métropolitaine : couverture et qualité de service. Plateforme ouverte des données publiques françaises. (src : https://www.data.gouv.fr/fr/reuses/antennes-5g-en-france/). 30 avril 2024

DecodeSystem. (2017). Iridium satellite time and location. Decode Systems. src: http://www.decodesystems.com/iridium.html.

del Peral-Rosado, J.A., López-Salcedo, J.A., Seco-Granados, G., Zanier F. & Crisci, M. (2012). Achievable localization accuracy of the positioning reference signal of 3GPP LTE. *Proceedings of the 25th International Technical Meeting of the Satellite Division of The Institute of Navigation (ION GNSS 2012), Nashville, TN, 650–659.*

Eissfeller, B., Pany, T., Dötterböck, D., & Förstner, R. (2024). A Comparative Study of LEO-PNT Systems and Concepts. *In Proceedings of the ION 2024 Pacific PNT Meeting*, Honolulu, Hawaii, April 2024, pp. 758-782. https://doi.org/10.33012/2024.19646

eoPortal. (2024). Pulsar. https://www.eoportal.org/satellite-missions/pulsar#eop-quick-facts-section. July 2024.

ETSI. (1993). Satellite Earth Stations (SES); Possible European standardisation of certain aspects of Satellite Personal Communications Networks (S-PCN). Phase 1 report. European Telecommunications Standards Institute. ETSI. 1993.

Farhangian F., & Landry, R. (2013). Multi-Constellation Software-Defined Receiver for Doppler Positioning with LEO Satellites. *Sensors*. Volume 20. Issue 20. Pages 5866. DOI: 10.3390/s20205866

FCC and Space Exploration Holdings, LLC. (2016). FCC Application Listing SAT-LOA-20161115-0011. SpaceX Non-Geostationary Satellite System. Attachment A. Internal Bureau FCC Selected Application Listing by File Number Report WR07, 15-Nov-2016.

FCC and Space Exploration Holdings, LLC. (2020). SpaceX Non-Geostationary Satellite System. Attachment A. Technical Information to Supplement Schedule S. 17 April 2020. p. 3.

FCC and Space Exploration Holdings, LLC. (2021a). LLC Request for Modification of the Authorization for the SpaceX NGSO Satellite System, IBFS File No. SAT-MOD-20200417- 00037; 2021.

FCC. (2021b). Starlink new Terminal Exhibit 1. FCC 0916-EX-ST-2021.

Gaffney, L.M., Hulkower, N.D., Klein, L., & Lam, DN. (1994). A reevaluation of selected mobile satellite communications systems: Ellipso; Globalstar, IRIDIUM and Odyssey. ESA/ESTEC February 1994. Contract N0. 9563/91/MIRE Rider 2. MTR 93B0000157

García-Molina, J. A. Wallner, S., Vazquez, C., De Pasquale, G., Del Peral-Rosado, J. A., Da Broi, G., Schmitt T., Melman, F., Parro, J. M., Soualle, F., Flochs, J. J., & Lopez-Risueno, G. (2022). Quasi-Pilot Signals: Acquisition and Fast Time Ambiguity Resolution. *In Proceedings of the 2022. 10th Workshop on Satellite Navigation Technology (NAVITEC)*, Noordwijk, The Netherlands, 5–7 April 2022.

Globalstar. (2000). Description of the Globalstar System. GS-TR-94-0001, Revision E December 07, 2000.

Graff, A.M., Blount, W. N., Iannucci, P. A., Andrews, J.G & Humphreys, T.E. (2021) Analysis of OFDM signals for ranging and communications. *Proceedings of the 34th International Technical Meeting of the Satellite Division of The Institute of Navigation (ION GNSS+ 2021) September 20 - 24, 2021.*

Graff, A. & Humphreys, T.E. (2024). Purposeful Co-Design of OFDM Signals for Ranging and Communications. *EURASIP Journal on Advances in Signal Processing*, 2024, N°1. https://doi.org/10.48550/arXiv.2309.03076

Hansen, A., Mackey, S., Wassaf, H., Shah, V., Wallischeck, E., Scarpone, C., Barzach, M. & Baskerville, E., (2021). Complementary PNT and GPS Backup Technologies Demonstration Report. US Department of Transportation. Sections 1 through 10. Office of the Assistant Secretary for Research and Technology, Department of Transportation. DOT-VNTSC-20-07

Huang, C., Qin, H., Zhao, C., & Liang, H. (2022). Phase-Time Method: Accurate Doppler Measurement for Iridium NEXT Signals. *in IEEE Transactions on Aerospace and Electronic Systems*, vol. 58, no. 6, pp. 5954-5962, Dec. 2022, doi: 10.1109/TAES.2022.3180702.

Humphreys, T. E., Iannucci, P. A., Komodromos, Z. M., & Graff, A. M. (2023). Signal structure of the Starlink Ku-band downlink. *IEEE Trans. Aerosp. Electron. Syst.*, vol. 59, no. 5, pp. 6016–6030, Oct. 2023.

Iannucci, P., & Humphreys, T. (2022). Fused Low-Earth-Orbit GNSS. *IEEE Transactions on Aerospace and Electronic Systems*, vol.60, no.4, pp.3730-3749, 2022. Doi: 10.48550/arXiv.2009.12334.

InLane Navigation Technology. (2018). Low Cost GNSS and Computer Vision Fusion for Accurate Lane Level Navigation and Enhanced Automatic Map Generation. D. 6.10, Ref. Ares(2018)4437744 - 29/08/2018, Standardization plan (final report).

ICG. (2022). Update on Frequency Band for Lunar In-Situ PNT/GNSS Constellations. International Committee on GNSS. ICG-16; Abu Dhabi. 10th Oct. 2022

ITU-R P.838-3. (2005). Specific attenuation model for rain for use in prediction methods. Recommendation. ITU-R P.838-3. International Telecommunications Union, Genf, (2005).

ITU-R M.1642-2. (2007). Methodology for assessing the maximum aggregate equivalent power flux-density at an aeronautical radionavigation service station from all radionavigation-satellite service systems operating in the 1 164-1 215 MHz band. Recommendation ITU-R M.1642-2. International Telecommunications Union, Genf, (10/2007).

ITU-R M.2219. (2011). Radionavigation-satellite service applications for the 5000-5010 MHz and 5010-5030 MHz bands. Report ITU-R M.2219. (10/2011), International Telecommunications Union, Genf, (10/2011).

ITU-R P.839-4. (2013). Rain height model for prediction methods. Recommendation. ITU-R P.839-4. International Telecommunications Union, Genf, (09/2013).

ITU-R M.1831. (2015). A coordination methodology for radionavigation-satellite service inter-system interference estimation. Recommendation ITU-R M.1831. International Telecommunications Union, Genf, (09/2015).

ITU-R P.837-7. (2017). Characteristics of precipitation for propagation modelling. Recommendation. ITU-R P.837-7. International Telecommunications Union, Genf, (06/2017).

ITU-R P.453-14. (2019). The radio refractive index: its formula and refractivity data. Recommendation. ITU-R P.453-14. International Telecommunications Union, Genf, (08/2019).

ITU-R P.676-13. (2022). Attenuation by atmospheric gases and related effects. Recommendation ITU-R P.676-13. International Telecommunications Union, Genf, (08/2022).

ITU-R P.618-14. (2023). Propagation data and prediction methods required for the design of Earth-space telecommunication systems. Recommendation ITU-R P.618-14. International Telecommunications Union, Genf, (08/2023).

Jardak, N., & Adam, R. (2023). Practical Use of Starlink Downlink Tones for Positioning. *Sensors, vol. 23, no. 6, p. 3234, 2023*.

Kassas, Z.M., Kozhaya, S., Kanj, H., Saroufim, J., Hayek, S.M., & Neinavaie M. (2023). Navigation with Multi-Constellation LEO Satellite Signals of Opportunity: Starlink, OneWeb, Orbcomm, and Iridium. *2023 IEEE/ION Position, Location and Navigation Symposium (PLANS), Monterey, CA, USA, 2023, pp. 338-343, doi: 10.1109/PLANS53410.2023.10140066*.

Kassas, Z., Khairallah, N., & Kozhaya, S. (2024). Ad astra: Simultaneous tracking and navigation with megaconstellation LEO satellites. *IEEE Aerospace and Electronic Systems Magazine PP(99):1-19*. 10.1109/MAES.2023.3267440.

Kozhaya, S., & Kassas, Z. H. (2024). LEO for Positioning, Navigation, and Timing. *ION GNSS+ 2024. September 16-20*. Baltimore, MD.

Langley, R. B. (1999). Dilution of Precision. GPS World, Vol. 10, No. 5, 1999, pp. 52-59

Leng, M., Lei, L., Razul, S. G., & See, C. M. S. (2015). Joint synchronization and localization using iridium ring alert signal. *10th International Conference on Information, Communications and Signal Processing (ICICS)*, Singapore, 2015, pp. 1-5, doi: 10.1109/ICICS.2015.7459985.

Lehtinen, A. (2002). Doppler Positioning with GPS [Master's Thesis, Tampere University of Technology]. Yumpu. https://www.yumpu.com/en/document/view/18205420/antti-lehtinen-doppler-positioning-with-gps-matematiikan-laitos.

Levanon, N. (1998). Quick position determination using 1 or 2 LEO satellites. *in IEEE Transactions on Aerospace and Electronic Systems*, vol. 34, no. 3, pp. 736-754, July 1998, doi: 10.1109/7.705883.

Levanon, N. (1999). Instant Active Positioning with One LEO Satellite. NAVIGATION, 46(2), 87–95. https://doi.org/10.1002/j.2161-4296.1999.tb02397.x

Leyva-Mayorga, I., Soret, B., Matthiesen, B., Röper, M., Wübben, D., Dekorsy, A., & Popovski, P. (2022), NGSO Constellation Design for Global Connectivity. In book: Non-Geostationary Satellite Communications Systems (pp.237-267). DOI:10.48550/arXiv.2203.16597.

Lichtenberger, C. A., Arizabaleta, M., Binder, F., Soualle, F., & Pany, T. (2024). On the Integration of Tone-Like Signals-of-Opportunity Within a Geodetic Grade GNSS SDR. *ION GNSS+ 2024*. September 16-20. Baltimore, MD.

Marathe, T., Reid, T.G.R., Neish, A., Gunning K., & Banville S. (2024). Xona PULSAR User Performance Assessment. *ION GNSS+ 2024*. September 16-20. Baltimore, MD.

Marini, J.W. (1972). Correction of Satellite Tracking Data for an Arbitrary Tropospheric Profile. Radio Science, 7, 223-231.

https://doi.org/10.1029/RS007i002p00223.

Narenthiran, K., Tafazolli, R., & Evans, B. G. (2000). Simple positioning method for location tracking in mobile satellite communications. *In Proceedings of the 18th AIAA International Communication Satellite Systems Conference*, Oakland USA, April 2000. DOI:10.2514/6.2000-1134.

Neinavaie, M., Khalife, J., & Kassas, Z. H. (2021). Doppler stretch estimation with application to tracking Globalstar satellite signals. *Proceedings of IEEE Military Communications Conference, November 2021, pp. 647–651*.

Neinavaie, M., & Kassas, Z. M. (2022). Unveiling Beamforming Strategies of Starlink LEO Satellites. *Proceedings of the 35th International Technical Meeting of the Satellite Division of The Institute of Navigation, Denver, CO, USA, Oct. 2022, pp. 2525–2531*.

Neinavaie, M., & Zaher M. Kassas. (2023). Signal Mode Transition Detection in Starlink LEO Satellite Downlink Signals. *IEEE Symposium on Position Location and Navigation (PLANS). 23-27 April 2023*.
Palacios, J., Gonzalez-Prelcic, N., Mosquera, C., Shimizu, T. & Wang, C.-H. (2021). A hybrid beamforming design for massive MIMO LEO satellite communications, 2021, arXiv:2104.11158.

Novella, A.G., Garcia -Pena, A., Macabiau, C., Martineau, A., & Ladoux P. (2022). GNSS Acquisition Thresholds for Civil Aviation GNSS Receivers. *Proceedings of the 35th International Technical Meeting of the Satellite Division of The Institute of Navigation (ION GNSS+ 2022)*. hal-04088236.

Orabi, M., Khalife J., & Kassas, Z. M. (2021). Opportunistic Navigation with Doppler Measurements from Iridium Next and Orbcomm LEO Satellites. 2021 IEEE Aerospace Conference (50100), Big Sky, MT, USA, 2021, pp. 1-9, doi: 10.1109/AERO50100.2021.9438454.

Pesyna, K.M., & Humphreys, T. E. (2013). Achieving the Cramer-Rao Lower Bound in GPS Time-of-Arrival Estimator, A Frequency Domain Weighted Least Square Estimator Approach. White Paper. The University of Texas at Austin.

Pressrelease. (2019). Globalstar and Echo Ridge Offer to Demonstrate GPS Backup Technology to Department of Transportation (src: https://www.businesswire.com/news/home/20190613005429/en/Globalstar-and-Echo-Ridge-Offer-to-Demonstrate-GPS-Backup-Technology-to-Department-of-Transportation)

Pressrelease (2020). Russia gears up for electronic warfare in space (part 2). Hendrickx, B. src: "https://www.thespacereview.com/article/4060/1". The Space Review. 02/11/2020.

Pressrelease. (2022) How the Russians tried to interfere with StarLink https://www.reddit.com/r/StarlinkEngineering/comments/ua87ep/how_the_russians_tried_to_interfere_with_starlink/?rdt=35013.

Pressrelease. (2024). China launches first satellites for Thousand Sails mega-constellation (src: https://spacenews.com/china-launches-first-satellites-for-thousand-sails-megaconstellation/). August 6, 2024

Reid, T. G. R. (2022). Launching Xona's Ravens: Commercial Satnav from LEO. Inside GNSS. 18 May 2022.

Reid, T. G. R., Gunning, K., Perkins, A.L.H., & Neish, A.M. (2023). Satellite Constellation System for Facilitating Enhanced Positioning and Nodes for User Therewith. US 2023/0120388 A1. Apr. 27, 2023

Rabinowitz, M., Parkinson, B. W., Cohen, C. E., O'Connor, M. L., & Lawrence, D. G. (1998). A system using LEO telecommunication satellites for rapid acquisition of integer cycle ambiguities. *IEEE 1998 Position Location and Navigation Symposium* (Cat. No.98CH36153), Palm Springs, CA, USA, 1998, pp. 137-145, doi: 10.1109/PLANS.1998.670034.

Satellesportal. src: https://satelles.com/

Schmitz-Peiffer, A., Stopfkuchen, L., Floch, J-J., Fernandez, A., Jorgensen, R., Eissfeller, B., Rodriguez, J.A., Wallner, S., Won, J-H., Anghileri, M., Lankl, B., Schüler, T., Balbach, O., & Colzi, E. (2009). Architecture for a future C-Band/L-Band GNSS Mission Part 2: Architecture for a future C-Band/L-Band GNSS Mission. *Inside GNSS*. July/August 2009.

Soualle, F., & Imparato, D. (2019). Preliminary Performance evaluation of positioning and timing techniques based on signals transmitted by "Mega" LEO Constellations. *ETC 2019 Toulouse*.

Tan, Z., Qin, H.L., Cong, L., & Zhao, C. (2019). New method for positioning using IRIDIUM satellite signals of opportunity.

in IEEE Access, vol. 7, pp. 83412-83423, 2019, doi: 10.1109/ACCESS.2019.2924470

Tan, Z., Qin, H., Cong, L., & Zhao, C. (2020). Positioning using iridium satellite signals of opportunity in weak signal environment. *Electronics*. Electronics 2020, Vol 9. Issue 1, page 37; 10.3390/electronics9010037.

Tufvesson, F., & Maseng, T. (1997). Pilot assisted channel estimation for OFDM in mobile cellular systems. *In Vehicular Technology Conference*, 1997, IEEE 47th, volume 3, pages 1639–1643. vol.3, May 1997. doi: 10.1109/VETEC.1997.605836.

Sayin, A., Cherniakov, M., & Antoniou, M. (2019). Passive Radar Using Starlink Transmissions: A Theoretical Study. *20th International Radar Symposium. 26-28 June 2019*, pp. 1–7

Shannon P. (2022). Leveraging a LEO Satellite Constellation for Accurate & Reliable PNT. PNTAB 27, Redondo Beach, CA. November 16, 2022.

Van Diggelen, F.S.T. (2009). A-GPS: Assisted GPS, GNSS, and SBAS, GNSS Technology and Applications Series. Artech House, March 2009.

Wang, D., Qin, H., & Huang, Z. (2023). Doppler Positioning of LEO Satellites Based on Orbit Error Compensation and Weighting. *IEEE Transactions on Instrumentation and Measurement, vol. 72, pp. 1-11, 2023, Art no. 5502911, doi: 10.1109/TIM.2023.3286001*

Wei, Q. H., Chen, X., & Zhan, Y. F. (2020). Exploring implicit pilots for precise estimation of LEO satellite downlink doppler frequency. *in IEEE Communications Letters*, vol. 24, no. 10, pp. 2270-2274, Oct. 2020, doi: 10.1109/LCOMM.2020.3003791

Won, J. H., Pany, T., & Eissfeller, B. (2012). Characteristics of kalman filters for GNSS signal tracking loop. *IEEE Transactions on Aerospace and Electronic Systems*, 48(4), 3671-3681. Article 6324756. https://doi.org/10.1109/TAES.2012.6324756.

Zhang, X., Zhan, X., Huang, J., Liu, J., & Y. Xiao (2024). Weiss–Weinstein Bound of Frequency Estimation Error for Very Weak GNSS Signals. *NAVIGATION: Journal of the Institute of Navigation*, 2024, № 3, p. navi.654. https://doi.org/10.33012/navi.654

APPENDIX POSITIONING ALGORITHMS

A.1 Generalized Position Equation for Single Point Positioning

The weighted least square (WLS) positioning solution, for example obtained after convergence of the Levenberg-Marquardt algorithm, is the most widely spread technique for single point positioning (SPP) exploiting broadcast GNSS ranging signals. As such, the literature provides an extensive number of references describing in details applicability and boundaries of this algorithm family. The intention of this section is therefore not to repeat such developments but rather to re-use the formalism and to broaden it for the different standalone or hybridized positioning scenarios.

The Equation (1), called position equation, obtained after linearisation of the pseudo-range (PR) measurement equation, relates the N PR residuals, $\Delta\rho_{UT}^{Sat_n}$, where N designates the number of ranging satellites, the state vector $\underline{S}$ comprising the residuals for the different UT parameters to be estimated and the measurement noise, $\underline{\varepsilon}$. Here, the matrix $\underline{H}$, called geometry or design matrix, is a key parameter building the bridge between ranging and positioning accuracy. This equation has been developed in the particular case of GNSSs or dedicated LEO-PNT systems broadcasting one-way-range (OWR) signals, from which ToA can be estimated. It also assumes that the UT has access to the time of transmission (for example disseminated in the navigation message). In that case, $\underline{S}$ comprises the 3 cartesian coordinates and clock offset of the UT.

$$\Delta \underline{\rho}_{UT} = \begin{bmatrix} \Delta \rho_{UT}^{Sat_1} \\ \Delta \rho_{UT}^{Sat_2} \\ . \\ \Delta \rho_{UT}^{Sat_N} \end{bmatrix} = \underline{\underline{H}} \begin{bmatrix} \Delta x_{UT} \\ \Delta y_{UT} \\ \Delta z_{UT} \\ c_0 b_{UT} \end{bmatrix} + \begin{bmatrix} \varepsilon_{\rho,Sat_1} \\ \varepsilon_{\rho,Sat_2} \\ . \\ \varepsilon_{\rho,Sat_n} \end{bmatrix} = \underline{\underline{H}} \cdot \underline{S} + \underline{\varepsilon}_{OWR} \qquad (1)$$

Besides OWR based positioning, Doppler positioning represents an important differentiator between LEO-PNT systems and GNSSs, as a direct consequence of the larger spacecraft velocity. One-way doppler (OWD) positioning allows deriving UT position from the Doppler measurements, which is primarily materialised by an offset of the received signal frequency due to relative velocity between UT and satellite (a second effect of Doppler is the compression or dilatation of the signal waveform for wideband signals as explained in Neinavaie et al., (2021)). The principle of Doppler positioning is well described, for instance, in Lehtinen (2002). Equation (2) provides the position equation for OWD positioning involving an equivalent design matrix, $\underline{\underline{G}}$, the N residuals of the range-rate $\Delta \dot{\rho}_{UT}^{Sat_n}$, the measurement noise, $\varepsilon_{\dot{\rho}}$, and finally the state vector $\underline{S}$ where the UT clock offset of OWR has been replaced with UT clock drift. It is noted that the derivation of this equation is obtained by neglecting the relative UT velocity w.r.t. satellite one, but also the UT clock acceleration, as explained in Wang et al., (2023).

$$\Delta \underline{\dot{\rho}}_{UT} = \begin{bmatrix} \Delta \dot{\rho}_{UT}^{Sat_1} \\ \Delta \dot{\rho}_{UT}^{Sat_2} \\ . \\ \Delta \dot{\rho}_{UT}^{Sat_N} \end{bmatrix} = \underline{\underline{G}} \begin{bmatrix} \Delta x_{UT} \\ \Delta y_{UT} \\ \Delta z_{UT} \\ c_0 \Delta \dot{b}_{UT} \end{bmatrix} + \begin{bmatrix} \varepsilon_{\dot{\rho},Sat_1} \\ \varepsilon_{\dot{\rho},Sat_2} \\ . \\ \varepsilon_{\dot{\rho},Sat_n} \end{bmatrix} = \underline{\underline{G}} \cdot \underline{S} + \underline{\varepsilon}_{OWD} \qquad (2)$$

Once expressed in a matrix form, the position equation derived in the OWR or OWD based positioning for cooperative PNT systems can be generalised when combining OWR and OWD, but also for different cooperative or opportunistic PNT scenarios applied to standalone or hybridised systems. The terms of the generalised position equation are synthetised in **TABLE 14**. To simplify notation the residuals for the UT states are expressed with the Δ prefix (e.g. x_{UT} in place of Δx_{UT}). Furthermore, to ease readability the design matrix $\underline{\underline{G}}$ derived for OWD is now also called $\underline{\underline{H}}$ (but with appropriate definition).

The following assessments justify the corresponding expressions but also the introduction of additional parameters (essentially related to timing).

• For standalone and opportunistic positioning, the UT cannot demodulate the LEO signal to access the transmission time. This situation is similar to snapshot GNSS positioning, for which another 5th unknown, with the synchronization error between UT and (GNSS) system time T_{Sys} has to be introduced, as explained in Van Diggelen (2009). The impact of a synchronization error expressed in seconds onto the pseudo-range for a LEO satellite observed with a radial velocity v_{rad}^{Sat} equals $v_{rad}^{Sat} \cdot T_{Sys}$ can reach several kilometres. Similar, it is shown in Wang et al., (2023) that the effect of the synchronization error onto the pseudo-range rate, proportional to the Doppler, is expressed as $a_{rad}^{Sat} \cdot T_{Sys}$, and where a_{rad}^{Sat} represents the satellite radial acceleration. Therefore, for opportunistic positioning the 5th unknown, called T_{SOoP}, reusing Wang et al., (2023) terminology, will complete the UT state vector.

• When hybridizing two LEO systems not sharing the same system time, a system time offset, playing the same role as the Galileo-to-GPS time offset (GGTO) has to be further included in the UT state vector. This offset is called LEO-LEO Time Offset (LLTO) in a LEO-PNT, or Alt-LEO-PNT context.

• An equivalent frequency offset will apply when hybridizing PNT systems for Doppler positioning, and is called LEO-LEO frequency offset (LLFO). It is worth noting that for cooperative and dedicated LEO-PNT systems (either with multi-tier or alternative architecture), the system time can be considered stable on a long-term scale, and the LLFO could be assumed as constant over a long period of time. This might be different for LEO-COM systems for which long term stability is not required.

• The generalized position equation, applicable for SPP, does not strictly apply in the particular case when the UT also estimates the satellite states (position, clock offset and drift) atop its own states. Here a dynamic filter known as STAN has been successfully experimented on the Starlink, Iridium, OneWeb and Orbcom systems. However, and in order to still anticipate SPP performance, the following CONOPS for an opportunistic UT implementing the STAN is proposed. In a first phase, both UT and satellites states are estimated with the STAN. A prediction model for the satellite orbit and clock, similar to the ones present in the navigation message of GNSS or dedicated LEO-PNT, is generated and applicable during a second phase. During this second phase the UT uses the information of the internally generated prediction model to correct the pseudo-range or pseudo-range rate. It is assumed that duration of the first phase is smaller than the one of the second phase (for example taking place during the first

quarter of the LEO satellite visibility window). For this specific CONOPS and during the second phase, the SPP becomes applicable and authorises exploitation of the generalized position equation.

TABLE 14: Different forms of the generalised position equation for OWR and/or OWD for standalone/hybridized PNT systems

Scenario	PR Equation	State Vector, $\underline{S}$	Design Matrix, $\underline{\underline{H}}$
Stand. Coop OWR	$\Delta\underline{\rho}_{UT}=\underline{\underline{H}}.\underline{S}+\underline{\varepsilon}_{OWR}$	$[x_{UT}, y_{UT}, z_{UT}, b_{UT}]^T$	$[\underline{\underline{U}} \quad -\underline{1}_{n\times1}]$
Stand. Coop OWD	$\Delta\underline{\dot{\rho}}_{UT}=\underline{\underline{H}}.\underline{S}+\underline{\varepsilon}_{OWD}$	$[x_{UT}, y_{UT}, z_{UT}, d_{UT}]^T$	$[\underline{\underline{V}} \quad -\underline{1}_{n\times1}]$
Stand. Coop OWR+OWD	$\begin{bmatrix}\Delta\underline{\rho}_{UT}\\\Delta\underline{\dot{\rho}}_{UT}\end{bmatrix}=\underline{\underline{H}}.\underline{S}+\begin{bmatrix}\underline{\varepsilon}_{OWR}\\\underline{\varepsilon}_{OWD}\end{bmatrix}$	$[x_{UT}, y_{UT}, z_{UT}, b_{UT}, d_{UT}]^T$	$\begin{bmatrix}\underline{\underline{U}} & -\underline{1}_{n\times1} & \underline{0}_{n\times1}\\\underline{\underline{V}} & \underline{0}_{n\times1} & -\underline{1}_{n\times1}\end{bmatrix}$
Stand. SooP OWR	$\Delta\underline{\rho}_{UT}==\underline{\underline{H}}.\underline{S}+\underline{\varepsilon}_{OWR}$	$[x_{UT}, y_{UT}, z_{UT}, b_{UT}, T_{Soop}]^T$	$[\underline{\underline{U}} \quad -\underline{1}_{n\times1} \quad \underline{P}_{n\times1}]$
Stand. SooP OWD	$\Delta\underline{\dot{\rho}}_{UT}=\underline{\underline{H}}.\underline{S}+\underline{\varepsilon}_{OWD}$	$[x_{UT}, y_{UT}, z_{UT}, d_{UT}, T_{Soop}]^T$	$[\underline{\underline{U}} \quad -\underline{1}_{n\times1} \quad \underline{A}_{n\times1}]$
Stand. SooP OWR+OWD	$\begin{bmatrix}\Delta\underline{\rho}_{UT}\\\Delta\underline{\dot{\rho}}_{UT}\end{bmatrix}=\underline{\underline{H}}.\underline{S}+\begin{bmatrix}\underline{\varepsilon}_{OWR}\\\underline{\varepsilon}_{OWD}\end{bmatrix}$	$[x_{UT}, y_{UT}, z_{UT}, b_{UT}, d_{UT}, T_{Soop}]^T$	$\begin{bmatrix}\underline{\underline{U}} & -\underline{1}_{n\times1} & \underline{0}_{n\times1} & \underline{P}_{n\times1}\\\underline{\underline{V}} & \underline{0}_{n\times1} & -\underline{1}_{n\times1} & \underline{A}_{n\times1}\end{bmatrix}$
Hybrid. Coop OWR	$\Delta\underline{\rho}_{UT}=\underline{\underline{H}}.\underline{S}+\underline{\varepsilon}_{OWR}$	$[x_{UT}, y_{UT}, z_{UT}, b_{UT}, T_{LLTO}]^T$	$\begin{bmatrix}\underline{\underline{U}}_{n_1} & -\underline{1}_{n_1\times1} & \underline{0}_{n_1\times1}\\\underline{\underline{U}}_{n_2} & -\underline{1}_{n_2\times1} & -\underline{1}_{n_2\times1}\end{bmatrix}$
Hybrid. Coop OWD	$\Delta\underline{\dot{\rho}}_{UT}=\underline{\underline{H}}.\underline{S}+\underline{\varepsilon}_{OWD}$	$[x_{UT}, y_{UT}, z_{UT}, d_{UT}, F_{LLFO}]^T$	$\begin{bmatrix}\underline{\underline{V}}_{n_1} & -\underline{1}_{n_1\times1} & \underline{0}_{n_1\times1}\\\underline{\underline{V}}_{n_2} & -\underline{1}_{n_2\times1} & -\underline{1}_{n_2\times1}\end{bmatrix}$
Hybrid. Coop OWR+OWD	$\begin{bmatrix}\Delta\underline{\rho}_{UT}\\\Delta\underline{\dot{\rho}}_{UT}\end{bmatrix}=\underline{\underline{H}}.\underline{S}+\begin{bmatrix}\underline{\varepsilon}_{OWR}\\\underline{\varepsilon}_{OWD}\end{bmatrix}$	$[x_{UT}, y_{UT}, z_{UT}, b_{UT}, T_{LLTO}, d_{UT}, F_{LLFO}]^T$	$\begin{bmatrix}\underline{\underline{U}}_{n_1} & -\underline{1}_{n_1\times1} & \underline{0}_{n_1\times1} & \underline{0}_{n_1\times1} & \underline{0}_{n_1\times1}\\\underline{\underline{U}}_{n_2} & -\underline{1}_{n_2\times1} & -\underline{1}_{n_2\times1} & \underline{0}_{n_2\times1} & \underline{0}_{n_2\times1}\\\underline{\underline{V}}_{n_1} & \underline{0}_{n_1\times1} & \underline{0}_{n_1\times1} & -\underline{1}_{n_1\times1} & \underline{0}_{n_1\times1}\\\underline{\underline{V}}_{n_2} & \underline{0}_{n_2\times1} & \underline{0}_{n_2\times1} & -\underline{1}_{n_2\times1} & -\underline{1}_{n_2\times1}\end{bmatrix}$
Hybrid. SooP OWR	$\Delta\underline{\rho}_{UT}==\underline{\underline{H}}.\underline{S}+\underline{\varepsilon}_{OWR}$	$[x_{UT}, y_{UT}, z_{UT}, b_{UT}, T_{Soop}, T_{LLTO}]^T$	$\begin{bmatrix}\underline{\underline{U}}_{n_1} & -\underline{1}_{n_1\times1} & \underline{P}_{n_1\times1} & \underline{0}_{n_1\times1}\\\underline{\underline{U}}_{n_2} & -\underline{1}_{n_2\times1} & \underline{P}_{n_2\times1} & -\underline{1}_{n_2\times1}\end{bmatrix}$
Hybrid. SooP OWD	$\Delta\underline{\dot{\rho}}_{UT}=\underline{\underline{H}}.\underline{S}+\underline{\varepsilon}_{OWD}$	$[x_{UT}, y_{UT}, z_{UT}, d_{UT}, T_{Soop}, F_{LLFO}]^T$	$\begin{bmatrix}\underline{\underline{V}}_{n_1} & -\underline{1}_{n_1\times1} & \underline{A}_{n_1\times1} & \underline{0}_{n_1\times1}\\\underline{\underline{V}}_{n_2} & -\underline{1}_{n_2\times1} & \underline{A}_{n_2\times1} & -\underline{1}_{n_2\times1}\end{bmatrix}$
Hybrid. SooP OWR+OWD	$\begin{bmatrix}\Delta\underline{\rho}_{UT}\\\Delta\underline{\dot{\rho}}_{UT}\end{bmatrix}=\underline{\underline{H}}.\underline{S}+\begin{bmatrix}\underline{\varepsilon}_{OWR}\\\underline{\varepsilon}_{OWD}\end{bmatrix}$	$[x_{UT}, y_{UT}, z_{UT}, b_{UT}, T_{LLTO}, d_{UT}, F_{LLFO}, T_{Soop}]^T$	$\begin{bmatrix}\underline{\underline{U}}_{n_1} & -\underline{1}_{n_1\times1} & \underline{0}_{n_1\times1} & \underline{0}_{n_1\times1} & \underline{0}_{n_1\times1} & \underline{P}_{n_1\times1}\\\underline{\underline{U}}_{n_2} & -\underline{1}_{n_2\times1} & -\underline{1}_{n_2\times1} & \underline{0}_{n_2\times1} & \underline{0}_{n_2\times1} & \underline{P}_{n_2\times1}\\\underline{\underline{V}}_{n_1} & \underline{0}_{n_1\times1} & \underline{0}_{n_1\times1} & -\underline{1}_{n_1\times1} & \underline{0}_{n_1\times1} & \underline{A}_{n_1\times1}\\\underline{\underline{V}}_{n_2} & \underline{0}_{n_2\times1} & \underline{0}_{n_2\times1} & -\underline{1}_{n_2\times1} & -\underline{1}_{n_2\times1} & \underline{A}_{n_2\times1}\end{bmatrix}$

The terms and components present in the different variants of the design matrix are defined as follows:

- n_1 and n_2 represents the number of exploitable lines of sights for the LEO-PNT systems 1 and 2.
- $\underline{0}_{n\times1}$ (resp. $\underline{1}_{n\times1}$) designates a column vector comprising n zeros (resp. ones).

- $\underline{\varepsilon}_{OWR}$ designates the vector of the measurements noise for the range : $\underline{\varepsilon}_{OWR} = \begin{bmatrix} \varepsilon_{\rho,Sat_1} \\ \varepsilon_{\rho,Sat_2} \\ . \\ \varepsilon_{\rho,Sat_n} \end{bmatrix}$, while $\underline{\varepsilon}_{OWD}$ designates the vector of the

measurements noise for the range-rate: $\underline{\varepsilon}_{OWD} = \begin{bmatrix} \varepsilon_{\dot{\rho},Sat_1} \\ \varepsilon_{\dot{\rho},Sat_2} \\ . \\ \varepsilon_{\dot{\rho},Sat_n} \end{bmatrix}$

- The vector, $\overrightarrow{u_{Sat_i}}$, represents the unit vector between the UT and the satellite, i: $\overrightarrow{u_{Sat_i}} = \frac{\overrightarrow{X_{Sat_i}} - \overrightarrow{X_{UT}}}{\|\overrightarrow{X_{Sat_i}} - \overrightarrow{X_{UT}}\|}$

- The vector $\underline{P}$ comprises the n relative radial velocities, while the vector $\underline{A}$ comprises the n relative radial accelerations:

$$\underline{P} = \begin{bmatrix} (\overrightarrow{u_{Sat_1}}).(\overrightarrow{V_{Sat_1}} - \overrightarrow{V_{UT}}) \\ (\overrightarrow{u_{Sat_2}}).(\overrightarrow{V_{Sat_2}} - \overrightarrow{V_{UT}}) \\ . \\ (\overrightarrow{u_{Sat_n}}).(\overrightarrow{V_{Sat_n}} - \overrightarrow{V_{UT}}) \end{bmatrix}_{n\times 1} \text{ and } \underline{A} = \begin{bmatrix} (\overrightarrow{u_{Sat_1}}).(\overrightarrow{A_{Sat_1}} - \overrightarrow{A_{UT}}) \\ (\overrightarrow{u_{Sat_2}}).(\overrightarrow{A_{Sat_2}} - \overrightarrow{A_{UT}}) \\ . \\ (\overrightarrow{u_{Sat_n}}).(\overrightarrow{A_{Sat_n}} - \overrightarrow{A_{UT}}) \end{bmatrix}_{n\times 1}$$

- Finally the matrices $\underline{\underline{U}}$ and $\underline{\underline{V}}$ combines respectively, the partial derivatives of range and delta-ranges (see Lehtinen (2002)):

$$\underline{\underline{U}} = \begin{bmatrix} \frac{(\overrightarrow{X_{Sat_1}} - \overrightarrow{X_{UT}})^T}{\|\overrightarrow{X_{Sat_1}} - \overrightarrow{X_{UT}}\|} \\ \frac{(\overrightarrow{X_{Sat_2}} - \overrightarrow{X_{UT}})^T}{\|\overrightarrow{X_{Sat_2}} - \overrightarrow{X_{UT}}\|} \\ . \\ \frac{(\overrightarrow{X_{Sat_n}} - \overrightarrow{X_{UT}})^T}{\|\overrightarrow{X_{Sat_n}} - \overrightarrow{X_{UT}}\|} \end{bmatrix}_{n\times 4} \text{ and } \underline{\underline{V}} = \begin{bmatrix} \left\{ \overrightarrow{u_{Sat_1}} \times \left(\overrightarrow{u_{Sat_1}} \times \frac{\|\overrightarrow{V_{Sat_1}} - \overrightarrow{V_{UT}}\|}{\|\overrightarrow{X_{Sat_1}} - \overrightarrow{X_{UT}}\|} \right) \right\}^T \\ \left\{ \overrightarrow{u_{Sat_2}} \times \left(\overrightarrow{u_{Sat_2}} \times \frac{\|\overrightarrow{V_{Sat_2}} - \overrightarrow{V_{UT}}\|}{\|\overrightarrow{X_{Sat_2}} - \overrightarrow{X_{UT}}\|} \right) \right\}^T \\ . \\ \left\{ \overrightarrow{u_{Sat_n}} \times \left(\overrightarrow{u_{Sat_n}} \times \frac{\|\overrightarrow{V_{Sat_n}} - \overrightarrow{V_{UT}}\|}{\|\overrightarrow{X_{Sat_n}} - \overrightarrow{X_{UT}}\|} \right) \right\}^T \end{bmatrix}_{n\times 4}$$

The availability of the SPP solution directly depends on the minimal number of satellites providing each, either ToA, FoA or both. The condition imposed by the observability equation states that the number of independent measurements (N_{Meas}) needs to be at least larger than the number of unknown parameters (N_{Param}) to be estimated. When hybridizing two systems, simulations showed that a further observability condition applies to the minimal number of independent measurements obtained from a specific LEO-PNT system when compared to the number of unknows specific to that system. Taking the example of the hybridization between a cooperative LEO-system and an opportunistic one and for a ToA based positioning, 4 unknowns (x_{UT}, y_{UT}, z_{UT}, b_{UT}) are common to both, while T_{Soop}, T_{LLTO} are specific to the introduction of the second system. Therefore at least 2 ToAs from the second LEO-system (and 4 ToA from first one) are necessary to ensure estimation of the 6 unknowns (in other words having 5 ToA from the first LEO-system and only 1 from the second one would not lead to the solution even if the overall number of unknowns equals 6). It is noted that the observability condition only infers about the existence but not the accuracy of the solution, which essentially depends on the ToA and FoA accuracies, and geometrical distribution of the satellites w.r.t. UT. **TABLE 15** provides the canonical SPP configurations based on ToA-, FoA-, or ToA&FoA, for both standalone or hybridized scenarios, also distinguishing opportunistic or cooperative positioning.

TABLE 15: Observability Requirements for Single Point Positioning

Single Point Algorithm	Observable		Standalone				Hybridized			
	Type	$N_{Meas/Sat}$	State	N_{Param}	$N_{Sat,min,obs}$	N_{Meas}	State	N_{Param}	$N_{Sat,min,obs}$	N_{Meas}
One-Way Range (OWR)	ToA	1	UT Pos, Clock Bias, (+T_SoOP[4])	4 $5^{(4)}$	**4** $\mathbf{5^{(4)}}$	4 $5^{(4)}$	UT Pos, UT Clock Bias, **LLTO,** (+T_SoOP[4])	5 $6^{(4)}$	**5** $\mathbf{6^{(4)}}$	5 $6^{(4)}$
One-Way Doppler (OWD)	FoA	1	UT Pos, Vel, Clock Drift, (+T_SoOP[4])	7 $8^{(4)}$	**7** $\mathbf{8^{(4)}}$	7 $8^{(4)}$	UT Pos, Vel, Clock Drift, **LLFO,** (+T_SoOP[4])	8 $9^{(4)}$	**8** $\mathbf{9^{(4)}}$	8 $9^{(4)}$
Simplified[1] OWD	FoA	1	UT Pos, Clock Drift, (+T_SoOP[4])	4 $5^{(4)}$	**4** $\mathbf{5^{(4)}}$	4 $5^{(4)}$	UT Pos, Clock Drift, **LLFO,** (+T_SoOP[4])	5 $6^{(4)}$	**5** $\mathbf{6^{(4)}}$	5 $6^{(4)}$
OWR + OWD[2]	ToA FoA	$2^{(3)}$	UT Pos, UT Vel, Clock Bias, Clock Drift, (+T_SoOP[4])	8 $9^{(4)}$	**4** $\mathbf{5^{(4)}}$	8 $10^{(4)}$	UT Pos, UT Vel, Clock Bias, Clock Drift, **LLTO, LLFO,** (+T_SoOP[4])	10 $11^{(4)}$	**5** $\mathbf{6^{(3)(4)}}$	10 $12^{(4)}$
OWR + Simplified[1, 2] OWD	ToA FoA	$2^{(3)}$	UT Pos, Clock Bias, Clock Drift, (+T_SoOP[4])	5 $6^{(4)}$	**3** $\mathbf{3^{(4)}}$	6 $6^{(4)}$	UT Pos, Clock Drift, **LLTO, LLFO,** (+T_SoOP[4])	7 $8^{(4)}$	$\mathbf{4^{(3)}}$ $\mathbf{4^{(3)(4)}}$	8 $8^{(4)}$
Notes		**(1):** User Velocity neglected w.r.t. Satellite one **(2):** All systems permit providing one ToA and one FoA per satellite (Starlink: ToA+FoA from PSS, 5G NTN: ToA+FoA from PRS, LEO-PNT: ToA+FoA from Pilot, Iridium: ToA+FoA from Burst Header). Exception applies to FoA only derived from the tone of Starlink signals, and ToA only derived from Pilot component. **(3):** When hybridizing Globalstar offering only FoA in opportunistic way, with other LEO Systems (Iridium, LEO-PNT or 5G NTN FR1), observability equation becomes $N_{Sat,Globalstar}+2\times N_{Sat,LEO}\geq 11$ (OWR+OWD), or 8 (OWR+OWD Simplified **(4):** T_{Soop} synchronization time offset introduced for all opportunistic scenarios **(5):** $N_{Meas} = N_{Sat} \times N_{Meas/Sat}$ and $N_{Meas} \geq N_{Param}$.								

As stated beforehand, the design matrix comprises the geometrical information for the different LoS involved in the SPP. Its exploitation permits expressing the positioning performance as function of the ToA or FoA accuracy. In the case of OWR and assuming a constant ToA accuracy, σ_{TOA}, the covariance $\underline{C_S}$ of the state estimation error can be expressed by Equation (3). Here an important Figure of Merit called dilution of precision (DOP), deeply analysed in Langley (1999), is given by Equation (4). A similar relationship presented with Equation (5), exists between the covariance $\underline{C_S}$ and the FoA accuracy σ_{FoA}. Here, the proportionality factor, is called Doppler dilution of precision DDOP, and is built with the design matrix $\underline{\mathbf{G}}$ derived for OWD, as explained in Lehtinen (2002).

$$\underline{C}_S = \underline{\underline{DOP}} \cdot \sigma_{ToA}^2 \tag{3}$$

$$\underline{\underline{DOP}} = \left(\underline{H}^T \underline{H}\right)^{-1} \tag{4}$$

$$\underline{C}_S = \underline{\underline{DDOP}} \cdot \sigma_{FoA}^2 \tag{5}$$

$$\underline{\underline{DOP}} = \left(\underline{G}^T \underline{G}\right)^{-1} \tag{6}$$

A.2 Atmospheric Contributions to Link Budget
Three main atmospheric contributions are considered for the link budget, with the rain attenuation, the Gaz absorption and finally the scintillations. Their quantitative evaluations have been enabled thanks to well-established ITU models summarized in **TABLE 16**. Digital maps providing the rain heigh (ITU-R P.839-4. (2013)) or the rainfall rate exceeded for 0.01% of an average year (ITU-R P.837-7. (2017)) supporting model evaluations have also been applied.

TABLE 16: ITU models for Atmospheric Contributions to Link Budget

Contribution	ITU Model
Rain Attenuation	ITU-R P.618-14 (2023)
	ITU-R P.837-7 (2013)
	ITU-R P.838-3 (2005)
Gaz Absorption	ITU-R P.676-13 (2022)
Scintillations	ITU-R P.453-14 (2019)

Notes: • The percentage p that the rain fall rate will exceeds over a yearly period is an important parameter dimensioning the link budget. The rain attenuation [dB] will increase with decreasing p. For the simulations, p is set to 0.01% (typical value).

• The ITU models are not applied for 5G NTN link budget calculations as 3GPP notes provide directly those values.

A.3 Thermal Noise Contribution to the Measurement Accuracy

A short compendium of analytical expressions enabling the evaluation of the ToA and FoA estimation accuracy is now proposed for the studied systems and signal processing scenarios. One of the most spread analytical expression used to derive those accuracy levels is the Cramèr-Rao Lower Bound (CRLB) providing the lowest estimation error level for an unbiased estimator (see Zhang et al., (2024)). The generic form of the CRLB shows that the estimator variance is inversely proportional to the signal-to-noise power ratio (SNR) evaluated over the coherent processing time, T_{int}. CRLB typically applies for block processing techniques aiming at estimating the ToA or FoA from matched filters applied to the signal snapshots. Similar analytical expressions to the CRLB have also been developed when applying tracking loop techniques (either for ToA estimation with delay lock loops (DLL), or FoA estimation with frequency lock loop (FLL), in which case additional configuration parameters, such as the closed loop bandwidth have to be accounted. As far as the FoA estimation is concerned two main situations are distinguished. The first one applies when estimating the carrier frequency of unmodulated tones (cases of Starlink or Iridium systems). The second one applies when estimating the carrier frequency of modulated signals, in which case the estimation is applied after wiping-off of the signal waveform (PRN sequence of LEO-PNT CDMA, or PSS of Starlink, or PRS sub-carriers for OFDM).

• **Analytical Expressions for Range Estimation Accuracy:**

Block Processing CDMA (see Pesyna et al., (2013))	Block Processing OFDM: (see del Peral-Rosado et al., (2012))	Loop CDMA (see Betz et al., (2009))
$$\sigma_{\text{PSR}}[m] = c_0 \sqrt{\frac{SL}{2(2\pi)^2 I_5 T_{int}\left(\frac{C}{N_0}\right)_{\text{eff}}}}$$ (7)	$$\sigma_i^2[m] \geq \text{CRB}(\tau_i)$$ $$= \frac{c_0^2}{8\pi^2 \cdot F_{\text{sc}}^2 \cdot \text{SNR}_i \cdot N_{\text{symb}} \cdot \sum_{n \in \mathcal{N}_{\text{PRS}}} p_n^2 \cdot n^2}$$ (8)	$$\sigma_{\text{DLL}}[m] = c_0 \sqrt{\frac{B_{DLL}\,(1 - 0.25 B_{DLL}\, T_{int}) I_1}{(2\pi)^2 \left(\frac{C_s}{N_0}\right)_{\text{eff}} I_2}\left[1 + \frac{I_3}{T_{int}\left(\frac{C}{N_0}\right)_{\text{eff}} I_4}\right]}$$ (9)
$$I_5 \doteq \frac{\int_{-\frac{B_{\text{RX}}}{2}}^{\frac{B_{\text{RX}}}{2}} \Gamma(f) f^2 df}{\int_{-\frac{B_{\text{RX}}}{2}}^{\frac{B_{\text{RX}}}{2}} \Gamma(f) df} \qquad (10)$$ • c_0 : Lightspeed [m/s] • f_0 : Carrier Frequency [Hz] • T_{Int}: Coherent Integration Time [s] • $\left(\frac{C}{N_0}\right)_{\text{eff}}$: Effective Signal-to-Noise PSD Ratio [Hz] • $SL \doteq 1 + \frac{1}{T_{int}\left(\frac{C}{N_0}\right)_{\text{eff}}}$: Squaring Losses reflecting the variance increase due to non-coherent processing • $\Gamma(f)$: PSD of the (ranging) signal normalised over the transmitted bandwidth	• c_0 : Lightspeed [m/s] • f_{SC}: OFDM subcarrier spacing [Hz] • SNR_i: Signal-to-Noise Power Ratio [-] • N_{Symb}: Number of PRS Symbol • $\mathcal{N}_{\text{PRS}}$: Subset of PRS Pilot Sub-Carrier • p_n^2: Relative power weight of subcarrier n.	$$I_1 \doteq \int_{-\frac{B_{\text{RX}}}{2}}^{\frac{B_{\text{RX}}}{2}} \Gamma(f) \sin^2(\pi f \Delta T_c) df$$ $$I_2 \doteq \left(\int_{-\frac{B_{\text{RX}}}{2}}^{\frac{B_{\text{RX}}}{2}} f \cdot \Gamma(f) \sin(\pi f \Delta T_c) df\right)^2$$ $$I_3 \doteq \int_{-\frac{B_{\text{RX}}}{2}}^{\frac{B_{\text{RX}}}{2}} \Gamma(f) \cos^2(\pi f \Delta T_c) df$$ $$I_4 \doteq \left(\int_{-\frac{B_{\text{RX}}}{2}}^{\frac{B_{\text{RX}}}{2}} \Gamma(f) \cos(\pi f \Delta T_c) df\right)^2$$ • c_0 : Lightspeed [m/s] • T_{Int}: Coherent Integration Time [s] • Δ: Early-Late Spacing [Chip] • T_c: Chip Duration • B_{Rx}: Two-Sided bandwidth of receiver front-end

TABLE 17: Analytical expressions for ToA estimation accuracy for block processing or DLL applied to CDMA or OFDM signals

- **Analytical expressions for Range-Rate Estimation Accuracy:**

Block Processing for Tone (see Borio et al., (2011)	Block Processing CDMA	Loop CDMA (see Borio et al., (2011)
$$\sigma_f\left[\frac{m}{s}\right] = \left(\frac{c_0}{f_0}\right)\frac{1}{2\pi T_{int}}\sqrt{\frac{\frac{6}{T_{int}}}{\left(\frac{C}{N_0}\right)_{eff}} \cdot \frac{N_{samp}^2}{N_{samp}^2 - 1}}$$ (11)	$$\sigma_v\left[\frac{m}{s}\right] = \left(\frac{c_0}{f_0}\right)\frac{1}{T_{PRN}}\sqrt{\frac{3}{2\pi^2 T_{int}\left(\frac{T_{coh}^2}{T_{PRN}^2} - 1\right)\left(\frac{C}{N_0}\right)_{eff}}}$$ (12)	$$\sigma_{FLL}^{\dot{\theta}}\left[\frac{m}{s}\right] = \left(\frac{c_0}{f_0}\right)\frac{1}{2\pi v_{PSP}T_{int}}\sqrt{\frac{4FB_{FLL}}{\left(\frac{C}{N_0}\right)_{eff}}\left(1 + \frac{1}{T_{int}\left(\frac{C}{N_0}\right)_{eff}}\right)}$$ (13)
- c_0 : Lightspeed [m/s] - f_0 : Carrier Frequency [Hz] - T_{Int}: Coherent Integration Time [s] - N_{Samp}: Sample Number in Signal Snapshot [-] - $\left(\frac{C}{N_0}\right)_{eff}$: Effective Signal-to-Noise PSD Ratio [Hz]	- c_0 : Lightspeed [m/s] - f_0 : Carrier Frequency [Hz] - T_{Int}: Coherent Integration Time [s] - T_{PRN}: PRN Code Period [s] - $\left(\frac{C}{N_0}\right)_{eff}$: Effective Signal-to-Noise PSD Ratio [Hz]	- c_0 : Lightspeed [m/s] - f_0 : Carrier Frequency [Hz] - T_{Int}: Coherent Integration Time [s] - N_{Samp}: Sample Number in Signal Snapshot - B_{FLL}: Closed Loop Bandwidth - $\left(\frac{C}{N_0}\right)_{eff}$: Effective Signal-to-Noise PSD Ratio [Hz] - F: Heuristic Coefficient with (F=2 for $\left(\frac{C}{N_0}\right)_{eff} < 35$ dB-Hz, F= 1 else)

TABLE 18: Analytical expressions for FoA estimation accuracy for block processing or FLL for unmodulated (i.e. Tones) or CDMA/OFDM modulated signals (post-correlation)

The aforementioned analytical expressions applicable for DLL/FLL tracking loops assume that the ranging signal is continuously transmitted and thereof received, as for GNSS signals. However, in some scenarios, the PSP only occupies a fraction of the coherent integration time, T_{int}. This is the case of the PSS which represents only $v_{PSP}=T_{Symb}/T_{OFDM}=0.33\%$ of the Starlink frame duration, or of the PRS symbol present with roughly $v_{PSP}=0.3\%$ (resp. 0.1%) every 5G Radio frame in FR1 (resp. FR2), for high PRS Rate. For those cases, the effective $(C/N_0)_{eff}$ to be injected in the analytical expressions of Equations (9) and (13) is derived by reducing the $(C/N_0)_{PSP}$ with $10\log_{10}(v_{PSP})$ where v_{PSP} represents the PSP duty cycle.

$$\left(\frac{C}{N_0}\right)_{eff} = \left(\frac{C}{N_0}\right)_{PSP} + 10 \cdot \boldsymbol{log}_{10}(v_{PSP})$$ (14)

This equation is derived, per analogy, from the analytical expressions developed for the estimation of the effective $(C/N_0)_{eff}$ in presence of powerful pulsed RFI signals (e.g. DME/TACAN in L5/E5 bands) and after application of blanking techniques consisting in zeroing samples contaminated by the pulses, after their detection, as explained in Novella et al., (2022).

For block processing techniques, the effective $(C/N_0)_{eff}$ directly equals the $(C/N_0)_{PSP}$. Furthermore, the SNR, which is relevant to express the lower sensitivity threshold, is defined by Equation (15), and where T_{PSP} represents the PSP duration equal to the coherent integration time (e.g. $T_{int} = T_{PSP} = T_{Symb}$ for Starlink and 5G NTN cases).

$$(SNR)_{PSP} = \left(\frac{C}{N_0}\right)_{PSP} + 10 \cdot \boldsymbol{log}_{10}(T_{PSP})$$ (15)

A.4 Performance Boards for Standalone and Hybridized Scenarios

A.4.1 Introduction

This section presents so-called "KPI performance boards", showing for each use case the main retained KPI (see section 3.4) and their statistics (minimum, maximum and median) evaluated for three canonical latitudes of 0°, 30° and 45°, and two UMA of 10° and 30° (45° for the dedicated LEO-PNT). The figure showing the $(C/N_0)_{PSP}$ also includes the ToA/FoA estimator threshold applicable for loop and block processing techniques (see **TABLE 10**). The difference between this threshold and the median provides an indication on the robustness margin for the link. Similarly, the minimal number of exploitable LoS ensuring solvability of the position equation ($N_{Sat,min,obs}$) has been included to highlight the robustness margin in the position domain.
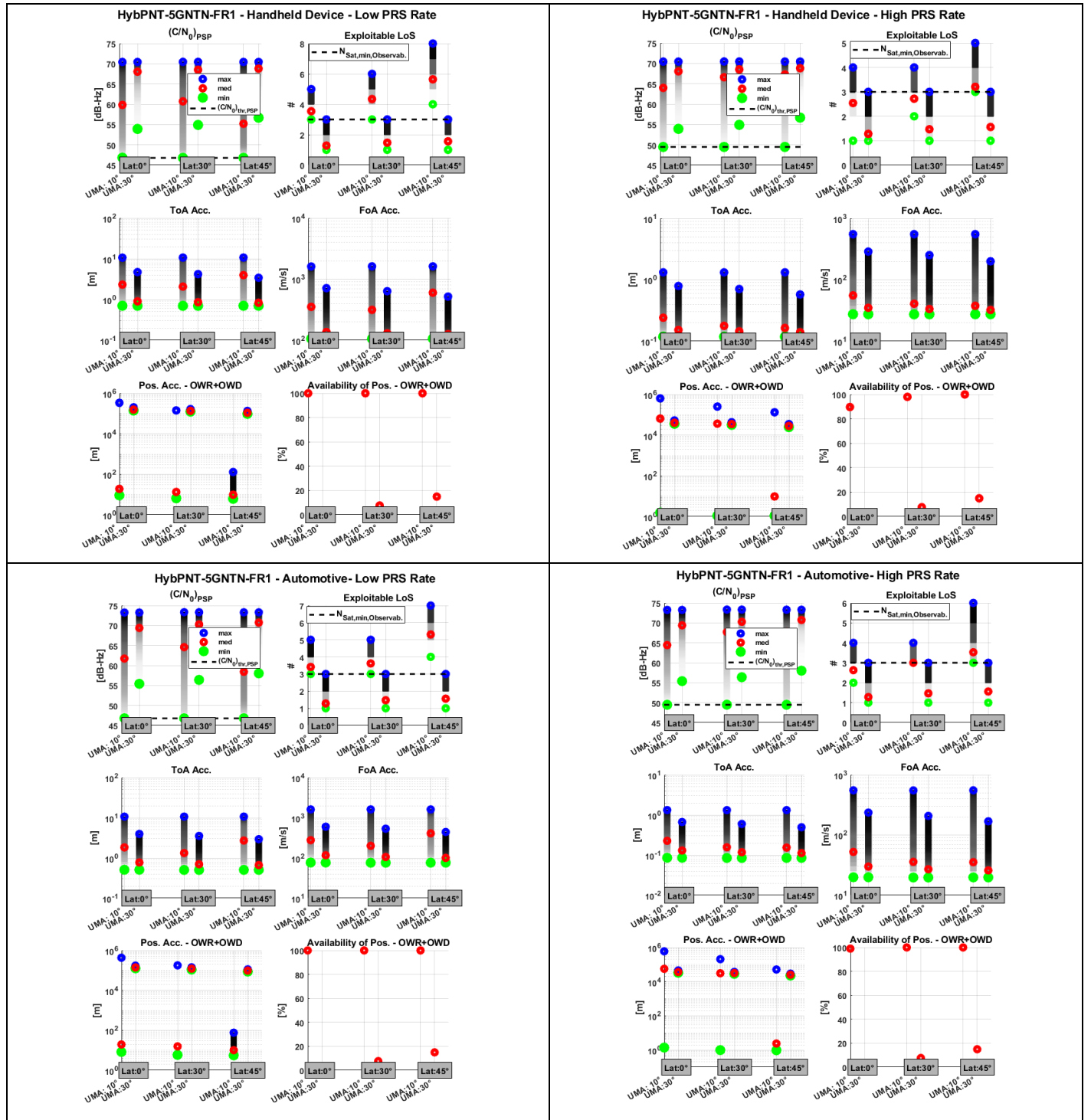
A.4.2 Performance Boards for Standalone 5G NTN in FR1

FIGURE 19: Performance board for Standalone 5G NTN at FR1 (Handheld/Car UT, Low/ High PRS Rate)

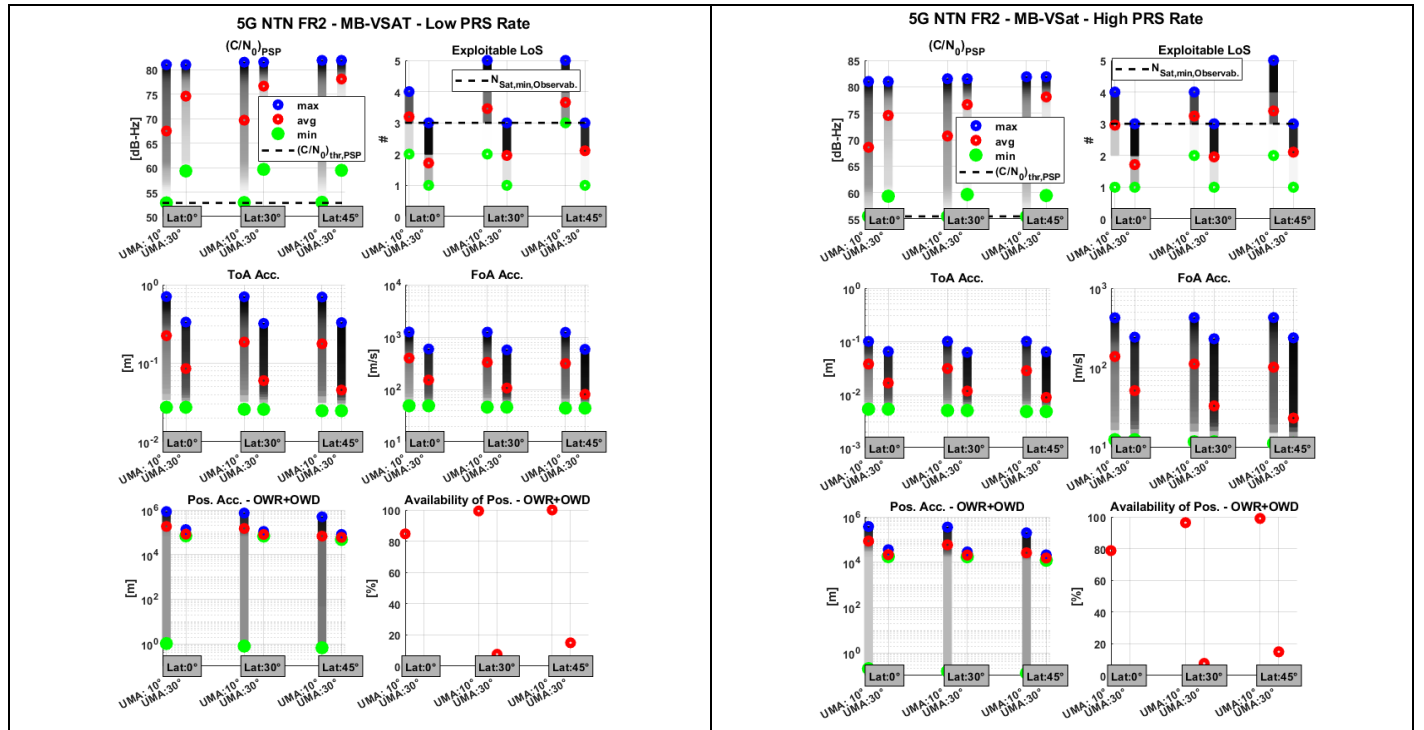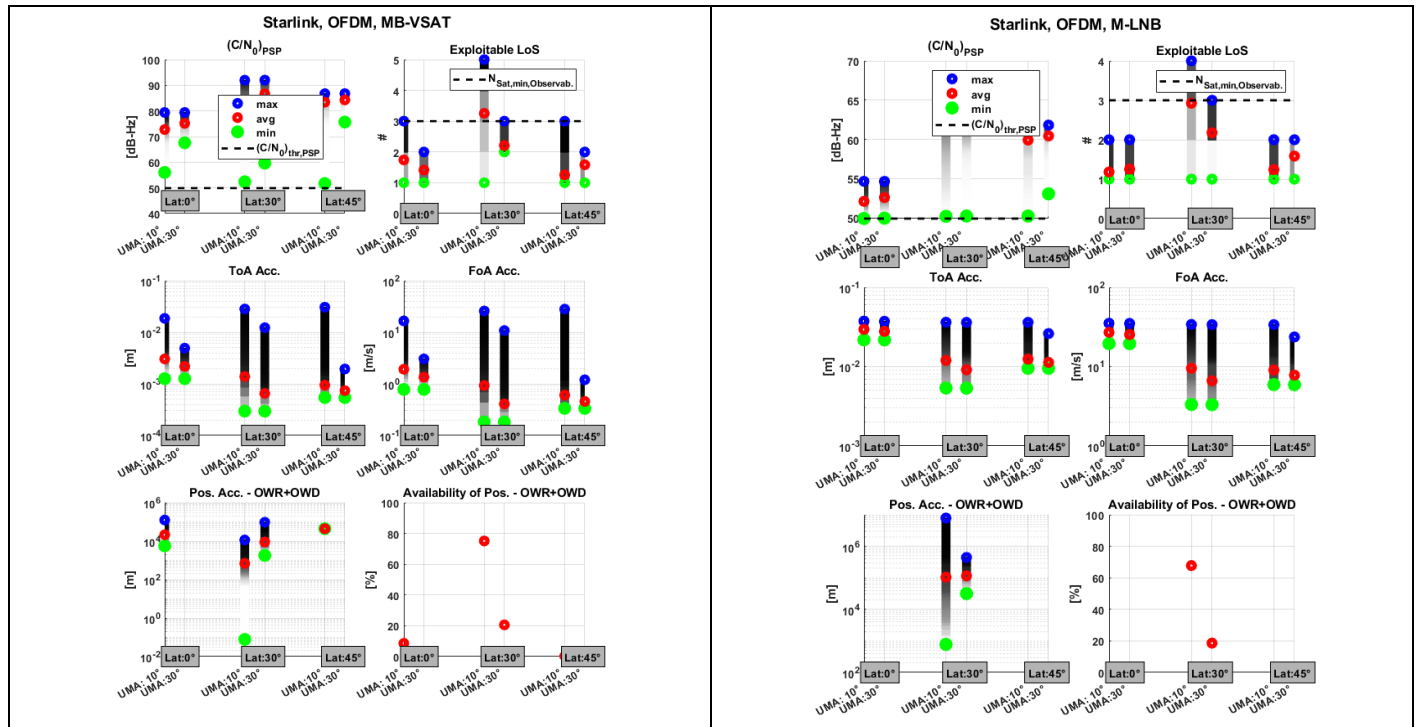## A.4.3 Performance Boards for Standalone 5G NTN in FR2

FIGURE 20: Performance board for Standalone 5G NTN at FR2 (Multi-Beam VSAT for Low and High PRS Rate)
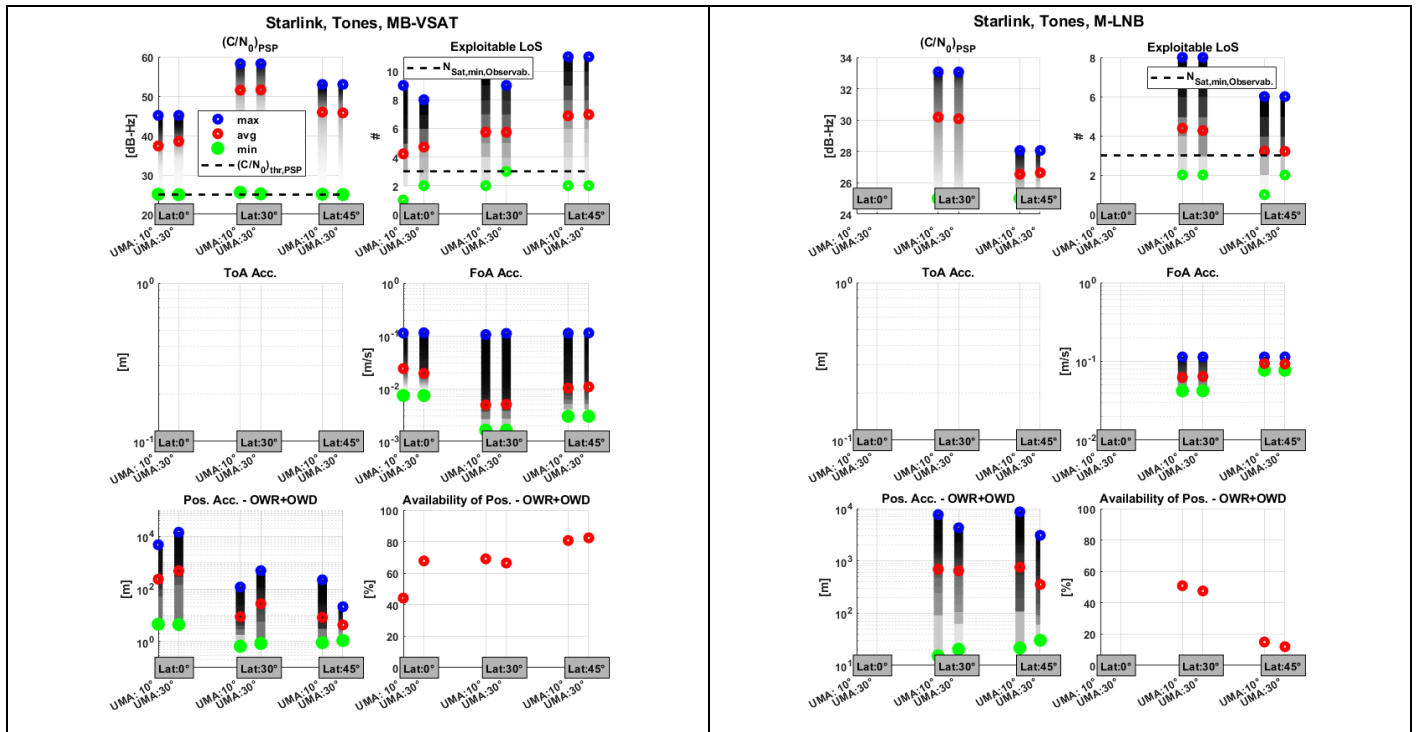
A.4.4 Performance Boards for Standalone Starlink

FIGURE 21: Performance board for Standalone Starlink (Multi-Beam VSAT/M-LNB for PSS and Tones)

A.4.5 Performance Boards for Standalone Dedicated LEO-PNT
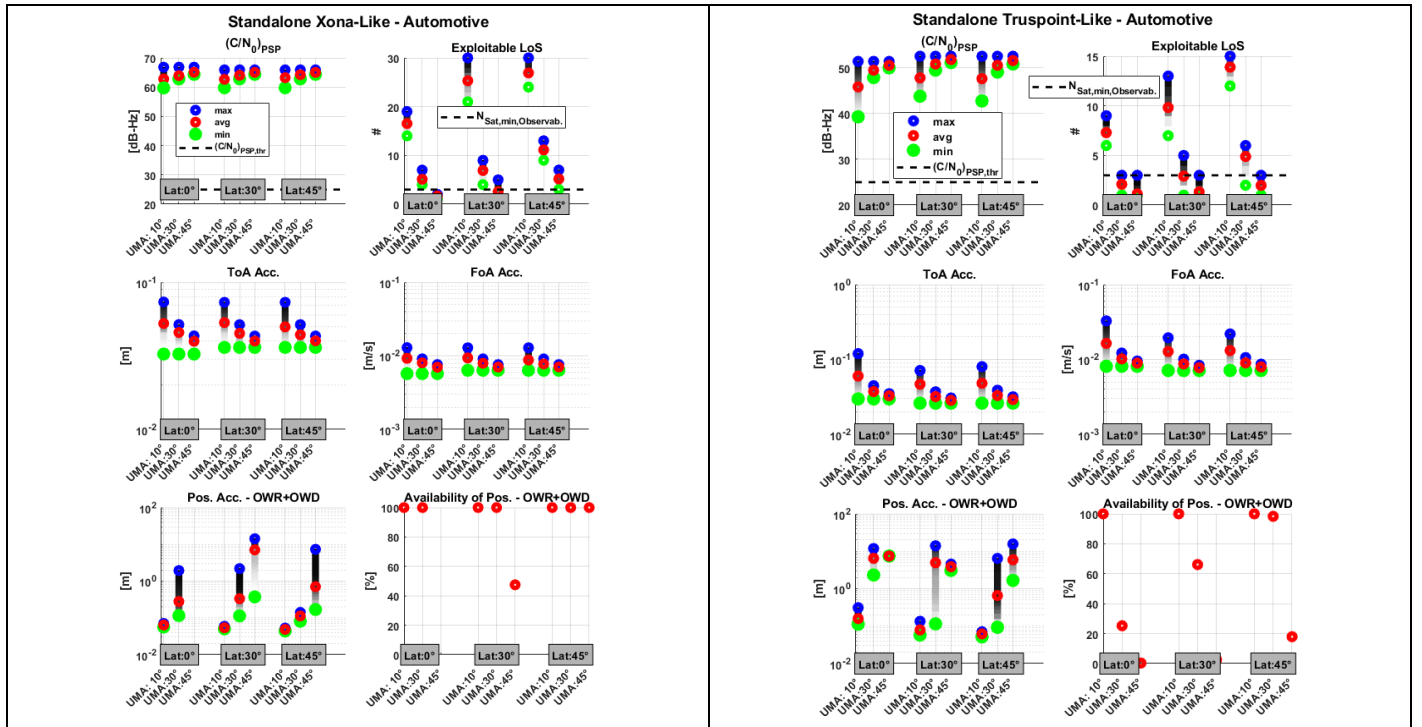
FIGURE 22: Performance board for Standalone Xona-Like (Hemispheric Ant.) and Trustpoint-Like System (CRPA 7 elements) for Automotive

A.4.6 Performance Boards for Hybridized 5G NTN, 5G TN and HAPS in FR1
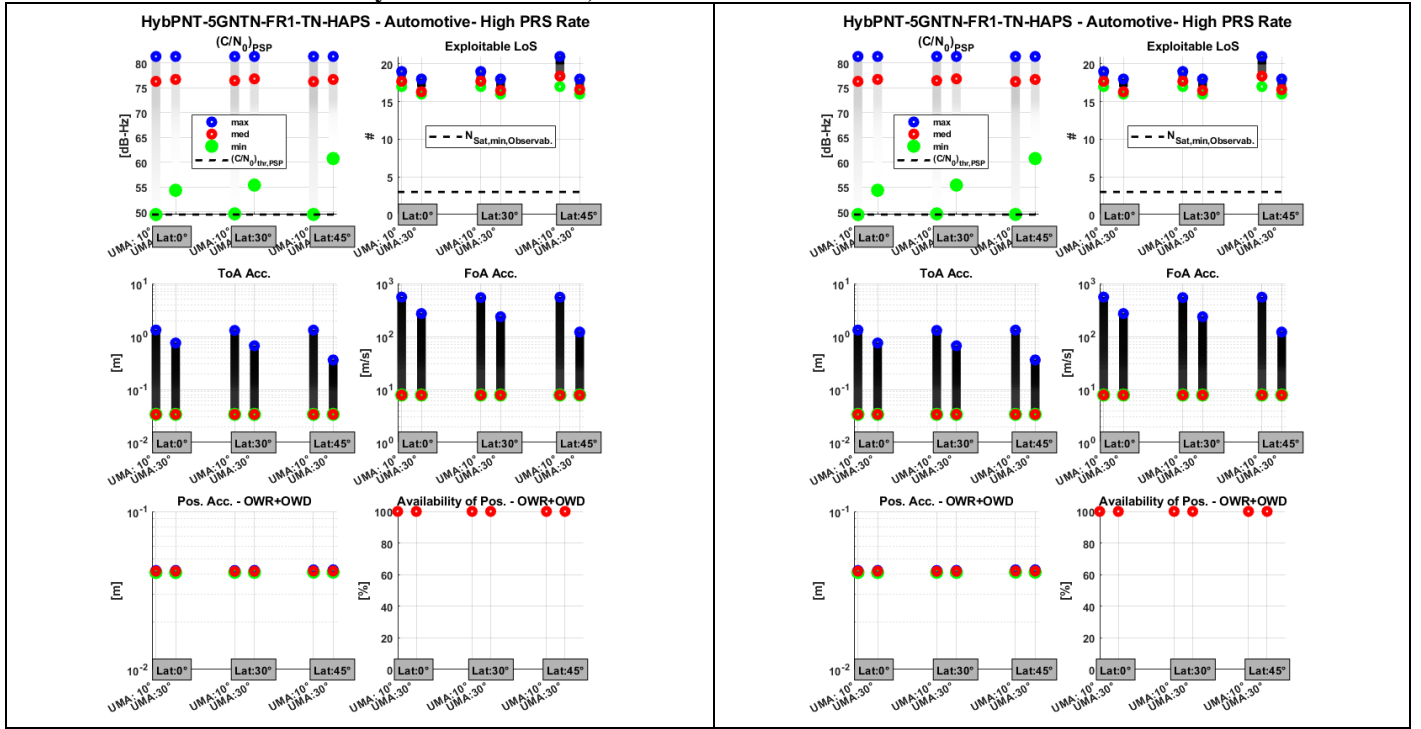

FIGURE 23: Performance board for hybridized 5G NTN, TN and HAPS at FR1 (Handheld/Car UT, Low/ High PRS Rate)

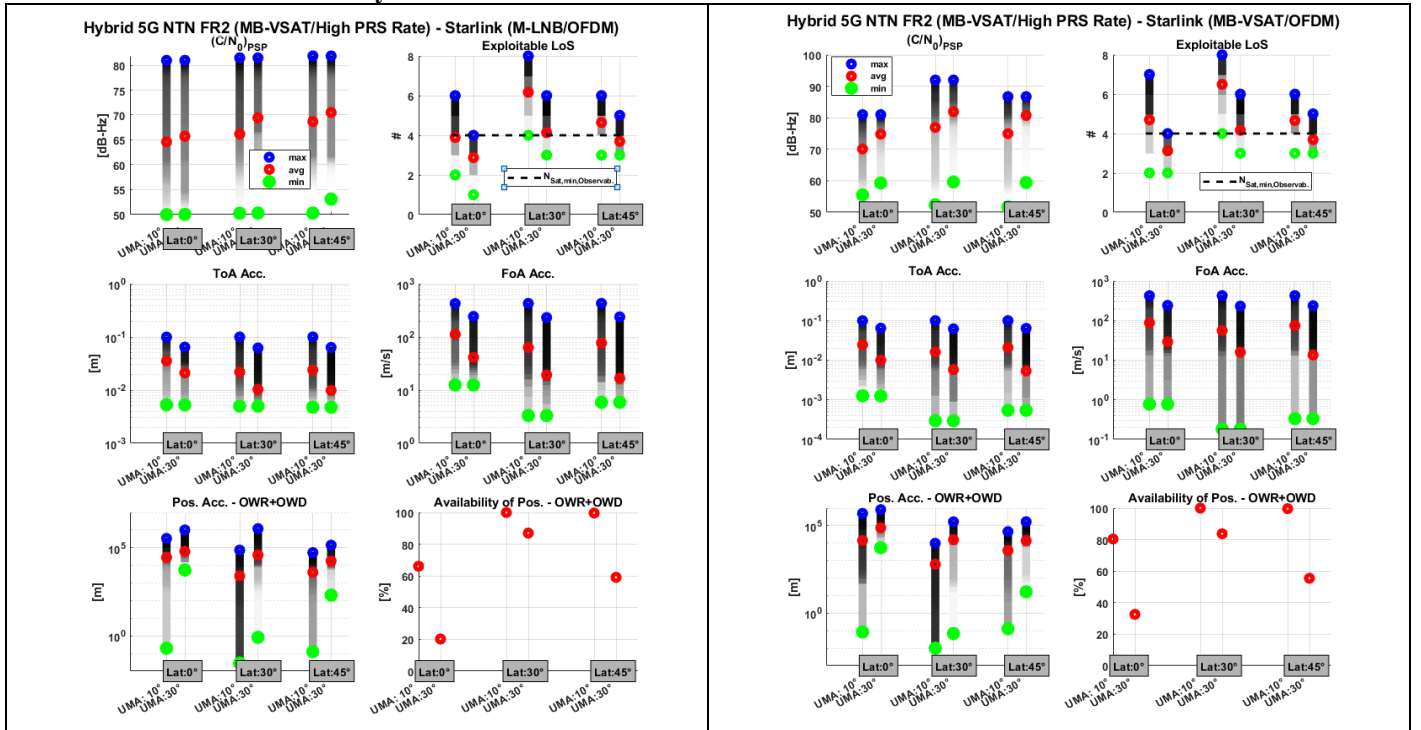## A.4.7 Performance Boards for Hybridized 5G NTN in FR2 and Starlink

FIGURE 24: Performance board for hybridized 5G NTN in FR2 (MB-VSAT) and Starlink (M-LNB/ MB-VSAT for PSS)

A.4.8 Performance Boards for Hybridized Xona-Like and Trustpoint-Like
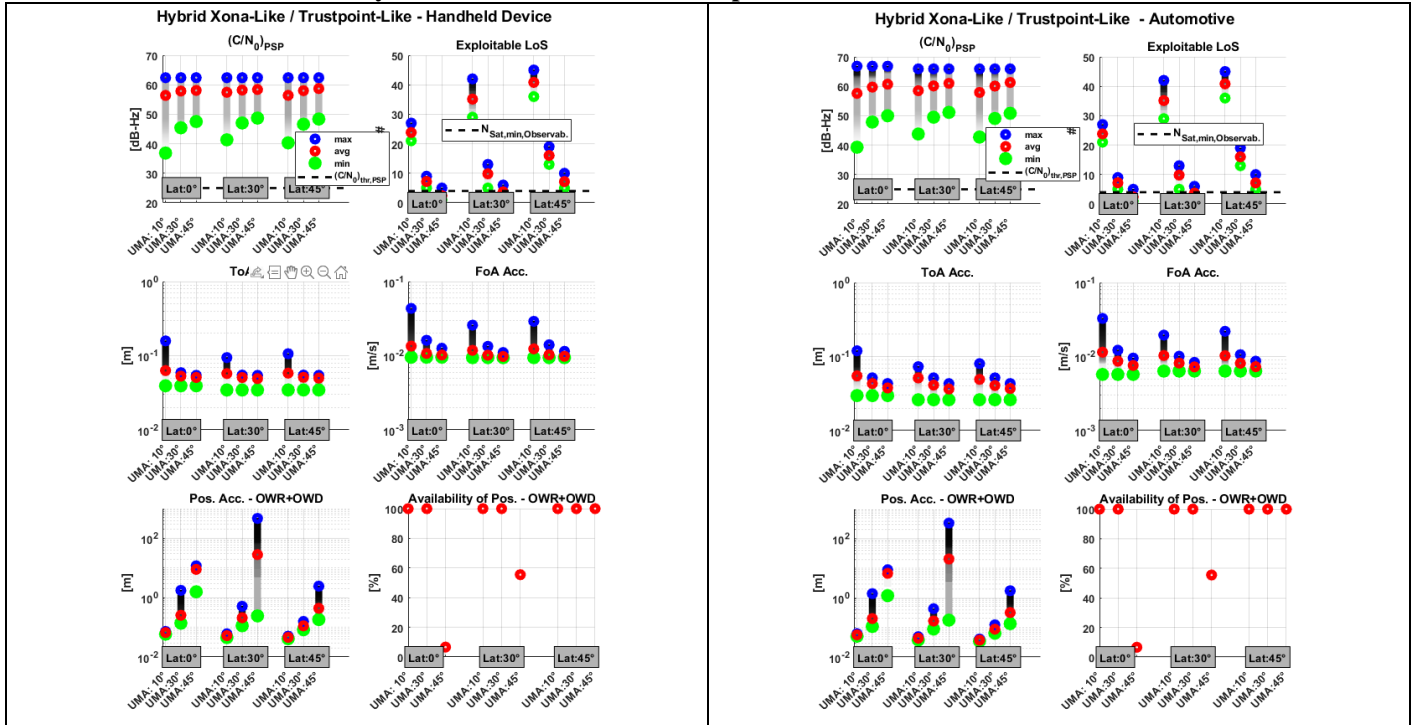

FIGURE 25: Performance board for hybridized LEO-PNT constellations (Xona-like and Trustpoint-like)